Republic of Iraq
Ministry of Higher Education
and Scientific Research
University of Babylon
College of Engineering
Department of Environmental Engineering

GIS and Satellite Imagery of Hilla River Basin Responses to Global Environmental Temperature Changes, Iraq

A Thesis

Submitted to the College of Engineering/University of Babylon

In Partial Fulfillment of the Requirements for the Degree

of Master in Engineering / Environmental Engineering

BY

Hiba Jasim Oudah Jasim ALmasaody

Supervised by

Asst. Prof. Dr. Hussein Ali Mahdi Al-Zubaidi

2022 A.D **1443 A.H**

بِسْمِ اللَّـهِ الرَّحْمَـٰنِ الرَّحِيمِ

قال تعالى: (اقْرَأْ بِاسْمِ رَبِّكَ الَّذِي خَلَقَ ۞ خَلَقَ الْإِنسَانَ مِنْ عَلَقٍ ۞ اقْرَأْ وَرَبُّكَ الْأَكْرَمُ ۞ الَّذِي عَلَّمَ بِالْقَلَمِ ۞ عَلَّمَ الْإِنسَانَ مَا لَمْ يَعْلَمْ).

صَدق الله العلي العظيم

سورة العلق

آية (19)

SUPERVISOR CERTIFICATION

I certify that the preparation of this thesis entitled

" GIS and Satellite Imagery of Hilla River Basin Responses to Global Environmental Temperature Changes, Iraq" was presented by "Hiba Jasim Oudah ALmasaody", and made under my supervision at the Department of Environmental Engineering, College of Engineering, University of Babylon, as a partial fulfillment of the requirements for the degree of Master in Engineering/ Environmental Engineering.

Signature:
Name **:** ***Asst. Prof. Dr. Hussein A. M. Al-Zubaidi*** **(Supervisor)**
Date: / 4 / 2022

Examining Committee's Certification

We certify that we have read this thesis entitled " **GIS and Satellite Imagery of Hilla River Basin Responses to Global Environmental Temperature Changes,** in **Iraq**", and as an examining committee, examined the student hiba jasim oudah its content and in what is connected with it and that our opinion, it meets the standard of a thesis for the Degree of Master of Science in Environmental

Signature:
Name: ***Prof. Dr. Saif Salah Alquzweeni*** *(Chairman)*
Date: / 4 / 2022

Signature:
Name : ***Prof. Dr. Isra'a Sadi Abdul-Amir*** *(Member)*
Date: / 4 / 2022

Signature:
Name: ***Prof. Dr. Hussein Janna*** *(Member)*
Date: / 4 / 2022

Signature:
Name: ***Asst. Prof. Dr. Hussein A. M. Al-Zubaidi*** *(Supervisor)*
Date: / 4 / 2022

Signature:
Name: ***Asst. Prof. Dr. Hussein A. M. Al-Zubaidi***
Address: Head of the Environmental Engineering Department
Date: / 4 / 2022

Approved by the Deanery of the College of Engineering.

Signature:
Name: ***Prof. Dr. Hatem Hadi Obeid Al-Taei***
Address: Dean of College of Engineering
Date: / 4 /2022
Engineering.

TO THOSE…

WHO HAVE THE BIGGEST HEARTS WHICH NEVER ASK, BUT ALWAYS GIVE

MY MOTHER

MY FATHER

MY HUSBAND, KADHUM

MY BROTHERS

AND ALL WHO HELPED ME IN THIS STUDY WITH LOVE AND RESPECT

Hiba jasim
2022

ACKNOWLEDGEMENTS

I sincerely thank God for the completion of this research.

I am very much delighted to express my profound gratitude to all the generous people for their help and suppot. My masters endeavor has been an amazing learning experience and this thesis would not have been accomplished without them .

First of all, I am very much grateful to my supervisor **Asst. Prof. Dr. Hussein Ali Mahdi Al-Zubaidi**, for his valuable suggestions and remarks, for his guidance and for taking the time to read the earlier drafts of this thesis .

My heartfelt thanks goes to my dear husband for his support. I also express my sincere gratitude to my parents and brothers for their inspirations, unconditional love and support.

I would like to thank all friends in university of Babylon for providing me with advice and support. I extend my sincere thanks to my professors and loyal friends in university of Babylon -College of Engineering, who have encouraged and supported me in getting the information and data that I needed.

This study could not have been conducted without help from many people. I would like to thank all others who have contributed directly and indirectly to the success of this research.

ABSTRACT

In the developing countries, the urbanization results in variation in land cover. This leads to spatial and temporal alteration in land surface temperature. This research highlights how land surface temperature (LST) varies spatially and temporally over the City of Babylon, Iraq. Images were taken from Landsat-8 during the period from 2013 to 2020, during June and July processed in QGIS software to indicate land surface temperature changes and link this variation with normalized difference vegetation index (NDVI).

The results showed that the maximum temperature was at barren lands (about 62 ºC), the mean temperature was between 45 and 51 ºC, and the minimum temperature was about 30 ºC. Also, the values of mean NDVI ranged between 0.15 and 0.17. Varying from low to high temperature values water, vegetation, bare areas occupied about (0.6 - 1.6) %, (10.2 - 22.6) %, and (76.1 - 89) % of the total area, respectively. It was found that the temperature distribution in the study area has been impacted by urban development during the study period.

Moreover, valid linear models were set up to forecast LST in terms of NDVI directly. The comparison between air temperature collected from meteorological stations and the determined Land Surface Temperature showed that high correlation is presented between the estimated and the observed values with 3 ^{0}C variation. The results also showed that LSTs in the center of Hilla River basin were higher than the other areas within the governorate. Temperature began to rise in 2013, and then became higher gradually in 2014 and 2015 to become significantly high in 2016, 2017, 2018 and 2019, but in 2020 the temperature droped slightly compared to previous years.

The results of Alsiha District showed increase in the bare and built-up land in the last eight years. Area increased from 2.6 km^2 in 2013 to 2.8 km^2 in 2020. Crops and vegetation have been decreased from 0.31 km^2 in 2013 to 0.18 km^2 in 2020 . Moreover, decrease has been observed in water body from 0.11 km^2 in 2013 to 0.06

km^2. Also, LST ranges from 36 ^{0}C to 50 ^{0}C in 2013 and from 40 ^{0}C to 54.6 ^{0}C in 2020. In this study, it was also found that the maximum LST for the entire land raised by 4 ^{0}C from 2013 to 2020, and the minimum temperature increased by the same rate from 36 ^{0}C to 40 ^{0}C. This can be attributed to the urbanization and replacement the vegetation cover by buildings.

In addition, the comparison between temperature data download from NASA (National Aeronautics and space Administration) website and the calculated temperature showed very good agreement in terms of RMSE (Root Mean Square Error) and MAE (Mean Absolute Error) regarding to the water body, vegetation and lands. The RMSE for water bodies was 0.9 ^{0}C and for plants was 1.2^{0}C, while for lands it was 1.5 ^{0}C. The MAE values were 0.6 and 0.9 ^{0}C for water and plants, respectively, while its value was 1.3 ^{0}C for lands.

TABLE OF CONTENTS

LIST OF FIGURES

LIST OF TABLES

LIST OF ABBREVIATIONS AND ACRONYMS

Abbreviation	Description
ArcGIS	: Aeronautical Reconnaissance Coverage GIS
ARVI	: Atmospherically resistant Vegetion Index
CL green	: Green Chlorophyll Index
DOS	: Discontinued Operating System
DVI	: Difference Vegettion Index
ERDAS	: Earth Resources Data analysis System
ESRI	: Environmental Systems Research Institute
EVI	: Enhanced Vegettion Index
GIS	: Geographic Information System
LSE	: Land Surface Emissivity
LST	: Land Surface Temperature
LULC	: Land Use Land Cover
MAE	: Mean Absolute Error
MSAVI	: Modified Soil Adjusted Vegetion Index
MSI	: Moisture Vegetion Index
NASA	: National Aeronautics and space Administration
NDBI	: Normalized Difference Built-up Index
NDVI	: Normalized Difference Vegetation Index
NDWI	: Normalized Difference Water Index
NIR	: Near Infrared
OLI	: Operational Land Image

QGIS : Quantum GIS

RMSE : Root Mean Square Error

ROIS : Regions Of Intersts

RS : Remote Sensing

R-squared : coefficient of determination

SAVI : Soil Adjusted Vegetion Index

SCP : Semi-Automatic Classification Plugin

TIRS : Thermal Infrared Sensor

UHI : Urban Heat Island

USGS : United States Geological Survey

CHAPTER ONE

INTRODUCTION

CHAPTER ONE

INTRODUCTION

1.1 General

The 21 century, especially in the African and Asian continent, has witnessed an unprecedented pace of urbanization and global urban population development (Njoku, 2019). Urban areas have a much greater socio-economic footprint than rural areas, caused by urban growth and a growing number of inhabitants in recent decades (Dissanayake et al., 2019). Land surface temperature can provide important information about the surface physical properties and climate which plays a role in many environmental processes(Al-Timimi et al., 2014). Remote sensing technology is an important source of earth observation from different platforms and sensors, and it offers work on a large scale with cheap, accurate (depending on the research design), and faster results compared. to the conventional methods. Thermal remote sensing is one of the branches of remote sensing that deals with the acquisition, processing, and interpretation of data acquired primarily in the Thermal Infrared (TIR) region of the electromagnetic. (EM) spectrum.Thermal remote sensing captures the radiation emitted from the ground primarily to estimate the surface temperature. In addition to surface temperature, surface emissivity, soil moisture,and evapotranspiration are the other crucial biophysical parameters estimated from TIR observations. Since these parameters govern the land-atmosphere interactions and the energy fluxes, their accurate evaluation is required to understand the behavior of the earth (Sekertekin and Bonafoni, 2020).

Land Surface Temperature (LST) is the surface temperature that can be determined when the surface of the ground is in direct contact (usually measured in Kelvin) with a measuring instrument. LST is the surface temperature of the crust of the earth where it absorbs, reflects and refracts heat and radiation from the sun. With a change in climate conditions and other human activities, LST shifts where the exact prediction becomes difficult (Anandababu et al., 2018).

One of the important variables measured by remote sensing satellites is surface temperature (Sameen and Al Kubaisy, 2014). Evolution of Land Surface Temperature (LST) based on remote sensing data depends on the spatial resolution of the sensors, as well as modelling process requiring a collection of mathematical equations for calculation the solar radiation parameters, vegetation indices and land surface temperature (Rolf and de By, 2001). The importance and effects of LST on different topics have been investigated by several researchers, including urban climate and Surface Heat Island (SHI) studies, evapotranspiration, forest fire monitoring, geological and geothermal studies (Sekertekin and Bonafoni, 2020). By replacing areas of vegetation with residential and commercial areas and their associated infrastructure, the development of urban areas has a direct effect on land use, this raises the surface temperature of the land (LST) (Beg, 2017). Using land-based observation stations, several studies have measured the relative warmth of cities by calculating the air temperature. Some experiments, along different roads, used temperature measurements using temperature sensors mounted on vehicles (Al-Timimi et al., 2014).

Due to its role in decreasing biodiversity and altering the regional climate and developing an Urban Heat Island (UHI) in cities, Land Cover (LC) changes have become a source of concern. Urban Heat Island (UHI)

refers to the phenomenon of higher urban air/surface temperatures than in non-urban regions (Zhibin et al., 2015). LC changes were caused by rapid urbanization that increased Land Surface Temperature (LST) (Ullah et al. , 2019). Remote Sensing (RS) techniques may be used to assess the most noticeable urban biophysical and environmental characteristics of spatial change (Ali et al., 2017). The surface of the land consists of trees, surfaces of water, surface materials that are impervious, soil and rocks. Impermeable surfaces leading to variation in land surface temperature of urban areas. LST depends on LC greatly for tropical and sub-tropical climate urban regions, where built-up areas have the highest LST relative to arid conditions in which bare soil has the highest LST. This rapid urban extensions will replace vegetation with LST-enhancing built-up areas, rising LSTs.

1.2 Study significance

To provide information and data for the study area, satellite images based on the newest remote sensing and GIS technologies were created to highlight the changes in LST spatially and temporally. This research is novel in finding the land surface temperature utilizing Landsat 8 Level 1 data and QGIS software **(**QGIS is a full-featured, user-friendly, free-and-open-source Geographical Information System (GIS) that runs on (Unix platforms, Windows, and MacOS **)** for Babylon Governorate, Iraq during the period from 2013 to 2020, indicating the relationship between LST and LC over time visually and quantitatively.

1.3 Study problem statement

The population growth and urbanization processes have altered the Land Cover (LC) distribution over the study region lately. These changes in addition to global climate changes, in turn, have impacted the Land Surface Temperature (LST) spatially and temporally. However, no information is available to display the trend of LST variation over time for the study area.

1.4 Study objectives

The main obectives of the study are:

1. To display land surface temperature spatially and temporally depending on Landsat 8 satalite images for the research area from 2013 to 2020.
2. To classify the study area land cover into classes.
3. To link LSTs to the land cover classes.
4. To correlate LSTs with Normalized Difference Vegetation Index (NDVI) and develop linear models for the study period.

1.5 Thesis structure

Five separate chapters contain the complete presentation of the thesis. Below is a short description of each chapter:

1. **Chapter One: Introduction**

The chapter introduces the study, study significance ,study problem statement , and the study objectives.

2. **Chapter Two: Theoritical Concepts**

The chapter gives a revision to the concepts related to the research. It begins with the geographic information systems followed by remote sensing. An overview about Landsat mission, Land-use/Land-cover basics and previous related studies were included too.

3. **Chapter Three: Data and Methods**

This chapter shows the techniques utilized in the research. It gives a description to the study area, datasets and methodology. It also provides the method of estimation of LST and NDVI.

4. **Chapter Four: Results and Discussion**

This chapter presents the results and discussion of this thesis.

5. **Chapter Five: Conclusions and Recommendations**

It includes the main findings of this study.

CHAPTER TWO

THEORETICAL CONCEPTS

CHAPTER TWO

THEORITICAL CONCEPTS

2.1 Introduction

This chapter involves the concepts adopted in this study . It gives description to the Geographic Information Systems (GIS), then the remote sensing is explained. Next, an overview about Landsat mission is presented, as well Land Use and Land Cover (LULC), estimation of NDVI, Land Surface Temperature (LST) and relationship between LULC and LST is achieved. Finally, in the section of literature review, the concepts of previous related studies that is related to this study are discussed.

2.2 Geographic Information Systems (GIS)

GIS is a system of software, hardware and data computers that allow data to be entered, manipulated, processed and displayed, and information that is connected to a position on the surface of the earth. (Ali and Ershad ,2020). GIS includes hardware, software, data, people, and organizational components. It flourished in the 1980s, inspired by the advent of Personal Computers (PCs) and graphical user interfaces. In resource control, emergency planning, crime analysis, public health, land record management, precision farming, and many other areas. Thus, GIS is now a valuable method.

Geospatial data is referenced spatially and can be either vector or raster data. Data collection, data management, data query, vector data analysis, raster data analysis, and data display are typical GIS operations. The incorporation of desktop GIS, web, and mobile technologies is a significant trend that has already led to the creation of location-based

services, collaborative web mapping, and voluntary geographic information (Packard, 2018). GIS data can be separated into two categories: spatially referenced data which is represented by vector and raster forms (including imagery).

- Raster data (also known as grid data) is based on cells, aerial or satellite imagery. There are two types of raster data: continuous and discrete data (Morais, 2000). A good example of raster data is LST raster as shown in Figure (2.1).

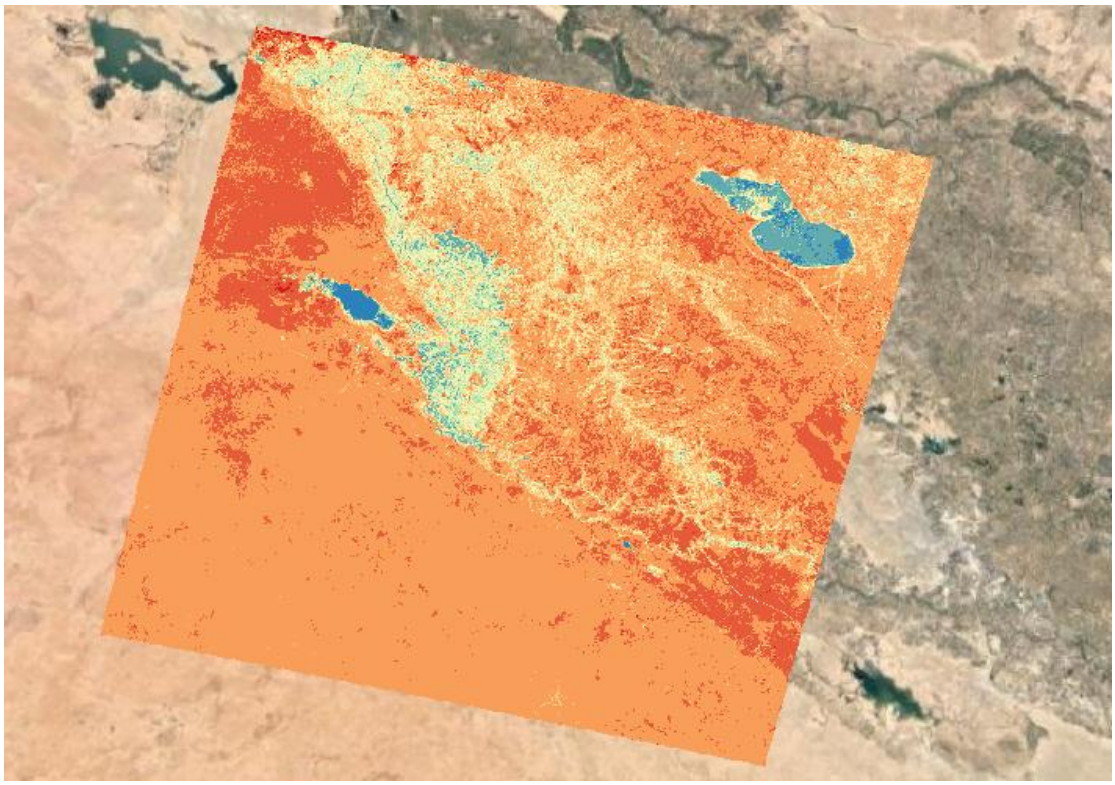

Fig. (2.1): Raster data of LST image generated from landsat-8 dataset for Babylon Governorate, Iraq.

- Vector data is split into three types: point, line, and polygon data (Figure 2.2).

- **Point data** is most widely used to describe nonadjacent attributes as well as individual data points. Since points have no dimensions, one can't quantify length or area with this dataset. Schools, points of interest, and, in the case below, bridge and culvert positions are all examples. Abstract points are also represented using point functions. Point coordinates, for example, may represent city locations or place names. An example of point data is Hilla city, Iraq.
- **Line data** is based to reflect linear characteristics, line (or arc) data is used. Rivers, trails, and streets are all popular examples. Due to the fact that line features only have one dimension, they can only be used to quantify length. There is a beginning and an end point for line functionality. Path centerlines and hydrology are two common examples. Line forms (solid lines or dotted lines) and variations of colors and line thicknesses are the most common symbols used to differentiate arc features from one another.
- **Polygons data** are used to represent places such as a city's border, a lake, or a forest on a large scale map. Since polygon features are two-dimensional, they can be used to calculate a geographic feature's area and perimeter.Thematic mapping symbology (tone schemes), patterns, or, in the case of numeric gradation, a color gradation system are the most popular ways to differentiate polygon features **.**An example is Babylon Governorate.

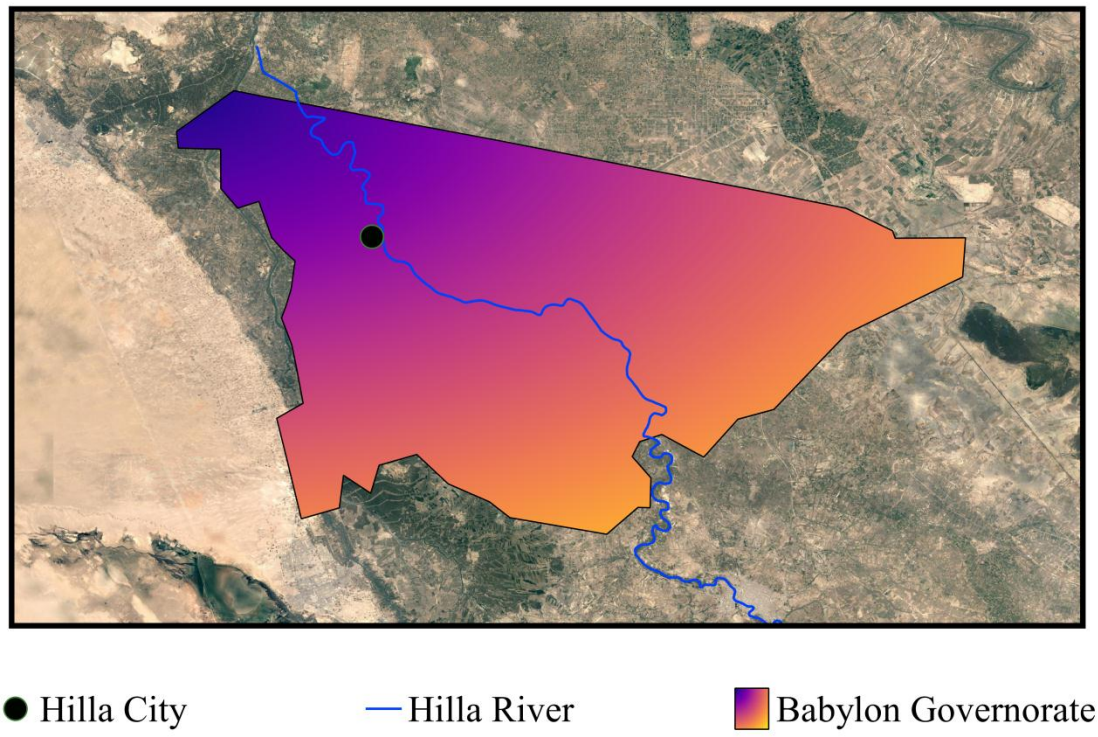

Fig. (2.2): An example of vector data: Hilla City is point data, Hilla River is line data, and Babylon Governorate is polygon data.

A simplified method of describing GIS is shown in Figure (2.3) as the one looks at the disposition of its data in layers. This system involves the specific location that has the same coordinate in all maps in groups of maps of the same portion of the territory. In this method, its thematic and spatial characteristics can be analyzed in order to gain a better understanding of the area (Hunter and Bishop, 2013).

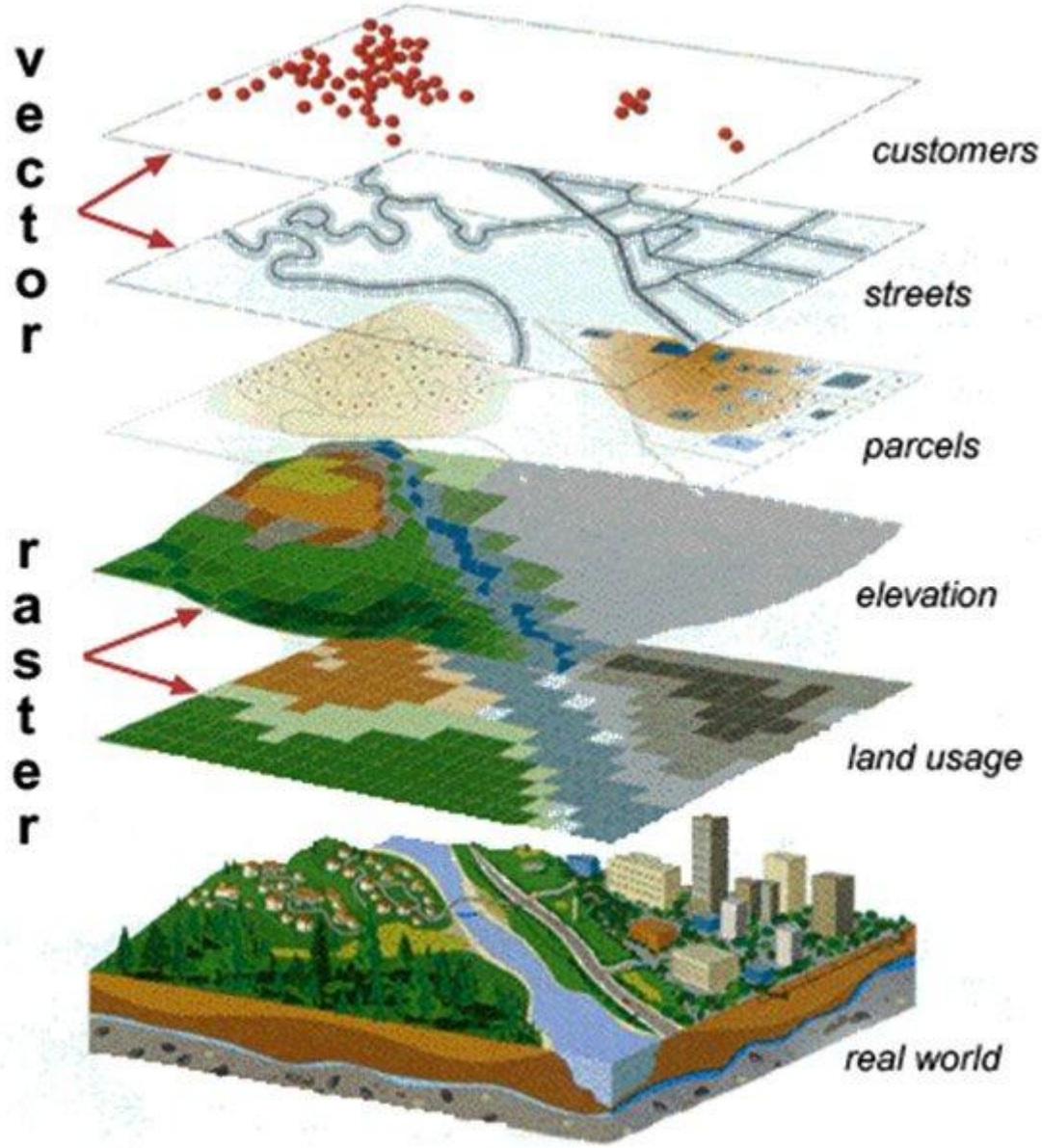

Fig. (2.3): The concept of layers (ESRI) (Hunter and Bishop, 2013).

2.3 Remote Sensing

It is the method of collecting data information using electromagnetic radiation or acoustic waves originating from the targets of interest, objects/substances which are not in direct contact with the sensor (Figure 2.4). An aerial picture is a typical example of a product that is remotely sensed (by camera and video, or now digital)(Ali, 2010)

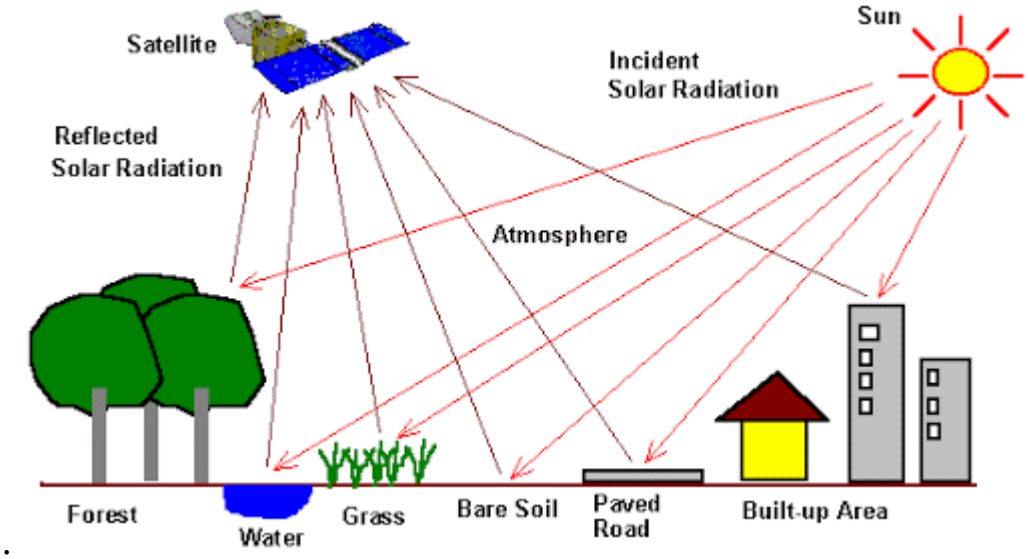

.

Fig. (2.4): Remote sensing process(Ali, 2010).

As technology progresses in producing remote sensing systems, the use of the techniques is growing increasingly, identifying new fields of application (Mårtensson, 2011). The screen emanates a physical quantity (light), that is a radiation source. The radiated light move s over a distance and hence “remote” to similar degres until encountering sensor and catching it. A singal is sent by each eye and recorded the data then interpreting this into data to a processor (your brain). By perceiving singals, either reflecting or emitting, passively or actively from objects to convey the information in pulues or waves, most human senses accumulate their knowledge of the external environment almost entirely (Al Ajmi and Saif ud din, 2009). Figure (2.5) shows image of Iraq by using remote sensing technique.

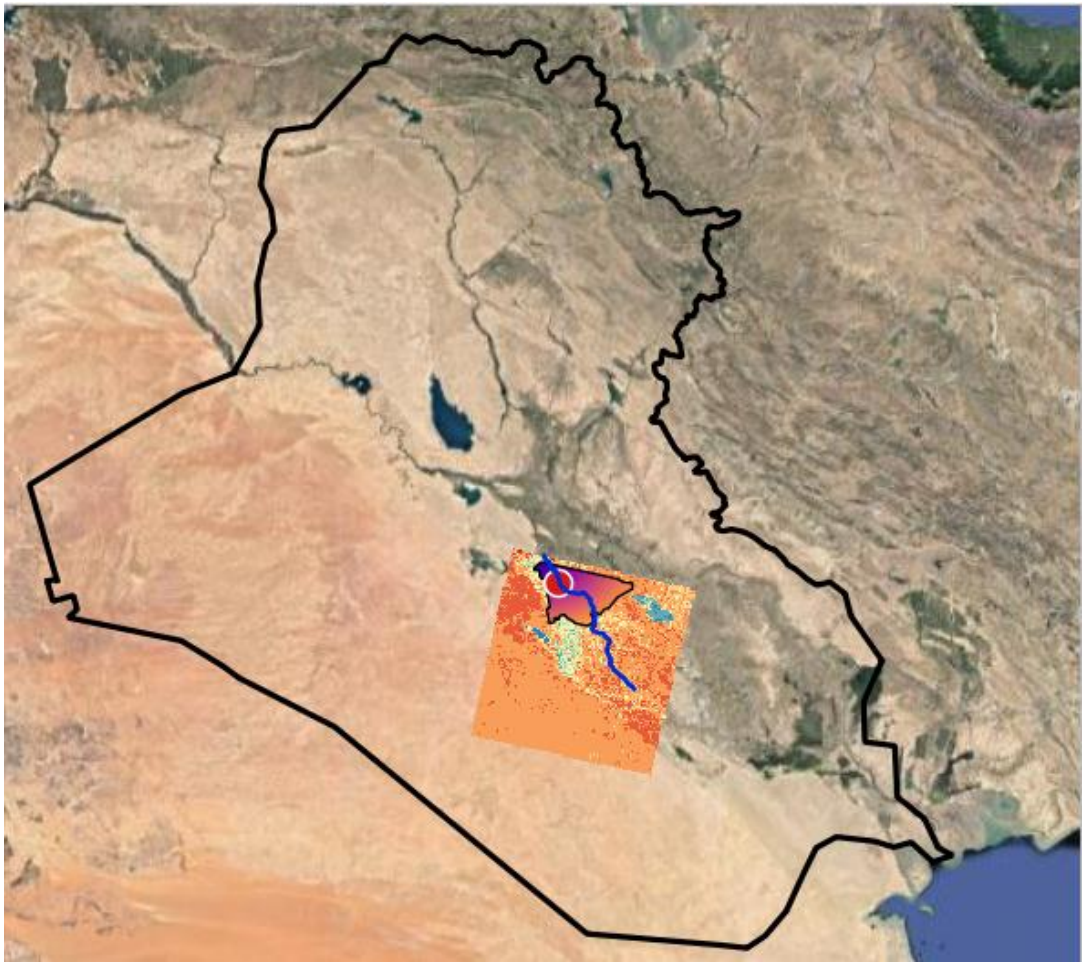

Fig. (2. 5): Satellite Image of Iraq.

Remote sensing technology is an essential source of earth observation from multiple platforms and sensors and provides inexpensive, precise (depending on the test design) and quicker results compared to traditional methods for large-scale work. One of the branches of remote sensing dealing with the collection, processing, and analysis of data required principally in the Electromagnetic (EM) spectrum Thermal Infrared (TIR) field is thermal remote sensing. To measure the surface temperature, thermal remote sensing mainly collects the radiation released by the earth. In addition to surface temperature, the other critical biophysical parameters estimated from TIR measurements are surface emissivity, soil moisture, and evapotranspiration. Since the land-atmosphere relationships and energy fluxes are controlled by these parameters, their detailed

measurement is important to understand the earth's nature (Sekertekin and Bonafoni, 2020) .

2.4 Landsat mission: An overview

Figure (2.6) displays the space planet of Landsat. The project gathers information on the urban lands, farms, freshwater and forests of our plant since the launching of the first Landsat satellite in 1972, forming the longest continuous record of its type. To understand environmental alterations, lots of agricultural practices are responding to natural disasters, distributing limited water supplies, decision-makers from around the world are using publicly available Landsat data (Jenner, 2019).

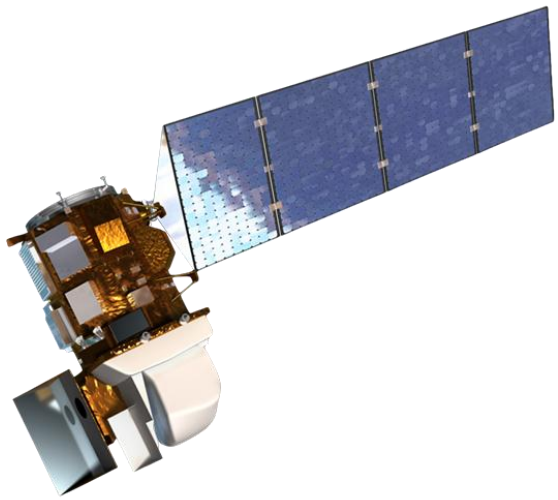

Fig. (2.6): Landsat Mission (NASA, 2013).

2.4.1 Previous Missions

Since the early 1970s, Landsat satellites have continuously produced multispectral images of the earth. A unique 46year data archive of the earth's land surface now exists thanks to these efforts. This one-of-a-kind retrospective portrait of the surface of the Planet has been used in many disciplines to obtain an improved understanding of the surfaces of the

earth's land and the environmental effects of humans. In a number of government, public, private, and national security applications, Landsat data has been used. Examples include land and water management, research on climate change, oil and mineral discovery, forecasting of agricultural yields, monitoring of emissions, identification of land surface change, and cartographic mapping, (Figure 2.7).

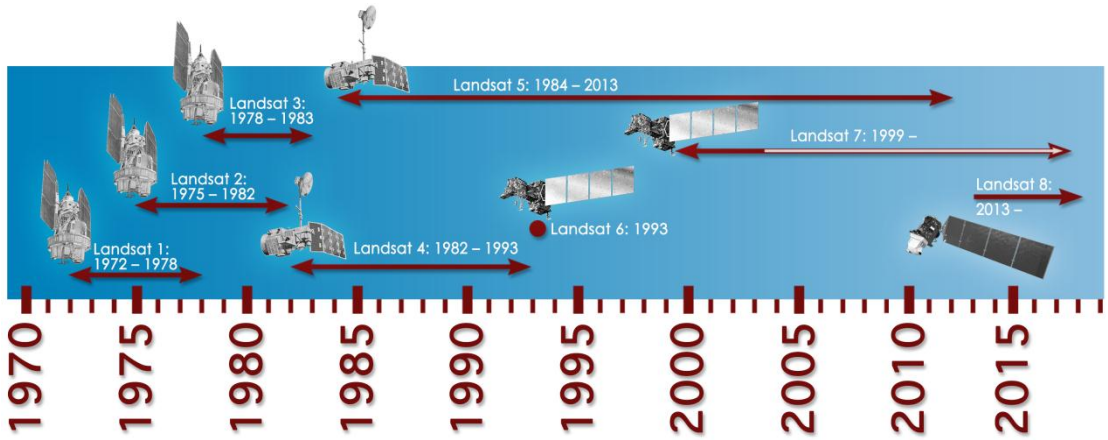

Fig. (2.7): The Landsat Missions Timeline (NASA, 2013).

In this sequence, L8 is the new satellite. In 1972, two earth-viewing imagers, a Return Beam Vidicon (RBV) and an 80-meter 4-band Multispectral Scanner System, launched the first (Landsat 1, originally known as ERTS-1, Earth Resources Technology Satellite 1) (MSS). Landsat 2 and Landsat 3, launched in 1975 and 1978, respectively, were similarly configured. Landsat 4 was released in 1984 with the MSS and a new method called the Thematic Mapper (TM). Improved ground resolution (30 meters) and 3 new channels/bands have been included in the instrument upgrades. Landsat 4 made use of the Multi Mission Modular Spacecraft (MMS), which replaced the Nimbus-based spacecraft configuration used for Landsat 1-Landsat 3, in addition to using an improved instrument. Landsat 5, a duplicate of Landsat 4, was launched

in 1984 and for 28 years, 23 years beyond its 5-year design life, returned scientifically viable results. Equipped with an extra 15-meter panchromatic (Pan) band, Landsat 6 failed to enter orbit in 1993.

L7 was introduced in 1999 and was nominally implemented until the Scan Line Corrector (SLC) of the Enhanced Thematic Mapper Plus (ETM+) sensor failed in May 2003. In the "SLC-off" mode, L7 has continued to acquire useful image data since that time. The high radiometric and geometric quality of all L7 SLC-off data is the same as the data collected prior to the SLC failure (ZANTER, 2019).

Figure (2.8) shows the continuity of multispectral data coverage provided by Landsat missions, beginning with Landsat 1 in 1972.

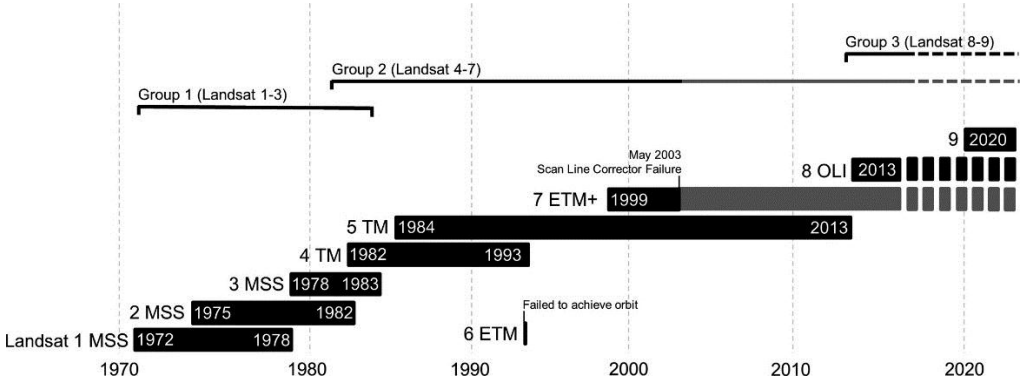

Fig. (2.8): A timeline of Landsat satellites and sensors. Landsat 9 launch date is based on recent congressional appropriations language, image source (Young et al. , 2017).

2.4.2 Landsat 8 Mission

Establishing and maintaining a global survey data archive is an essential operational strategy of the L8 mission. Worldwide Reference Framework (WRF) utilized in L8 is the same that of Landsat 4, 5 and 7 enabling sensors to view the entire planet (Figure 2.9).

Furthermore, L8 activities aim to capture Sun-lit in systematic way, substantially photographs that is free of clouds of the entire land surface of the Planet. The Long-Term Acquisition Plan (LTAP) for L8, initially built for L7, specifies the acquisition pattern for the project to establish and update the archive of the earth in order to gurantue global continuity.

The purpose of the L8 project is to give highly-visible, timely and infrared photos of whole earth's landmass and areas close to coastal, in constant way refreshing an established Landsat database. In terms of calibration, coverage, geometry, and spectral properties, data entry into the system is sufficiently compatible with current archived data to permit deterction of regional and global alterations and comparsion of characterization (ZANTER, 2019).

Fig. (2.9): Landsat 8 Mission (U.S. Geological Survey, 2018).

2.4.3 Landsat 8 Station

On the board of Landsat Data Cobtinity Mission (LDCM) spacecraft, the first photographs were taken in 2013. It was for the Thermal Infrared Sensor (TIRS) and Operational Land Imager (OLI). In an 8-day offset from Landsat 7, the Landsat 8 satellite pictures the entire World every 16 days . It promises to create images at a far higher pace than Landsat 7. (up to 400 scenes per day). Both sensors have enhanced radiometric signal-to-noise (SNR) output quantized over a dynamic spectrum of 12 bits. Improved signal to noise ratio makes for improved characterization of the status and quality of land cover, (Figure 2.10).

Data obtained by the computers on board the satellite can be accessed free of charge from Glo Vis, earth explorer or from the Landsat Look Viewer within 24 hours of reception . The estimated covered land is 183 km east-west and 170 km north-south and compressed into 1 GB file.

There is compliance between the standard level-1 data products created utilizing Landsat 1 to Landsat 7 and that of Landsat 8. It consists of Digital Numbers (DN) reflecting mult-spectral photo data gathered by Thermal Infrared Sensor (TIRS) and the Operational Land Imager (OLI). The goods are provided in unsigned integer format of 16-bit and could be rescaled to radiance or reflectance at the top of the atmosphere (TOA) utilizing radiometric rescaling coefficients given in the metadata file (MTL file). This file also includes the thermal constants needed to translate TIRS data to the at-satellite brightness temperature.the spatial resolution (level of detail) could be the most significant part of observing a satellite photograph, but the use of variations in irradiative power expressed by various surface materials to classify characteristics of interest is less understood. Landsat 8 maintains compatibility with previous sensors and also helps further analysis in the future with the

inclusion of new multispectral and thermal bands (Dev Acharya and Yang, 2015).

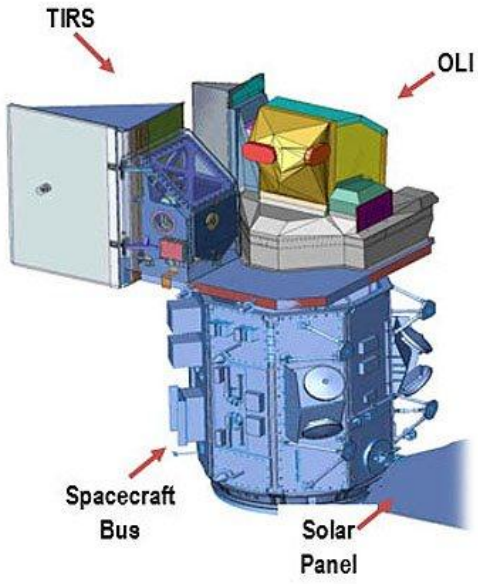

Fig. (2.10): Illustration of Landsat 8 Observatory (ZANTER, 2019).

Landsat 8 which the Landsat Data Continity Flight (LDCF) was released on Feb 2013 from Vandenberg Air Force Base, California. This landsat is considered the newest released Landsat satellite carrying a two-sensor payload, NASA (NASA stands for National Aeronautics and Space Administration). NASA was started on October 1, 1958, as a part of the United States government. NASA is in charge of U.S. science and technology that has to do with airplanes or space, GSFC-built TIRS and the BATC-built OLI. Each scene is continousely photographed by the TIRS and OLI sensors, but can be utilized in separate way in case of presence of issue with either sensor. Regularly, the sensors view the plant at-nadir on the orbital raw coordinate system of the sun-synchronous Worldwide Reference System 2 (WRS-2). Nevertheless, it is possible to schedule special collections off-nadir. The sensors provide technological

improvements over previous Landsat tools. The spacecraft is referred to as the L8 observatory, with its two integrated sensors.

In a sun-synchronous, close-polar orbit, at 705 km (438 mi) altitude, sloped at 98.2^0, Landsat 8 orbits the earth and completes one orbit of the earth every 99 minutes. With an equatorial crossing time, the satellite has cycle repeated in a 16-day: 10:00 a.m. +/- 15 mins.

● Operational Land Imager (OLI)

The OLI sensor (Figure 2.11) has a design life of five years with the design being similar to that of Advanced Land Imager (ALI) that was incopporated on Earth Observing 1 (EO-1) representing a remarkable technological advancement over L7's ETM+ sensor. For all bands, the OLI sensor collects photo for 9 shortwave spectral bands over a 190 km stretch with a spatial resolution of 30 m. To avoid atmospheric absorption characteristics within ETM+ bands, it is required to refine the widths of some OLI bands. In OLI band 5, the remarkable enhancement occurs so that a water vapour absorption feature is elimated at 0.825 μm in the center of ETM+. To generate more variation between vegetated lands and non-vegetated ones, OLI pan band, band 8 is also narrower in compared with ETM+ pan band. OLI has two bands in addition to the legacy Landsat bands which are 1-5, 7, and pan. The coastal/aerosol band (band1) is similar to ALI band1 particularly utilized for ocean color measurements, and the current Cirrus band (Band 9; 1.36-1.38 μm) with the purpose of identifying thin clouds forming of snow drops (cirrus clouds looks bright, meanwhile the majpority of land surface looks dark).

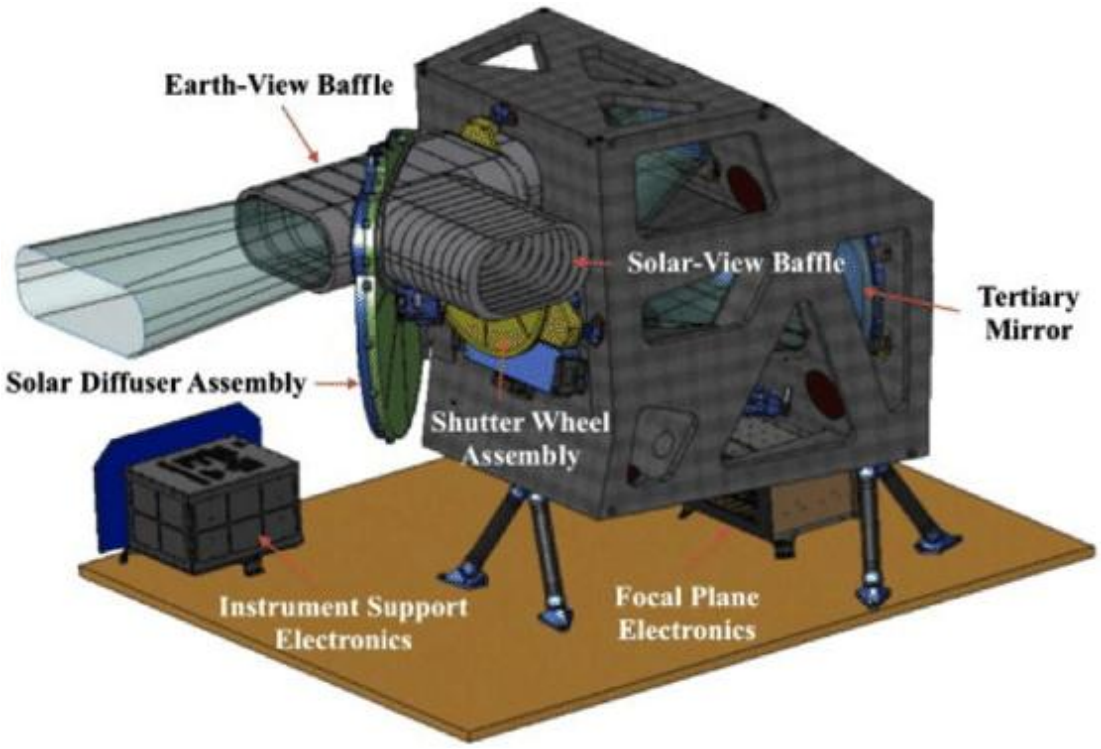

Fig. (2.11): OLI Instrument (ZANTER, 2019).

- **Thermal Infrared Sensor (TIRS)**

Like OLI, TIRS (Figure 2.12) is a push-broom sensor with long arrays of photosensitive detectors utilizing a focal plane. To quantify longwave Thermal Infrared (TIR) radiation released by the surface of the earth, the amplitude of which is a function of surface temperature, TIRS uses Quantum Well Infrared Photodetectors (QWIPs). Two thermal infrared wavelength bands are adaptive to the TIRS QWIPs, causing the temperature of the earth's surface to be isolated from that of the atmosphere.

The TIRS sensor, which has a design life of three years, gathers image data for two thermal bands with a spatial resolution of 100 m over a 190 km span. The two thermal infrared bands encompass the wavelength spectrum of the larger thermal bands (10.0-12.5 μm) of TM and ETM+ and reflect an improvement over the thermal data of the single band.

TIRS-generated data is quantized to 12 bits . While TIRS has a lower spatial resolution than the 60 m ETM+ band 6, technically, the dual thermal bands could allow surface temperature to be recovered, but the use of this method is prevented by stray light problems with band 11 (ZANTER, 2019).

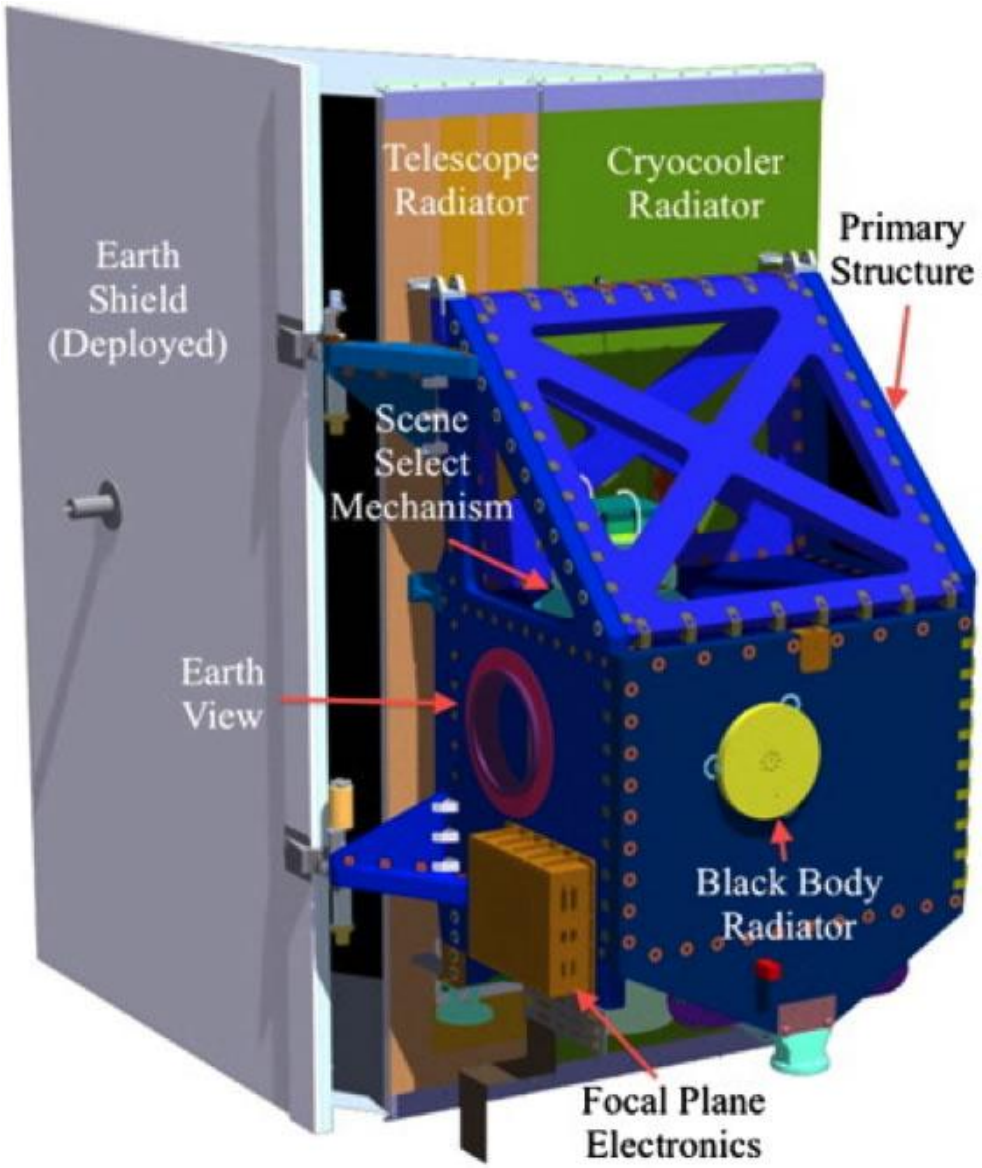

Fig. (2.12): TIRS Instrument with Earth Shield Deployed (ZANTER, 2019).

2.5 Land-use/Land-cover

For monitoring ecological changes and management of natural sources, land cover/land use is used (Hussain et al., 2020) . A distinct concept is applied to the classification of the surface of the earth. Land-cover is defined as visible landscape features and land-use is defined on the landscape as human activity (Weih Jr and White Jr, 2008) (Figure 2.13).

Fig. (2.13) Land Use /Land Cover (Luman, 2021).

Lots of information are available about current land use/land cover and alterations in them. Local planning agencies utilized the detailed information created during ground surveying including obervatation and enumeration (Anderson, 1976).

Owing to some natural reasons and other societal effects, the surface of the planet shifts easily every day. The hottest topics in the remote sensing field and Geographic Information System (GIS) ecosystems have developed over the last few decades from studying the earth's existence

(MohanRajan et al., 2020). For many fields of research, industry and management, Land Use/Land Cover (LULC) data is important. Land cover explains a region on the earth has a certain surface: cotton fields, wetland and concrete roads, for instance. While land use specifies the human activity the land is being used for: commercial, manufacturing and residential land uses, for instance. Some changes in land use that cause immediate land cover conversion and affect air temperature and environment are meteorologically important (Bobrinskaya, 2012). For environmental research and land use/land cover studies, multispectral remote sensing has been used since the beginning of the first earth Resources Technology Satellite in 1972, there has been a notable bustle linked to mapping and tracking environmental change resulting from man-made activities and natural events (Erasu, 2017).

2.6 Estimation of NDVI

Normalized Difference Vegetation Index (NDVI) is utilized to indicate water distrubtion and vegetation health. NDVI is also utilized throughout the global to monitor water distrubtion, drought, estimateagricultural production, predicting fire areas and desert maps. In order to encourage crop scouting, farming apps such as Crop Monitoring incorporate NDVI and provide accuracy to the application of fertilizer and irrigation, among other field treatment activities, at unique growth stages. NDVI is favourable for montoring vegetation throughout the world because it assits in adjusting for alterations in lighting situations (Beg, 2018).

According to Beg (2018), NDVI can be determined as follows:

$$NDVI = \frac{NIR-R}{NIR+R} \quad \text{.....(2.1)}$$

Where :

NIR: near-infrared band (Band 5)

RED: red band (Band 4).

Based on the equation, at a specific point in the image, the density of vegetation (NDVI) equalt to the variation between the intensities of the reflected light of the infrarded and red ranges divided by the sum of the intensities, (Figure 2.14).

Fig. (2.14) NDVI – Normalized Difference Vegetation Index Explained (Dynamics, 2015).

The index is suitable for values ranged from (-1 to 1) most importantly reflecting greens, wheras clouds, snow and water give the negative values, near zero values gained from soil bare and rocks. NDVI function has a very small values (0.1 or less) indicating empety areas of sand, rock or snow. Shrubs and meadows are characterized by moderate values ranged from 0.2 to 0.3, while high values ranged from (0.6 to 0.8) reflect temperate and tropical forests as shown in Figure (2.15). This scale is effectively used by Crop Monitoring to show farmers which parts of their fields at any given moment have thick, moderate, or sparse vegetation (Hashim et al., 2019).

Fig. (2.15) Scale of NDVI values (Bentuk et al. ,2021).

But, NDVI can simply be defined as a measurement to plant health depending on reflection of the plant to the light at specific frequencies (some waves are reflected while others are absorbed). Chlorophyll (a health indicator) deeply absorbs visible light, and the cellular structure of the leaves closely mirrors near-infrared light. If the plant becomes dehydrated, exhausted, tainted with sickness, etc., the spongy layer deteriorates, and the plant absorbs some of the near-infrared light instead of reflecting it. Therefore, by examining how NIR shifts compared to red light, an accurate indication of the presence of chlorophyll that correlates with plant health is provided as shown in Figure (2.16) (Pavlovic et al., 2015).

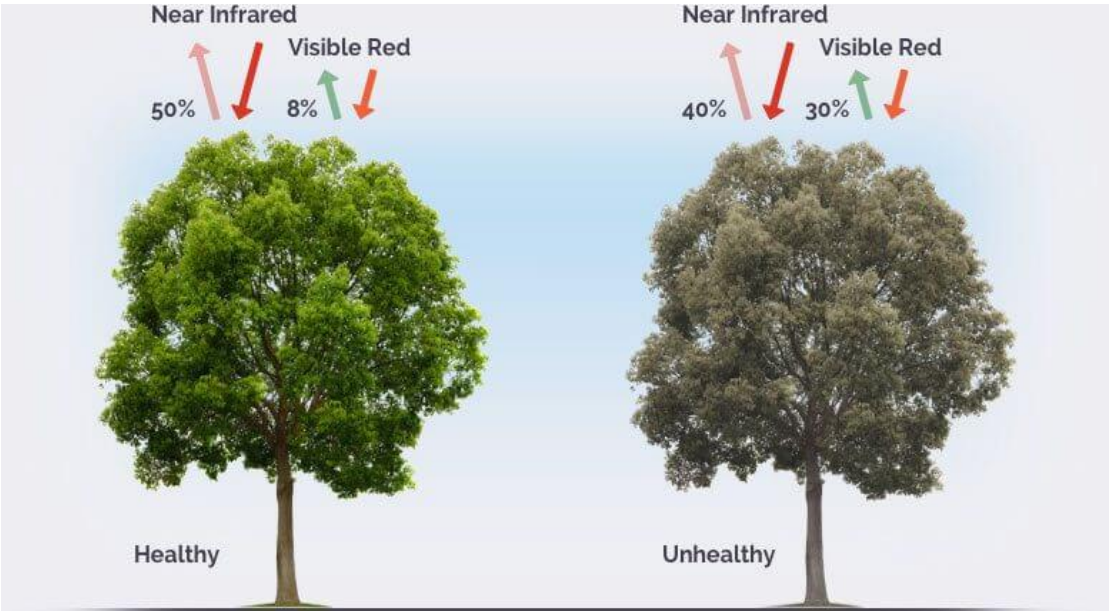

Fig. (2.16) NDVI: Normalized Difference Vegetation Index For Agriculture (Earth Observing System, 2020).

Ground surveys would permit a highly precise classification of Land Use Land Cover (LULC), but they are time-consuming, burdensome and costly, highlighting an obvious and preferred alternative to remote sensing. Medium spatial resolution data, such as that from Landsat, is suitable for regional local scale land cover or vegetation mapping**.** Two sensors are included in Landsat 8, i.e. the Operational Land Imager (OLI) and the Thermal Infrared Sensor (TIRS). OLI collects data at a spatial resolution of 30 m with eight bands located in the electromagnetic spectrum's visible and near-infrared and shortwave infrared regions, and an additional spatial resolution of 15 m in the panchromatic band. Using two bands located in the atmospheric window between 10 and 12 μm, TIRS senses the TIR radiance at a spatial resolution of 100 m (Figure 2.17). To find LST, thermal infrared band10 (TIR) was used (Jeevalakshmi et al., 2017).

2.7 Land Surface Temperature Determination

Among environmental scientists, there is a growing knowledge that remote sensing can and must play a role in providing the data required to evaluate conditions of habitats and control of change on all special scales (Avdan and Jovanovska, 2016) .A change in the urban environment involves a change in the city's microclimate, which directly influences the change in the surface temperature of the earth, it is possible to quantify these changes using field measurements and methods remotely.The earth's far-infrared satellite imagery is used as source data for remote temperature analysis methods (Gosteva et al., 2019) .

The rapid urbanization process has led to many eco-environmental problems, such as dramatic land use changes and urban heat island growth (Jiang and Tian, 2010). Urbanization and climate change are causing changes in the surface temperature of urban land that pose a danger to human health and the environment. The reseacher must be able to observe land surface temperatures inside spatially diverse urban environments to overcome this problem (Naughton and McDonald, 2019). Satellite-based remote sensing technologies are commonly used in rapid urban expansion to investigate urban thermal environments (Yang et al., 2020).

Landsat 8 is the most recently launched Landsat satellite, launched on February 11, 2013. Valuable data and images used in agriculture, education, industry, research, and government are gathered. Two main segments are the Landsat 8 satellite system: the observatory and the ground system. The observatory consists of two earth-observing cameras, the Operational Land Imager (OLI) and the Thermal Infrared Sensor, a spacecraft bus and its payload (TIRS). Land Surface Temperature (LST) is a primary environmental climate indicator derived from Thermal Infrared (TIR) data used in ecological studies and climate analysis in

surface energy balance models. For regions in various parts of the world, study in this field is carried out (Gosteva et al., 2019). Landsat8 bands, wavelength and resolution are as given in Table (2.1) (Anandababu et al., 2018).

Table (2.1): LANDSAT8_OLI and TIRS (Anandababu et al., 2018).

Bands	Wavelength (micrometers)	Resolution (meters)
Band 1 - Ultra Blue (coastal/aerosol)	0.435 - 0.451	30
Band 2 – Blue	0.452 - 0.512	30
Band 3 – Green	0.533 - 0.590	30
Band 4 – Red	0.636 - 0.673	30
Band 5 - Near Infrared (NIR)	0.851 - 0.879	30
Band 6 - Shortwave Infrared (SWIR) 1	1.566 - 1.651	30
Band 7 - Shortwave Infrared (SWIR) 2	2.107 - 2.294	30
Band 8 – Panchromatic	0.503 - 0.676	15
Band 9 – Cirrus	1.363 - 1.384	30
Band 10 - Thermal Infrared (TIRS) 1	10.60 - 11.19	100
Band 11 - Thermal Infrared (TIRS) 2	11.50 - 12.51	100

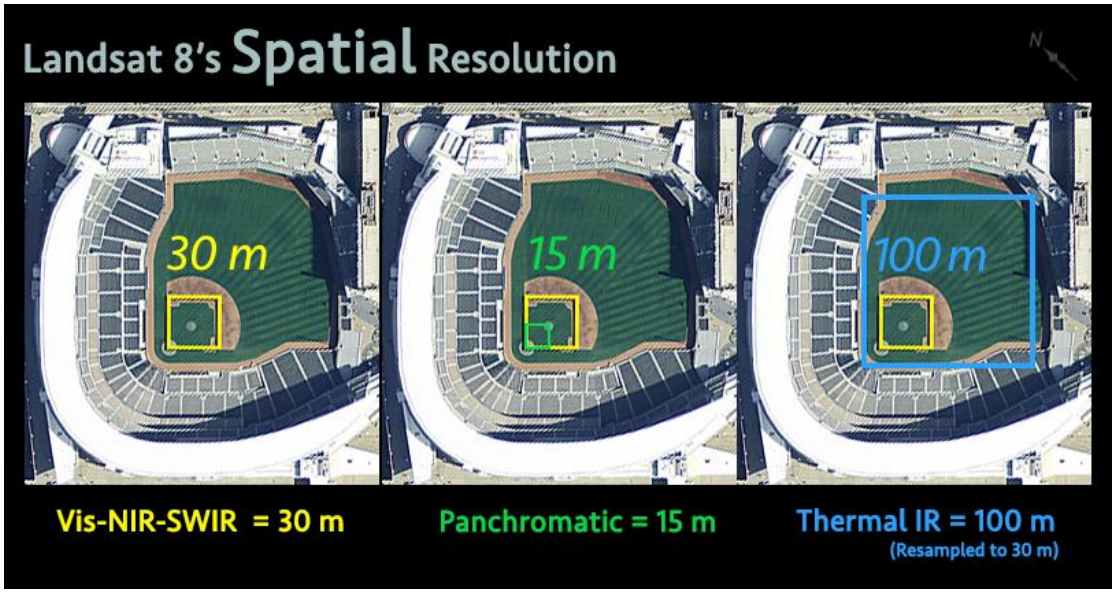

Fig. (2.17): Spatial Resolution (Irons et al., 2013).

Currently, through numerous processes like heat flux and water, land, air, surface wind intensity, and boundary layer turbulence, a strong consensus on the influence of land use/land cover transition on regional climate has been achieved. A common research topic has been the exploration of the mechanism of interaction between LULC change and local climate. Therefore, to better resolve regional environmental concerns and offer a framework for regional planning, the relationship between LST and LUC improvements should be explored (Tan et al., 2020).

2.8 Relationship Between LULC and LST

Surface temperature of land is the movement of the energy in the interaction between the atmosphere and the land surface and between biosphere and land surface. Alteration in LST is intuitive regional climate reaction to climate change occurred around the global and has substantial implications in some fields like hydrology, agricultural, atmosphere, biodiversity and biogeochemistry. LULC is the material and energy

exchange interfacing between the the biosphere and atmosphere and has a direct impact on LST. The change in LULC directly induces changes in the physical properties of the ground surface, influencing a number of regional temperature deciding factors, such as the exchange of radiation, humidity, and water vapor. The transition in LULC also affects the structure of surface attachments, such as the form of vegetation and density of vegetation. Furthermore, the change in LULC has related consequences, such as population shifts and geographic chemical composition changes. This interaction results in alterations in terrestrial carbon reserves and its currents, leading to a number of effects, including changes in greenhouse gas emissions in the atmosphere (Tan et al., 2020).

There is a close relationship between the surface temperature of urban areas and the surface structure and texture. Anthropogenic urban areas have the ability to generate heat that affects the temperature of the air. The LST shift is not only related to the conversion of the land use/land cover form, but also to the presence and increase of the greenhouse effect. Many studies deal with other variables and indexes relevant to LST. LST is linked to various forms of human activities, but only the relationships between the distribution of LST and LULC types have been reported and confirmed so far. The relationship of the LST with vegetation cover and NDVI is especially well known. Others also state that not only the form of vegetation, but also the moisture and density of the soil are susceptible to LST (Bobrinskaya, 2012).

Brightness temperature, especially in studies related to urban development with surface temperature, is the most common way of recovering soil surface temperature. In these studies, Landsat 8 (TIRS) data is commonly used as it meets the criteria for analysis of land

use/land cover transition. In addition, there is a general consensus that there is a negative link between the surface temperature of the soil and NDVI (Saied, 2015).

2.9 Previous related studies

Sameen & Al Kubaisy (2014) utilized photo processed by algorithms and ArcGIS geoprocessing equipment to examine Automatic Surface Temperature Mapping for Al Habbaniyah Lake. By this research, two bands of Landsat 8 were used which are bands 10 and 11. The results of the presented model showed the ability of ArcGIS software with the integration of ENVI tools on automating complex maps production processes with high accuracy and fast. The study also showed that there is a difference between the temperature values that has calculated from band 10 and band 11. The results indicated that thermal bands of Landsat and the model were measurable due to the hot weather at that session. Hence, the temperature values that were created ranged between 52 and 63C◦ were reliable.

Al-Timimi et al. (2014) investigated the land surface temperature for various areas within Iraq utilizing thermal band of ETM+ sensor mounted in the Landsat 7 satellite. To represent land surface temperature, thermal photo were converted into thermatic maps utilizing ERDAS 8.4 software. The estimated land surface temperatures for the following cities in Iraq: Al-Mousl=29.7°C, Taleafer =31.8°C, Al-Ramadi =17°C, Heet =17.8°C, Kerbela =17°C, Al-Hai 20.6°C and Al-Basrah stations =30.2°C. Also, it was indicated that the correlation between the predicated data and the obsereved ones is high with 0.96 variation.

Ilayaraja et al. (2016) utilized open source softwares such as Geographic Resources Analysis Support System (GRASS GIS) and Quantum GIS (QGIS) to examine the land surface temperature of the Chennai Metropolitan Area (CMA). To classify land use/land cover, Landsat (TM5) reflected band such as bands 1-5 & 7 were utilized. Band 6 was utilized to compute the land surface temperature (LST) for the research region. The normal Normalized Difference Vegetation Index (NDVI) was classified utilizing band 3 and 4. Onscreen digitzation with visual interpretation was utilized to conduct land use/land cover pattern in CMA with the use of Survey of India topo sheet (1970). The sensitivity photo was prepared and land use/land cover classes were indicated with emissivity in the range between 0.97 and 0.99. Land surface temperature of 2006 was taken with values ranging from 18.5 to 34.56 ^{0}C and 19.20 to 35.9 ^{0}C for the year 2009.

Ali et al. (2017) compared between Surface Urban Heat Island (SUHI) in Baghdad and Londan due to the variation in the weather, environment and level of urbanization. To charchterize the land surface, supervised classification and spectral indices utilizing Landsat 8 and was retrived from Landsat band 10 with calibration for emissivity by utilizing QGIS. In July, 2013, two Landsats 8 were utilized to ensure that the surface temperatures in both capitals are at the maximum level. The results indicated that the hottest surface type varies in both captials. On the other hand, covering the soil in London increases surface temperature and as consequence increase urban heat island influence, while in Baghdad it decreases under similar conditions.

Jeevalakshmi et al. (2017) utilized thermal infrared sensor and operational line imager of landsat 8 to examine land surface temperature of Chittoor region in India. Estimation for the land surface emissitivty required to apply th method is indicated from a procedure utilize near and visiblr infrared bands. The research concentrated on improving the processing method of ERDAS IMAGINE image utilizing Landsat 8 band 10 data. By comparing the data gained from Automatic Weather Station and that of retrived LST, it was indicated that there is variation in temperature by ±3 ^{0}C. based on the comparsion results, it was indicated that the standard deviation in the first case was 1.02 ^{0}C, while for the second one, it was 1.79 ^{0}C.

Ibrahim (2017) examined the influence of land use alterations on LST in Duhok City. Three Landsat photos were utilized for collecting data which are (two Landsat TM and Landsat OLI_TIRS-8) in 1990, 2000 and 2016. Supervised classification was utilized for calculating land use/cover types, and to create land surface temperature maps, mono- window algorithm was utilized. The results indicated that barren area and bult-up regions are associated with the highest temperatures ranging between 47, 50 and 56 ^{0}C. Meanwhile, water bodies and forest recorded the lowest temperatures ranging between 25, 26 and 29 ^{0}C in the years 1990, 2000 and 2016, respectively. In addition, it was found that the correlation between NDBI and NDBAI is positive with high temperatures, while the correlation between NDVI and NDWI is negative with low temperatures.

Beg (2018) examined the spatial and temporal variation of LST utilizing various dated satellite photos of Landsat 4, 7 and 8 at 037 raw and 168 path in July 1989, April 2000, April 2006 and May 2016 in the city of Bagdad. To determine the LST paramters, eight analysis models builing up utilizing ERDAS 2014 software are adopted while ENVI v.5.3

software was used in the classification of land use/land cover (LULC) types. The results indicated increase in the built-up land by 23% in association with decline in the vegetation by 6% and open space by 26%. In bare regions, the maximum surface temperature indicated ranged from 26 to 41 ^{0}C while it was between 25 to 34 ^{0}C for areas covered by vegetation. Moreover, LST and NDVI have an inverse correlation ranging from -0.5 to -0.81.

Anandababu et al. (2018) investigated land surface temperature utilizing Landsat 8 data and Arc GIS in Hosur area in Krishnagiri in India. Brightness temperature is estimated by using the TIR band 10 and 11, while band 4 and 5 were utilized to create NDVI of the research region. Satellite data in the period from April to Novemeber 2017 was adopted in the research. The results showed that the estimated values of LST in April was 62.82% of the total region, and surface temperature is between 32 to 34 ^{0}C, while in Novemeber, it was 74.52% of the total area and the surface temperature is between 25 and 28 ^{0}C.

Gosteva et al. (2019) examined the LST in the city of Krasnoyarsk for two years from september 2016 to september 2018 utilizing the analysis of Landsat-8 satellite photos. The pixel temperature value is derived from the MOD11L swath product. The results showed that the temperatures have changed by 4 degrees or more over two years, it is clear that this is due to a change in urban development, for example, the construction of new micro districts, shopping mall, and a change in the natural landscape, for example, destruction of forests.

UllAh et al. (2019) investigated the alterations in LULC and LST in the period from 1990 to 2017 in Himalayan areas of Pakistan utilizing data

provided by the Landsat and the Support Vector Mechine (SVM) technique. The results revealed an increase in bare soil and built-up regions by 4.22% and 5.75%, respectively, with decrease in vegetation by 9.88% for the period from 1990 to 2017.

CHAPTER THREE

DATA AND METHODOLGY

CHAPTER THREE

DATA AND METHODOLGY

3.1 Study area description

Babylon Governorate is located in the middle of Iraq and shares internal boundaries with the governorates of Baghdad, Anbar, Kerbala, Najaf, Qadissiya and Wassit, about 100 km to the south of the Iraqi capital, Baghdad. It is situated between latitude 32°5'41" N and 33°7'36" N, and longitude 44°2'43" E and 45°12'11" E, (Figure 3.1).

The total area of Babylon Governorate is 5315 square kilometers, representing 1.3% of the total area of Iraq , the area of Hilla City is 878 square kilometers. It has population of 2,092,998 cpita (2015 census), distributed throughout its main cities (Al-ansari and Chabuk, 2021). The governorate is characterized by comparatively flat and inclining land. The northern part of the Babylon Governorate rises to about 60 m above mean sea level, and the southern part falls to about 20 m above mean sea level. The lands of the Babylon Governorate are fertile, and the Hilla River passes through most cities in the governorate. Babylon Governorate has a typical dry, desert climate with temperatures easily exceeding 40°C in summer. Rainfall is very limited and restricted to the period between November and April months.

Hilla River is one of the most famous river in Iraq and the most important in terms of water resources. Its length is more than 101 km with coordinates 32 ° 3'16 'N and 44 ° 46'29' E. The Euphrates River is the source for the river, which the river originates from the border Northern Babylon Governorate and going to Diwaniyah Governorate.

Hilla River is the only source of water for the purposes of agriculture and drinking, as drinking water projects that extend along the course of the river depend on it, whether in the city center of Hilla or the districts and sub-districts of Babylon Governorate, as well as the river is an important tourist attraction.

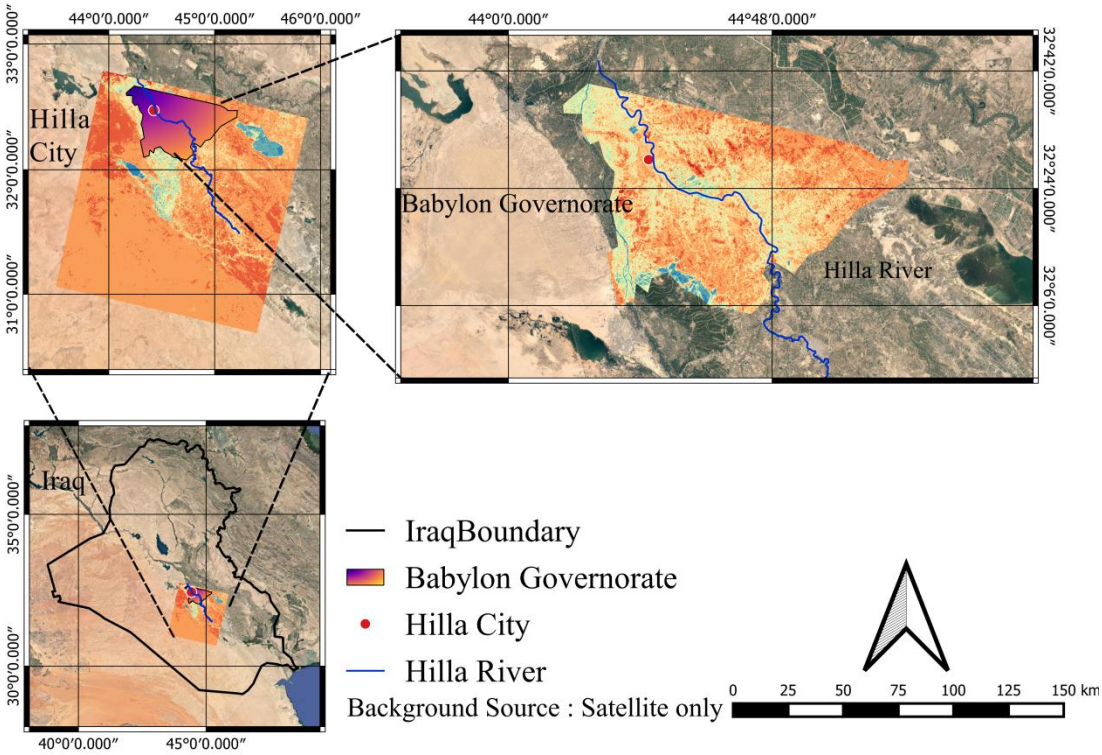

Fig. (3.1): The study area.

3.2 Datasets

Landsat 8 was launched in for the first time in 2013 since the first launching of satellite in 1972. The data provided by landsat satellite is very confidential and credible. All 7 successful missions have multispectral data of high quality around the world and have been utilized for different scientific purposes. Around the world, there are multispectral data of 40 years in the archive of landsat. Hence, it can be considered the landsat data an fundamental source of collecting data for

change detection researches, particularly to indicate alterations in land cover/ land utilization.

Landsat 8 is one of the landsat series of a federal agency that oversees aviation. Geologic Institute of the U.S makes the informtion of Landsat 8 on the market Earth Explorer website freely. The data of Landsat 8 (OLI and TIRS) was provided by the United State Geological Survey and was gained in the form of a photo file tagged geographically. In this research, the TIR band 10 was utilized to examine the Land Surface temperature while for the generation of the research location NDVI, band 4 and 5 were utilized. Satellite data was used for these years in the Hilla region (24/6/2013, 27/6/2014, 30/6/2015, 2/7/2016, 19/6/2017, 22/6/2018, 25/6/2019 and 27/6/2020).

For assessing improvements in the regimes of LULC, Emissivity, NDVI and LST and to generate qualified and precise results, the following characteristics were gathered: (I) cloud-free images, (II) daytime dry-season data, approximate 10% of the whole landsat scene cloud was covered during the entire period. A pretreatment method was applied before LULC classification to eliminate the atmospheric influences from Landsat photos for LULC (Dissanayake et al., 2019).

In addition, the summer season in which the atmosphere was not considerably affected by the absorption and dispersion and free of clouds were utilized in this research these senses, used in this work, were selected from the USGS website. The reference information for LULC indication, Google earth photos with high resolution were utilized. As remote sensing and GIS software, QGIS 3.10 was used to evaluate the data and gain the last results during the whole analysis. All important data

needed like rescaling factor values, thermal constants, etc., are provided in the metadata file supplied with each sense, (Table 3.1).

Table (3.1): Details of Landsat-8 senses used in this study.

Landsat-8 Sense Identifier	Sensor	Path/Row	Acquisition Date	Center Latitude	Center Longitude	Bands (used)
LC81680382013175LGN01	OLI/TIRS	168/38	2013/06/24	31°44'30.98"N	44°41'36.42"E	2-7 and 10
LC81680382014178LGN01			2014/06/27	31°44'31.24"N	44°42'16.13"E	
LC81680382015181LGN02			2015/06/30	31°44'30.95"N	44°41'35.34"E	
LC81680382015184LGN01			2016/07/02	31°44'31.09"N	44°41'35.05"E	
LC81680382017170LGN00			2017/06/19	31°44'32.28"N	44°41'09.60"E	
LC81680382018173LGN00			2018/06/22	31°44'31.67"N	44°41'59.35"E	
LC81680382019176LGN00			2019/06/25	31°44'31.67"N	44°40'57.58"E	
LC81680382020179LGN00			2020/06/27	31°44'32.64"N	44°41'13.24"E	

3.3 Methodology

In this research, the brightness temperature was determined based on Landsat 8 band 10, while band 4 and 5 were utilized to calculate NDVI. The flowchart in Figure (3.2) shows the entire methodology applied in this study.

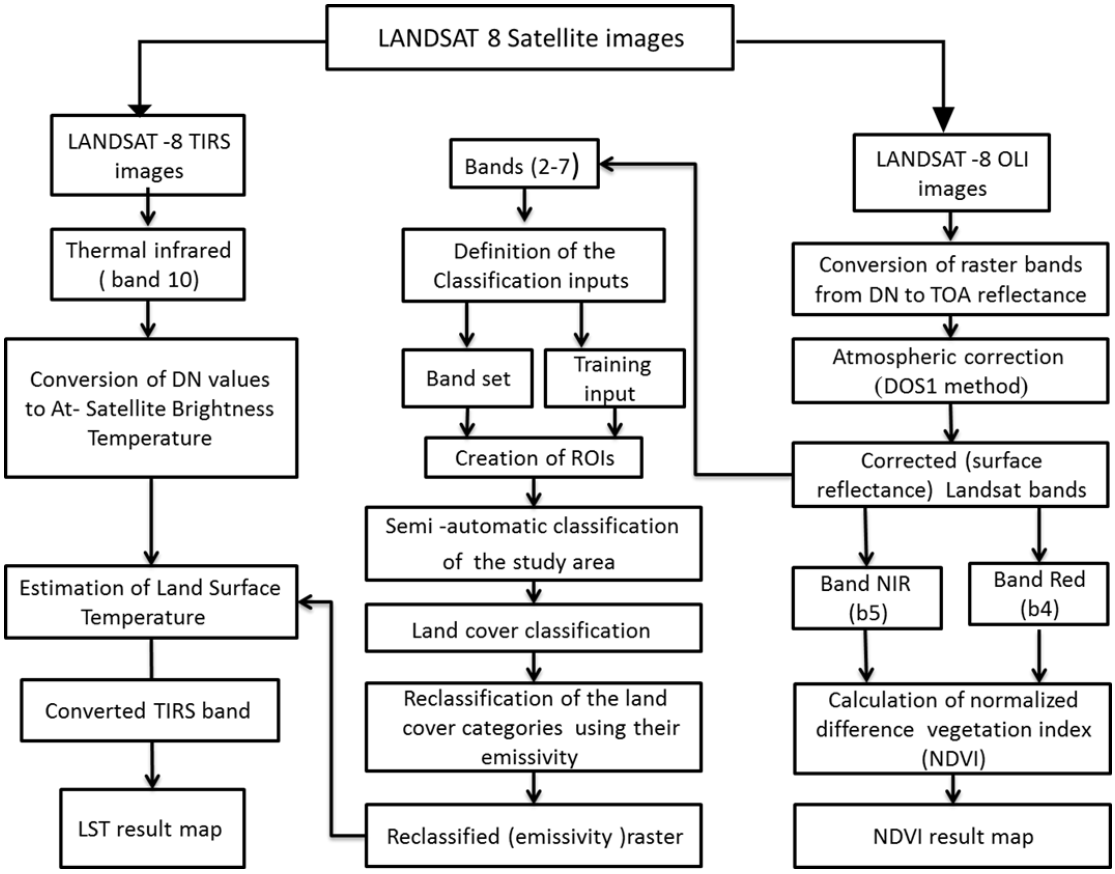

Fig. (3.2): Flowchart of the methodology.

Landsat 8 (OLI and TIRS) data from 2013 to 2020 was selected. For the same time, images on July with an interval of 8 years were assessed ellaborating summer situations. The digital numbers (DN) of TIRS and OLI bands were transformed to spectral radiance and Top Of Atmosphere (TOA) planetary reflecting for the purpose of pre-processing the satelliate photos. Band 10 is used to determine the temperature of brightness in this analysis and bands 4 and 5 are used to determine NDVI.

For these images, steps were made before performaing classification which are image adujstment and layer stacking as shown in the below workflow diagram. The stacking step of the layer requires the production of color images. Each band has specific wavelengths in a separate image that are similar to black and white digital photography.

The bands from various wavelengths should be mixed together to create the color picture (Band set). Utilizing three bands which are Band 2-Near Infra-red, Band3-Green and Band 4-Red with the utilization of the standard False Colour Composite (FCC) combination. Combaing these bands is considered very logical and beneficial in supervised classification procedures using Landsat 8 images, (Figure 3.3).

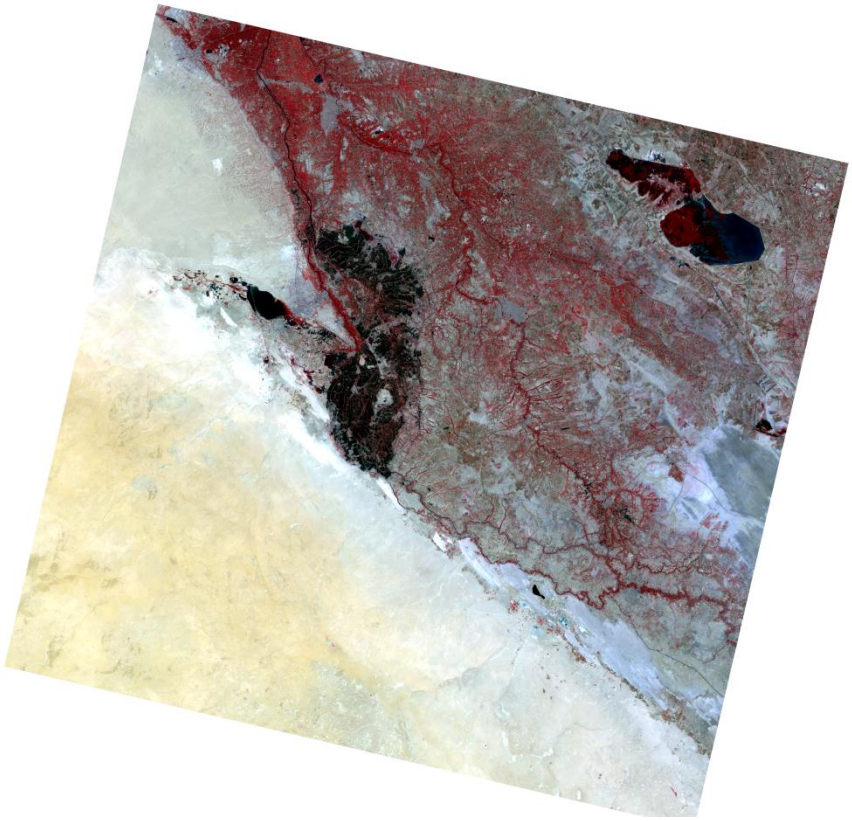

Fig. (3.3): Virtual band set.

According to the settings defined in Landsat 8; the DOS1 correction algorthim has been applied. Bands from 2 to 7 will be converted to reflectance and band 10 will be converted to At-Satellite Brightness Temperature by using SCP plugin in QGIS 3.10 (Congedo, 2016), (Figure 3.4).

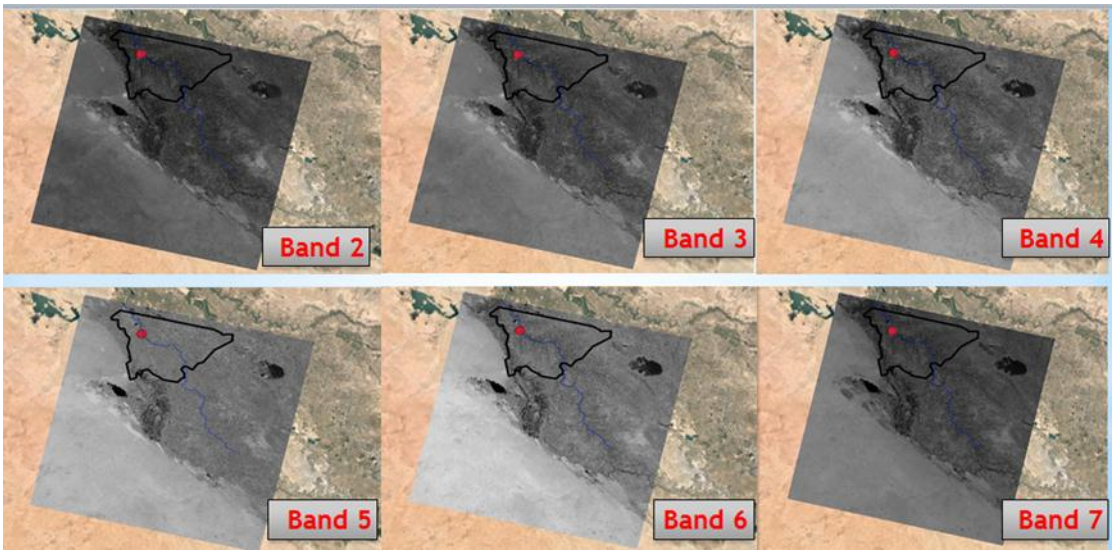

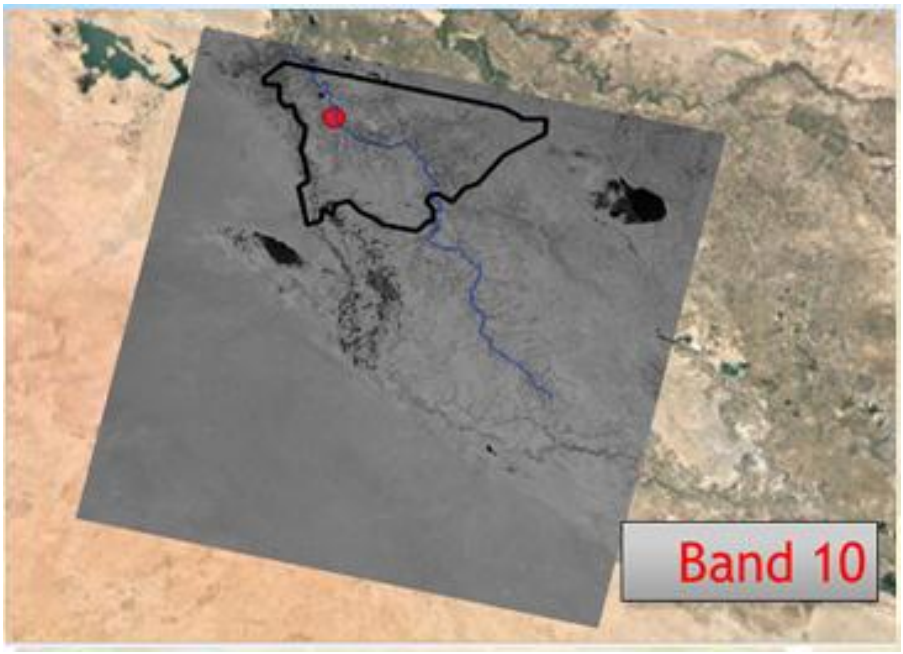

Fig. (3.4): Reflectance and brightness temperature.

Land cover has been classified, which will be used later for the creation of the emissivity raster as shown in the Table (3.2 and 3.3).

Table (3.2): Land cover classes

Macroclass name	Macroclass ID
Water	1
Vegetation	2
Buildings & bare lands	3

Reclassifying Land Cover Classification to Emissivity Values, the reclassification of the classification raster has been achieved by utilizing the land surface emissivity values as given in Figure (3.5).

In term of classes for the land cover, the emissivity (e) is given in Table (3.3) (Congedo, 2016).

Table (3.3): Emissivity values for each land coverage classes

Land Surface class	Emissivity
Water	0.98
Vegetation	0.98
Built up & Bare lands	0.93

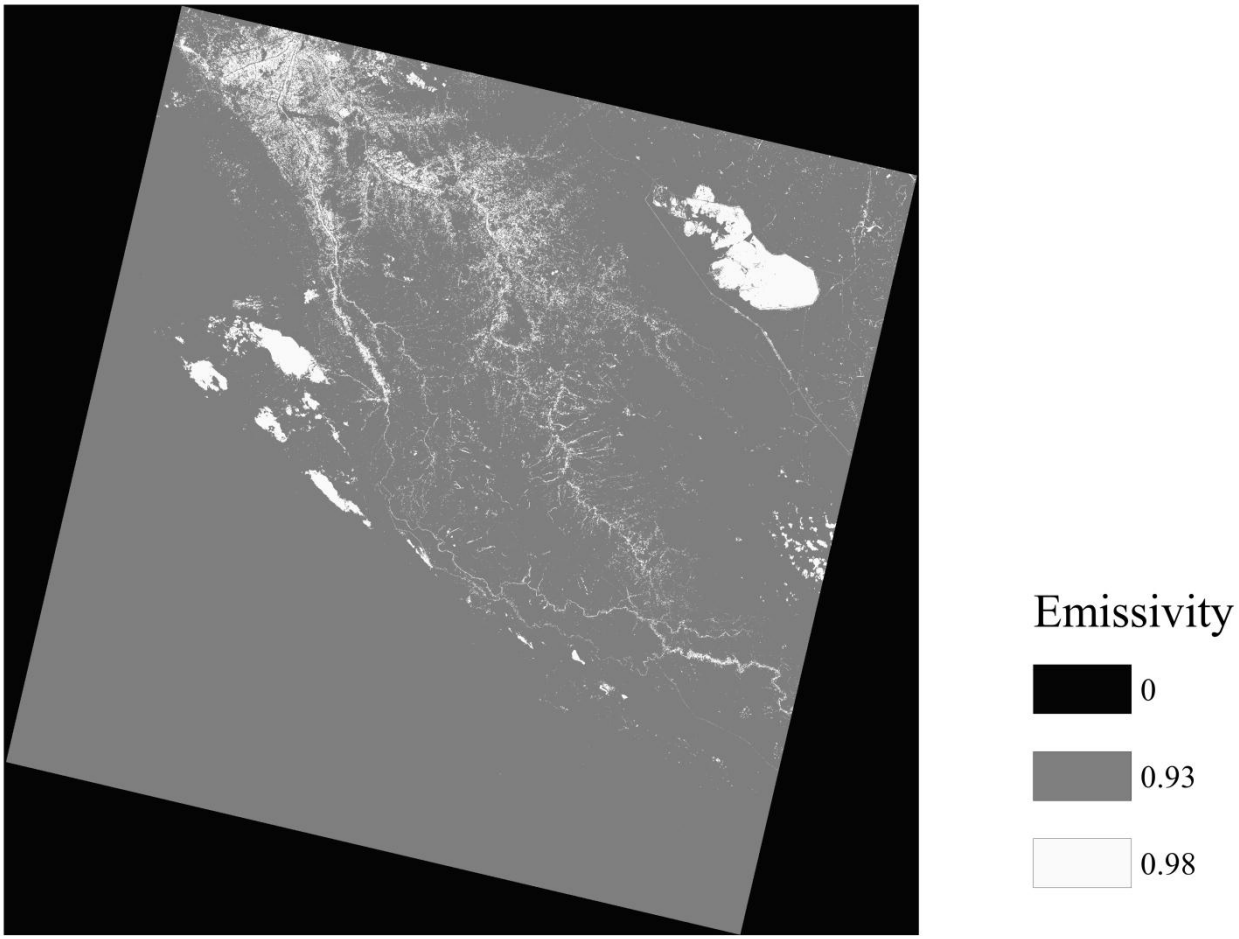

Fig. (3.5): Emissivity values.

NDVI was calculated utilizing band NIR (4) and band Red (5) by equation using Raster Calculator in QGIS 3.10 .

Analysising the alterations in LU–LC types and temperature and in this research area, required applying the NDVI for measuring the correlation with derived LST.

To create the tables, graphs, charts and figures, Microsoft Excel and Matlab software were utilized.

3.4 Estimation of LST

The images were converted to reflectance in QGIS as follows:

a) Radiance at the Sensor's Aperture

The below equation is used for Landsat 1 G Level product with the purpose of restoring spectral radiance values from DNs: Landsat images, scaled prior to output, are supplied in radiance. (L_λ , in terms of W /(m^2 x µm x sr)) is indicated through (Congedo, 2016):

$$L\lambda = AL + Qcal * ML \quad \ldots\ldots\ldots\ldots\ldots(3.1)$$

where:

AL= factor of band specific additive rescaling obtained from meta-data of Landsat

Q calorie = typical pixel that has been quantized and calibrated numbers

ML: factor at band specific multi-plicative rescaling obtained also from metadata of Landsat metadata.

(Jeevalakshmi et al., 2017)indicated the method of producing At-Satellite Brightness Temperature to be used in the thermal bands by converting DN.

b) Top Of Atmosphere (TOA) Reflectance

The variability between senses could be minimized by utilizing solar irradiance, transforming radiance photos to reflectance of TOA (atmospheric reflectance and joint surface). The TOA reflectance is the reflected power measured as a ratio of the total one which is determined from the equation below (Beg, 2018) :

$$\rho_\rho = (d^2 * \pi * L\lambda) / (\cos\theta s * ESUN\lambda) \ldots(3.2)$$

where:

$L\lambda$ is indicated as spectral radiance at the amount of light that is emitted.

d is the space between the sun and earth measured in items of astronomy.

$ESUN\lambda$ is solar orbital spaceflight in its mean value

θs is the same as maximum position of the sun

It should be noted that band-specific rescaling factors are given for Landsat 8 images permitting converting DN directly to TOA reflectance.

c) Surface Reflectance determination

Reflectance on the ground is calculated, it is crucial to consider the influences of the atmosphere; i.e. reflectance disturbances that vary from the wavelength. The land surface reflectance (ρ) is indicated by (Moran et al ,. 1992) as following:

$$\rho = [\pi * d^2 * (L\lambda - Lp)]/[E_{down} + Tv * Tz * ((\cos\theta s * ESUN\lambda * Tz))] \quad \text{……………………………………………(3.3)}$$

where:

Tv: in the view direction representing the permeability of the air

Tz: inside that illustration path representing the permeability of the air

E_{down}: down welling diffuse irradiance.

Lp: radiance of the path

d) Converting to temperature

This topic offers basic details on converting SCP to Land Surface Temperature Estimation and At-Satellite Brightness Temperature.

e) Converting to At-Satellite Brightness Temperature

For thermal bands, the conversion of DN to At-Satellite Brightness Temperature is given by (Jeevalakshmi et al., 2017):

$$TB = K2 / \ln [(K1 / L\lambda /) + 1] \ldots\ldots\ldots\ldots (3.4)$$

where:

K1 is constant of thermal conversion of band-specific measured by (wts/meter squared x ster xμm).

K2 is constant of thermal conversion of band-specific measured in $\overset{o}{K}$.

L λ is the Spectra Radiant at the Device's Window in terms of K1.

In Landsat 8, the values of K1and K2 are given in photo metadata file.

f) Establishment of LST

Land Surface Temperature is estimated by many researches. Ilayaraja et al. (2016) and Weng et al. (2004) determined Land Surface Temperature from Satellite Brightness Temperature as following:

$$T = TB / [1 + (\lambda * TB / c2) * \ln(e)] \ldots\ldots (3.5)$$

The resulting temperature is calculated in Kelvin, after which the researcher convert it to a temperature in Celsius according to the following equation:

$$LST\ (C°) = LST\ (K°) - 273 \ldots\ldots\ldots\ldots (3.6)$$

3.5 NDVI determination

After converting DN to reflectance, (NDVI) was measured for the near infrared and red (NIR) from the equation below (Ibrahim, 2017):

$$NDVI = \frac{NIR - RED}{NIR + RED} \ldots\ldots\ldots\ldots\ldots\ldots\ldots\ldots (3.7)$$

Where :

NIR – represents the near-infrared band (Band 5) .

RED – represents the red band (Band 4).

CHAPTER FOUR

RESULTS AND DISCUSSION

CHAPTER FOUR

RESULTS AND DISCUSSION

4.1 classified land cover types for Babylon Governorate from 2013 to 2020

Landsat 8 Operational Land Imager (OLI) spectral bands is incorporated in the range of 0.45 µm (blue/visible) to 2.29 µm (infrared/nonvisible) with two Thermal Infrared Sensor (TIRS) bands. OLI has a high horizontal resolution that enables the frequent to sweep of the satellite over the same corridor and be visible at 16 days intervals. This is available freely at the USGS. During the hot periods (in June and July) in Babylon Governorate, eight Landsat photos were needed.

The description of types of land cover for Babylon Governorate from 2013 to 2020 is shown in Figure (4.1). As shown in Table (4.1), the LST statistics are summarized according to LULC showing that the lowest average ranged from 35.4 to 39 ^{o}C and covered area of 0.6 to 1.6 % of study area. This is followed by vegetation area represented by garden, green land, and cropland with an average of LST ranging between 39.3 and 45 ^{0}C. The highest LST was found in barren area which are roads, residential area, parks and bare area with values ranging between 47 and 54 ^{0}C. This barren land occupies approximate 76.1% to 89% of the overall land of the research land (3560.5 km^{2}), while the vegetation occupies 10.2% to 22.6% of the land extending along Hilla River.

The LST determined from Landsat-8 Level-1 photograph was taken on July from 2013 to 2020. In fact, the increase in the barren areas

particularly in residential lands would result in increase in LSTs and in the summer period, it leads to warmer local climate.

Each type of land cover represents a specific class of LST interval, and in this case, the relationship between the dependent and independent parameters is valid. Therefore, the detection of LST patterns utilizing kinds of land cover is a viable method for investigating UHI's spatial variance.

Summarization for the land indicated for land use/land cover classes of the selected region derived from the classification results is given in Table (4.1). The dominant kind of land cover during the whole period of eight years is open area covering about 86.4%, 79.5%, 89%, 81.4%, 88.1%, 81.1%, 76.1%, and 84% of the total land in 2013, 3014, 2015, 2016, 2017, 2018 2019, and 2020, respectively. The second greatest land utilization kind is agriculture occupying about 12.8% of the total area in 2013, 19% in 2014, 10.2% in 2015, 17.8% in 2016, 11.3% in 2017, 16.6% in 2018, 22.6% in 2019, and 15 in 2020. The lowest land cover is water taking about 1.5% of the total area.

Table (4.1): Statistical parameters of LST of various LULC classes for Babylon Governorate from 2013 to 2020.

2013			
Land use/ land cover type	Area (km^2)	% area	Avg. T. (^oc)
Water	54.2	1.5	35.4
Vegetation	430	12.8	41.6
Buildings & Bare lands	3076.3	86.4	50.6

2014			
Water	53.3	1.5	36
Vegetation	677.2	19	43.4
Buildings & Bare lands	2830	79.5	52.7
2015			
Water	27	0.8	35
Vegetation	368	10.2	41
Buildings & Bare lands	3166	89	49
2016			
Water	28.2	0.8	35.4
Vegetation	635	17.8	42
Buildings & Bare lands	2897.3	81.4	50
2017			
Water	22	0.6	37.4
Vegetation	403	11.3	44
Buildings & Bare lands	3135.3	88.1	53
2018			
Water	58	1.6	39
Vegetation	589.4	16.6	39.3
Buildings & Bare lands	2913.3	81.1	47
2019			
Water	47.5	1.3	38
Vegetation	804.5	22.6	45

Buildings & Bare lands	2708.5	76.1	54
2020			
Water	36	1	36.6
Vegetation	530.6	15	44
Buildings & Bare lands	2994	84	53

The area of land use/land cover given in Table (4.1) is represented graphically in Figure (4.1), also. The figure shows that the principle LULC kind is open area, water covers small fracture of the whole land then vegetation then buildings & bare lands. There is a significant increase in the buildings & bare lands in 2015, while opposite trend can be seen for vegetation. Water has observed slight changes during the study period.

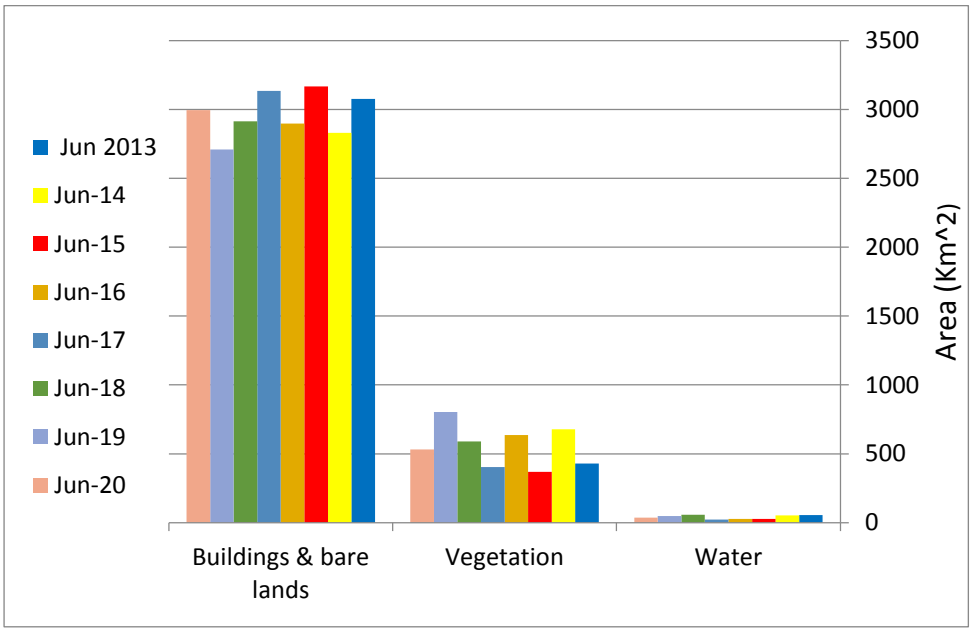

Fig. (4.1): Land use land cover areas in different years.

To gain a comprehensive thought about the relationship between land cover and LST, it is necessary to investigate the thermal signature of each

type of LULC. Therefore, a comparison of LULC and LST was conducted. By combining all consistent pixels of a given LULC category, the mean temperature of land use cover type was determined. In the rock outcrops, the results showed the highest LST, while the lowest was registered for water bodies. In vegetated regions and water bodies, cold anchor pixels were found, while the warmest were rock, built-up areas or bare soils. The pixel surface temperature varied from 47 Cº to 54 Cº.

Over the entire study period, buildings and bare lands were the predominant land use type (89%) during 2015 and reached to only 76.1% in 2019 (Figure 4.1 and Table 4.1). Remarkable decrease in the vegetation area occurs in urban area. Water coverage decreases gradually from 1.5% in 2013 to 1% in 2020. In term of temperature, water temperature is lower than that of other kinds of lands. Thermal processes in urban regions are changed by increasing impervious surface and lowering vegetative canopy coverage, thereby producing 8-9 ° C warmer temperature regimes compared to rural areas.

The analysis of the LSTs and LULC relationship shows that the spatial distribution of LSTs in the study area is dominated by two key land use/land cover, i.e. barren lands (built up area and bare lands) and density of vegetation cover. During the study period, the vegetation cover shows a temperature difference of 8-9 Cº less than the barren lands, suggesting their positive effect on the reduction of LST in the study region.

An successful method for retrieving LST maps for wide areas is satellite imagery. Forms of land cover and the materials used as surface structure directly affect LST. Therefore, it should be considered not to use

materials that absorb too much of the sun's radiation for urban heat island effect in city centers.

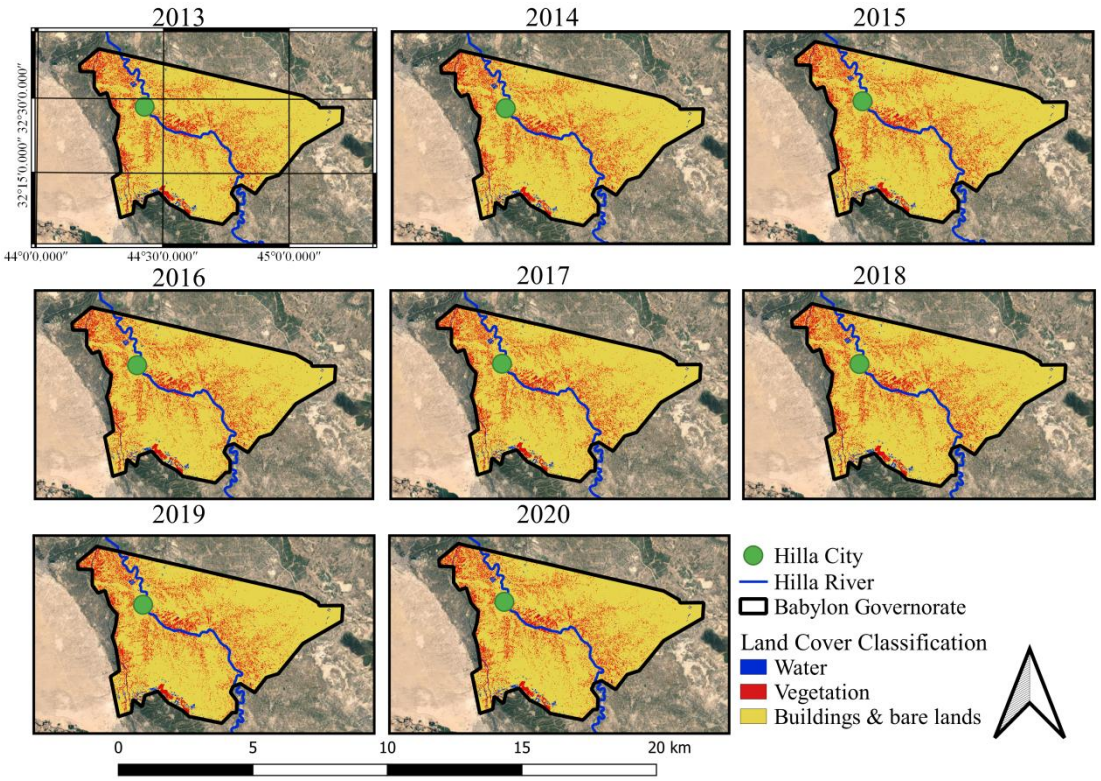

Fig. (4.2): Land cover spatial-temporal variation for Babylon Governorate from 2013 to 2020 (Appendix C).

Figure (4.2) shows classification maps for the Babylon Governorate from 2013 to 2020, where the blue color represents water, and the red color represents plants, while buildings and arid lands are represented in yellow.

(Mahmou et al., 2021) examines how the land surface temperature (LST) is influenced by land cover and watch the spatial distribution pattern of LST in the city of Karbala, Iraq. To evaluate the LST and the normalized difference vegetation index (NDVI) in 2013, 2015 and 2017, Landsat 8-OLI photographs were utilized. The results indicated that there is linear correlation between the increase in LST and the increase in the built-up land. It was also found that vegetation coverage lowers the LST value.

4.1.1 Accuracy assessment for Land Cover Classification

A Spectral Signature Plot was made for the years from 2013 to 2020 to examine how accurate the land cover classification is for those years by QGIS program using the SCP tool.

Several functions are available in the window Spectral Signature Plot for presenting spectral signature values as a function of wavelength (defined in the Band set). The SCP dock may be used to add signatures to the Spectral Signature Plot.

Land cover spectral examination with QGIS 3.10 and Semi-Automatic Classification Plugin (SCP) occurred by these steps from SCP tool to band set tool , open the Band set; (Bands 2-7) and choose Landsat 8 OLI bands 2, 3, 4, 5, 6, and 7 and then make training input, created with SCP, open a training input file, new file: generate an empty training input file (scp); the vector component of the training input is imported in QGIS; when the training input file is saved, a backup file is produced (a file.scp.backup in the same directory as the file.scp).Finally from SCP tool to post processing to class signature select the layer of Land cover classification and choose the output file and click run .

The spectral signatures are created by combining the bands in the picture. Because each substance interacts differently with electromagnetic radiation, it is characterized as a distinct response pattern. A categorization is based on identifying portions of the electromagnetic spectrum where the nature of the interaction varies for the elements inside the picture as shown in Figure (4.3).

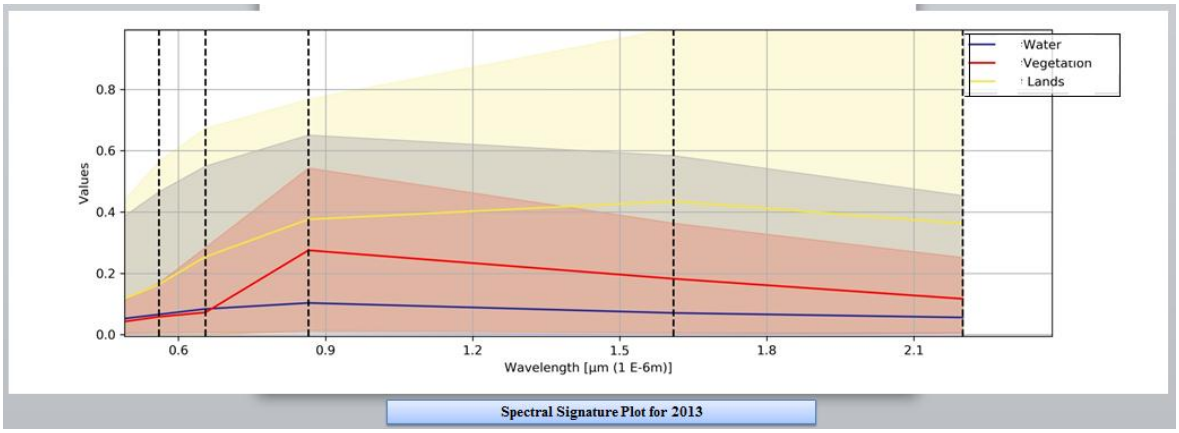

Spectral Signature Plot for 2013

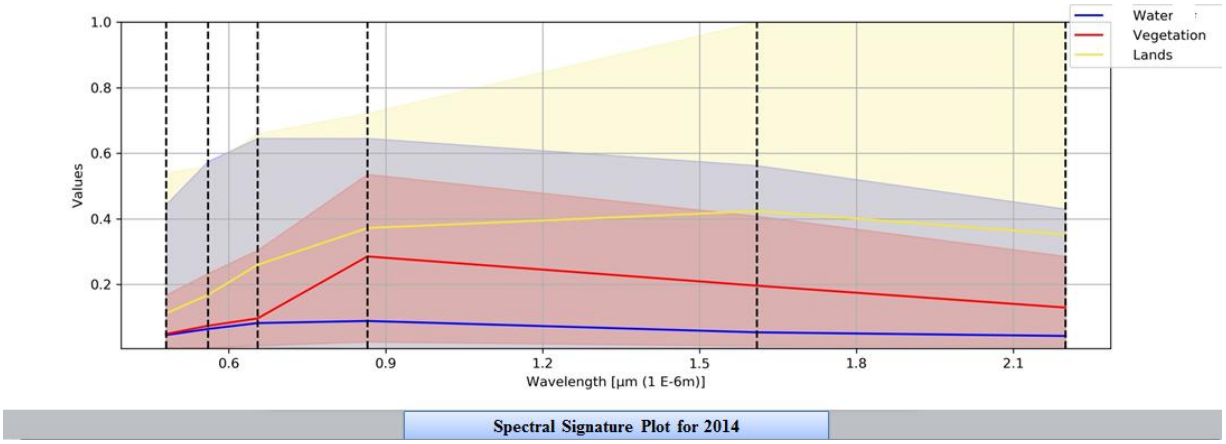

Spectral Signature Plot for 2014

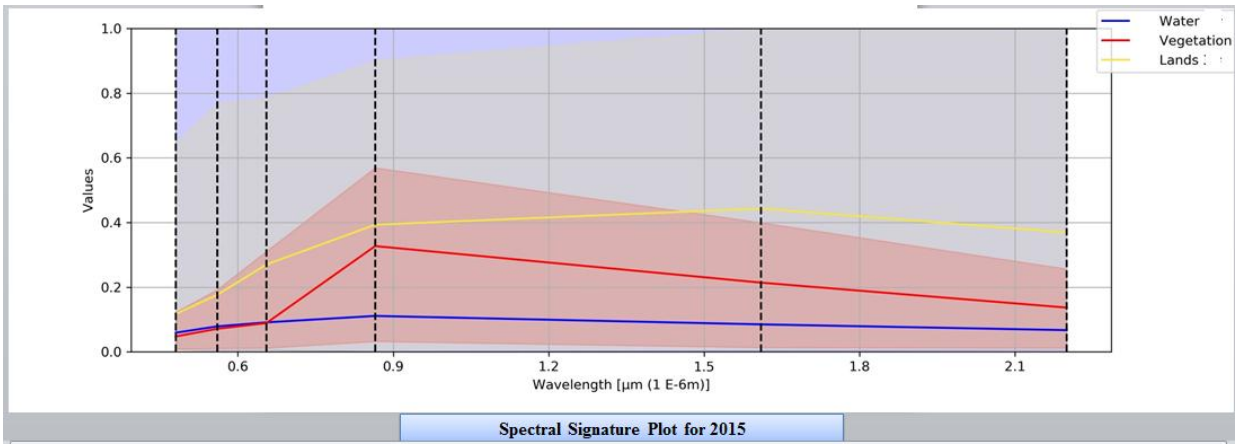

Spectral Signature Plot for 2015

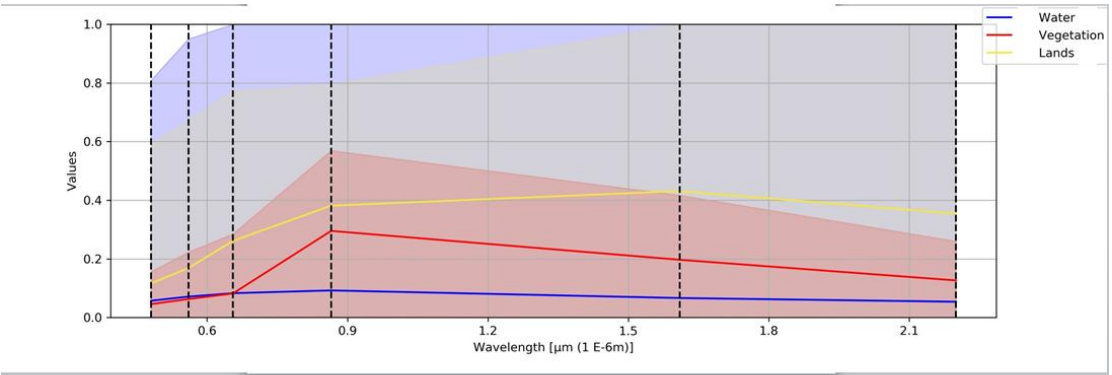

Spectral Signature Plot for 2016

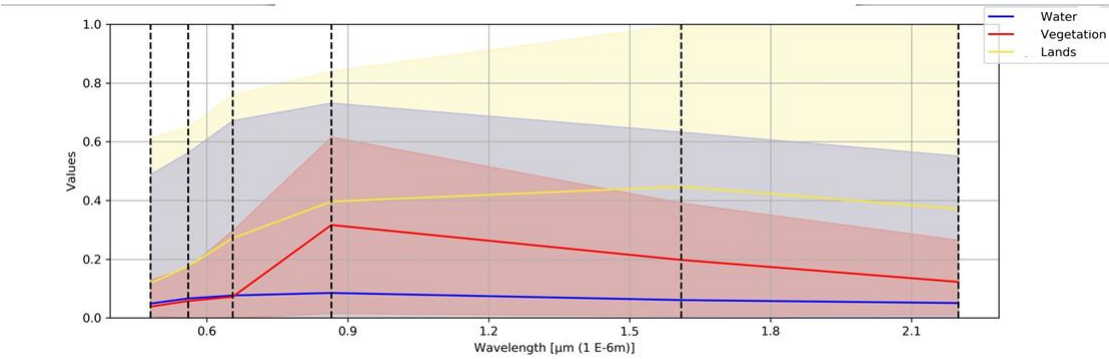

Spectral Signature Plot for 2017

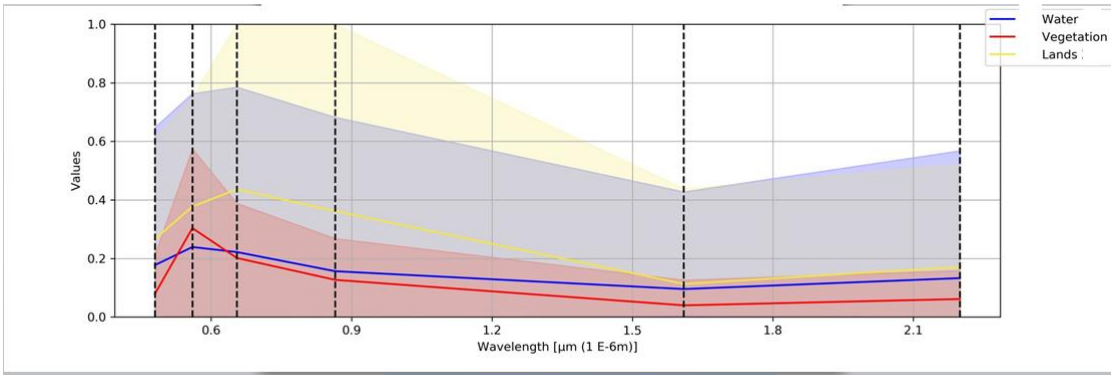

Spectral Signature Plot for 2018

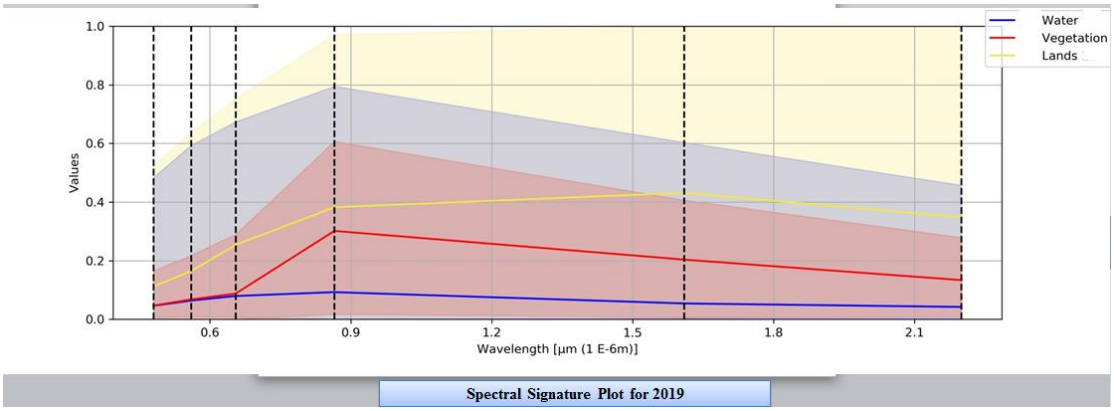

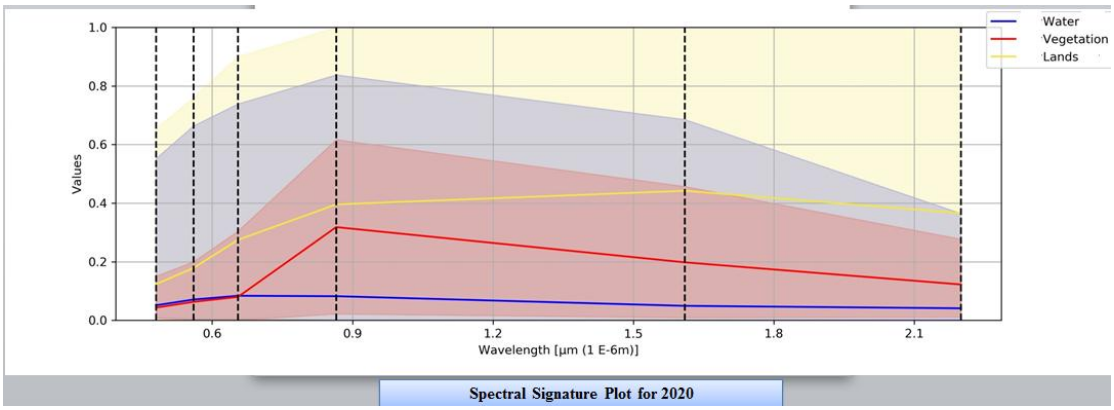

Fig. (4.3): Land cover spectral signatures for years from 2013 to 2020.

Spectral signature is indicated a function of wavelength as the reflectance. Classification algorithms employ spectral fingerprints to label the pixels in a picture. The spectral fingerprints of several materials can be quite similar (water, lands and vegetation cover).

4.1.2 Water's spectral signature and its behavior

The quantity of reflected radiation is detected as a function of wavelength responding to the spectral signature, declining towards the infrared. The behavior is characteristic of lacustrine waters, since the reflectance at any wavelength falls as the depth of the bodies of water increases as shown in Figure (4.4).

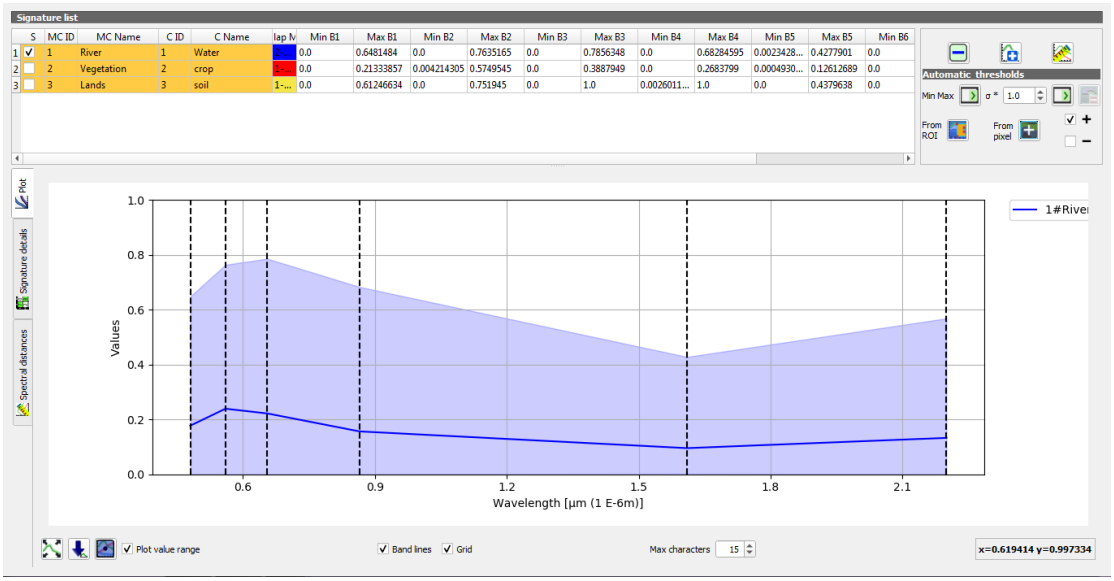

Fig. (4.4):Land cover spectral signature for water.

4.1.3 Spectral signature of vegetation behavior

Vegetation is a resource that depends on lots of properties such as types of species to be assessed (trunks, stems, leaves and others), particularly since the coverage has been subjected to different environmental alterations such as low reflectance in the visible with rise in green color because of chlorophyll, which is a property of leaves. Because plants have a limited absorption of energy, reflectance rises in the near infrared. Because the water in the plant absorbs the energy, there is a large drop along the wavelengths in the mid-infrared as shown in Figure (4.5).

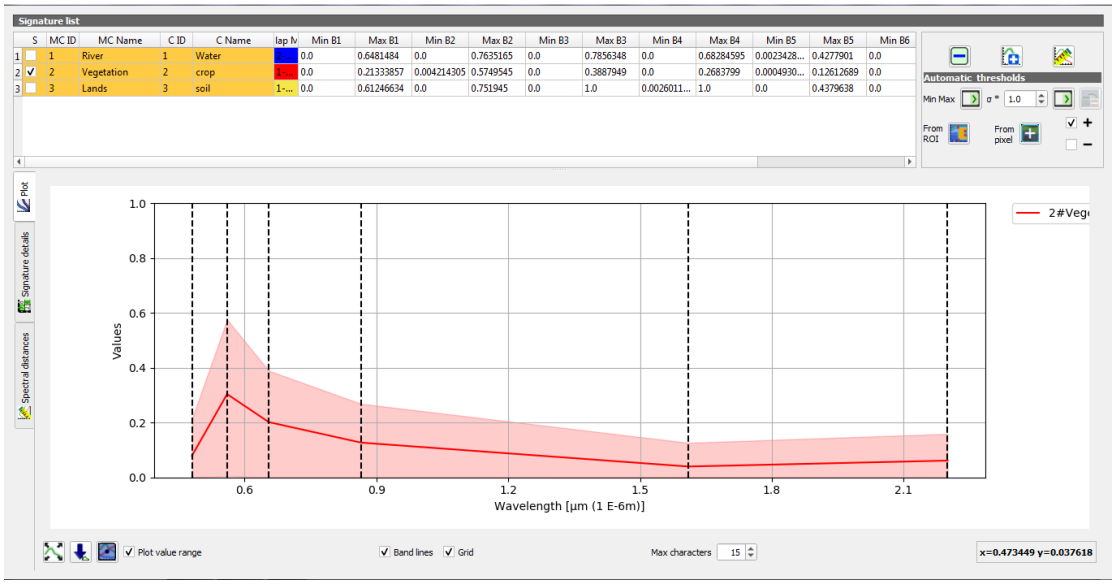

Fig. (4.5): Land cover spectral signature for vegetation.

4.1.4 The spectral signature of dry soils and its behavior

The comparison between the spectral signature of crop covering and the spectral signature of uncultivated (dry) soils showed that there is no longer possible to proof the summit in the green of the visible area, and because plants is no longer capable of absorbing water, reflectance along wavelength increases as shown in Figure (4.6).

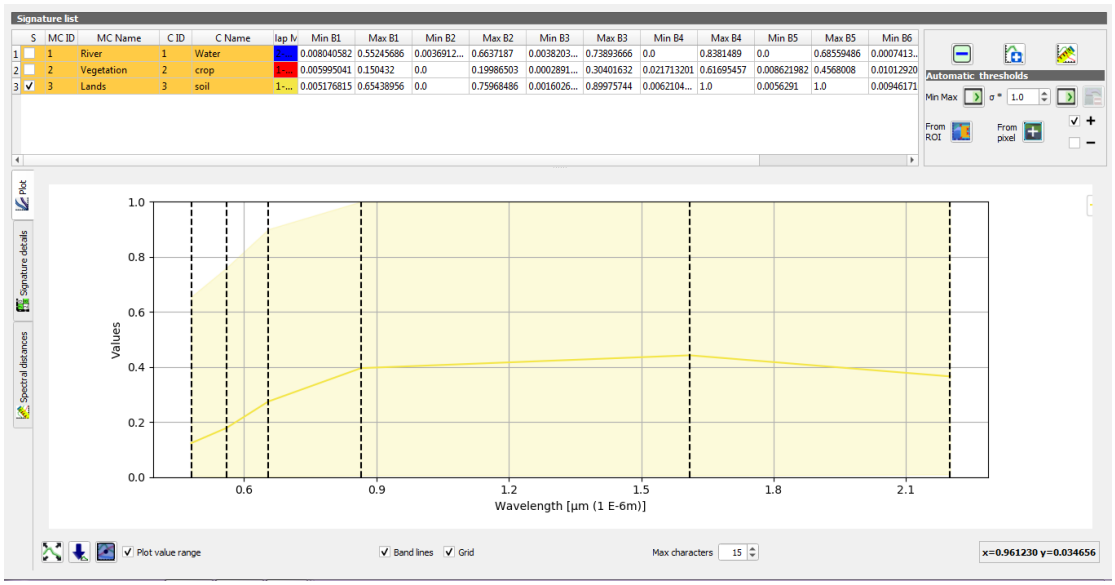

Fig. (4.6): Land cover spectral signature for soil.

4.2 Spatial pattern of LST and NDVI with LULC indices

4.2.1 Land Surface Temperature

The result of the study is creating a map of the absolute value of LST of the research area. The spatial – temporal variations of LSTs are illustrated in distribution maps (Figure 4.7), during the periods (2013-2020). The results extracted from Landsat - 8 image Level 1are processed using QGIS (3.10).The results show that the lowest temperature about 30 ^{o}C , followed by mean ranging from 45 to 51 ^{o}C, while the highest LST was about 62 ^{o}C .

The highest temperature was found in the years 2013, 2014, 2017, 2019 and 2020, while the years 2015, 2016 and 2018 recorded a lower temperature. The sudden fall in the maximum temperature during 2015 ,2016 and 2018 can be considered rational because in the past, some days of the years are hotter in spite of the effect of urban warming phenomena resulted from increase in the urbanization over time (Thapa , 2017).

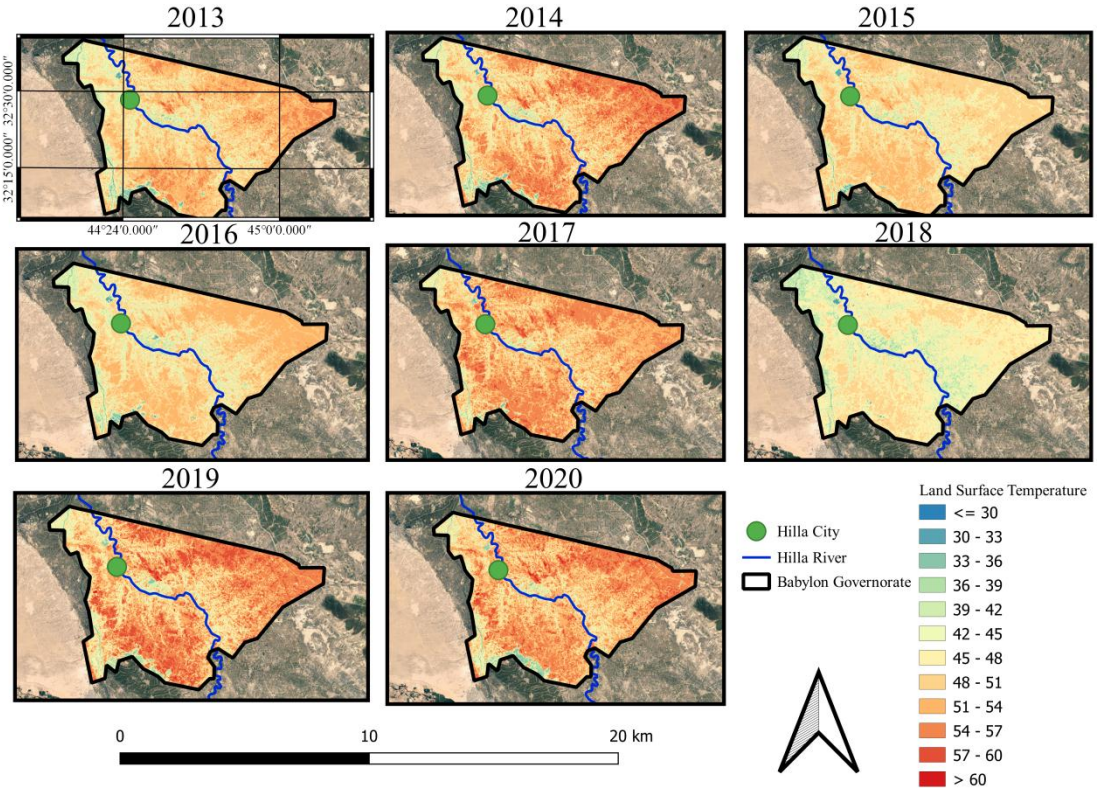

Fig. (4.7): LSTs spatial-temporal variation for Babylon Governorate from 2013 to 2020 (Appendix B).

The analysis of LST pattern showed that in all maps, the blue tone refers to low temperature and stands for the water coverage. High LST indicated by red color represents the impervious surface of the buildings & bare soil. The yellow area represents the vegetation land. The QGIS Histogram Plugin used to investigate the distribution of numerical values for raster layer (Appendix A).

The analysis of spatial pattern of LST in the research region shows that the spatial pattern of LST in the research field, a spatial statistical approach was required. A spatial autocorrelation analysis was then carried out using the SCP method in QGIS 3.10 for years from (2013 to 2020). The SCP outcomes characterize the spatial pattern of the LST for the various seasons and the study area for all the years. The spatial autocorrelation of LST was calculated in the current research by simultaneously considering both the position of the LST points and the

point's attribute (value) to determine whether the expressed pattern is clustered, scattered, or random.

Figure (4.8) indicates the mean LST within the land use land cover (LULC) class in the research zone. The lowest mean LST in all eight years was recorded in water LULC category which are (35.4 C^{o} in 2013, 36 in 2014, 35 in 2015, 35.4 in 2016 , 37.4 in 2017, 39 in 2018, 38 in 2019 and 36.6 in 2020). The maximum mean LST in the selected period is gained in the vegetation area (41.6 in 2013, 43.4 in 2014, 41 in 2015 ,42 in 2016, 44 in 2017, 39.3 in 2018, 45 in 2019 and 44 in 2020). After vegetation, buildings & bare lands got the highest mean LST values (50.6 in 2013, 52.7in 2014, 49 in 2015 ,50 in 2016, 53 in 2017, 47 in 2018, 54 in 2019 and 53 in 2020). Hence, low mean LST values is in water, the medium is in agriculture, and the high values are in buildings & bare lands.

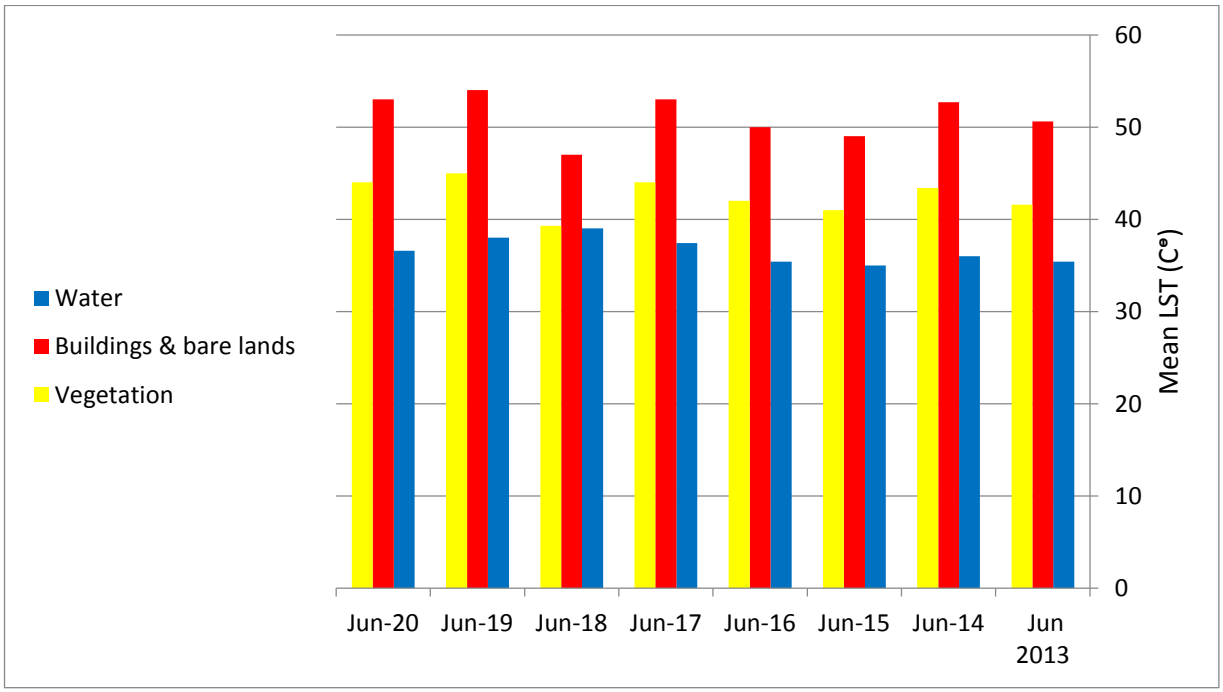

Fig. (4.8): Mean LST for each LULC class in different years.

4.2.2 Normalized Difference Vegetation Index

The spatial distribution of NDVI in the research zone is shown in Figure (4.9). A zymology was made for the map and zoning according to the values shown, as the red color represents water bodies and its value is less than zero, while the yellow color represents bare lands and its values from 0-0.2 and the green color represents vegetation with values greater than 0.2 (Kaplan and Avdan, 2018).

The area having the greatest NDVI is observed to be concentrated particularly in the central zone, low values of NDVI showed in the edges. The lowest values of NDVI were recorded in rivers and ponds which appeared as thin curvilinear features and small dark red patches respectively.

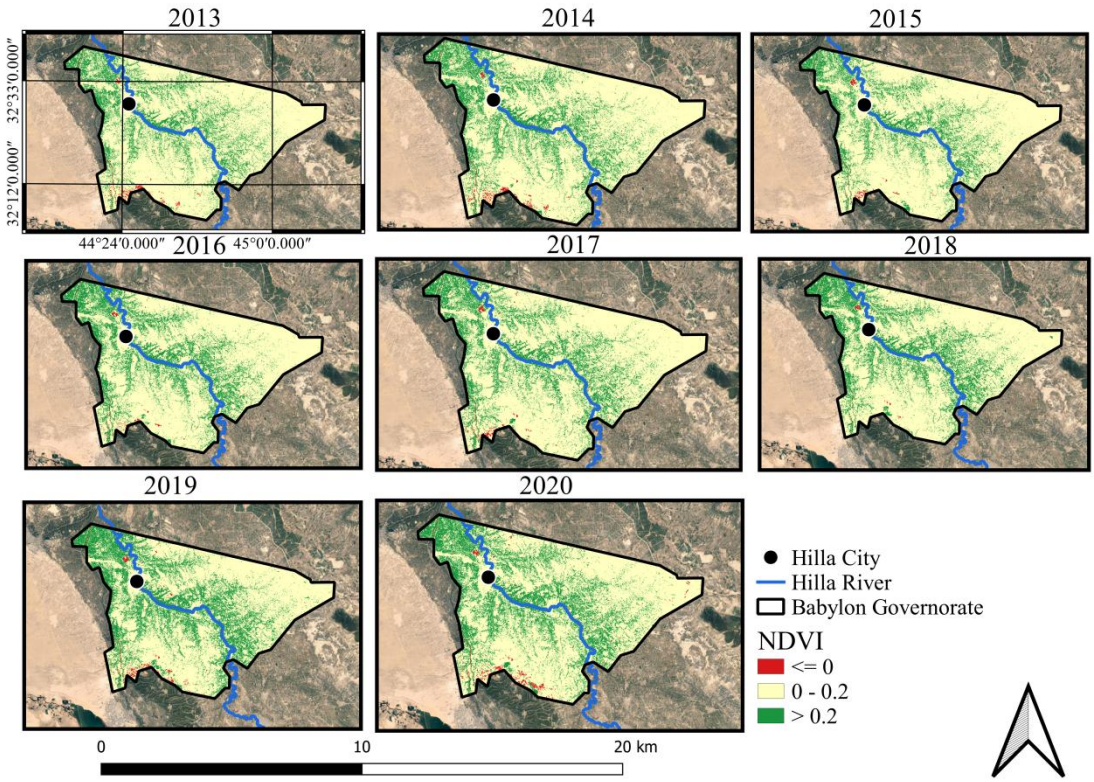

Fig. (4.9): NDVI spatial-temporal variation for Babylon Governorate from 2013 to 2020 (Appendix D).

The bar chart of mean values of NDVI for all LULC classes is shown in (Figure 4.10). Agriculture is the area with the LULC class that has the highest mean NDVI value ranging from 0.28 to 0.34. This can be attributed to the predominance of vegetation coverage. Water is associated with the lowest NDVI ranging from -0.016 to 0.073 because of the lack of vegetation in water. Nevertheless, the value tends to raise with time because of the growth of vegetation in water with the increase in contamination level. For both bare soil and urban area, NDVI value is 0.13 approximately.

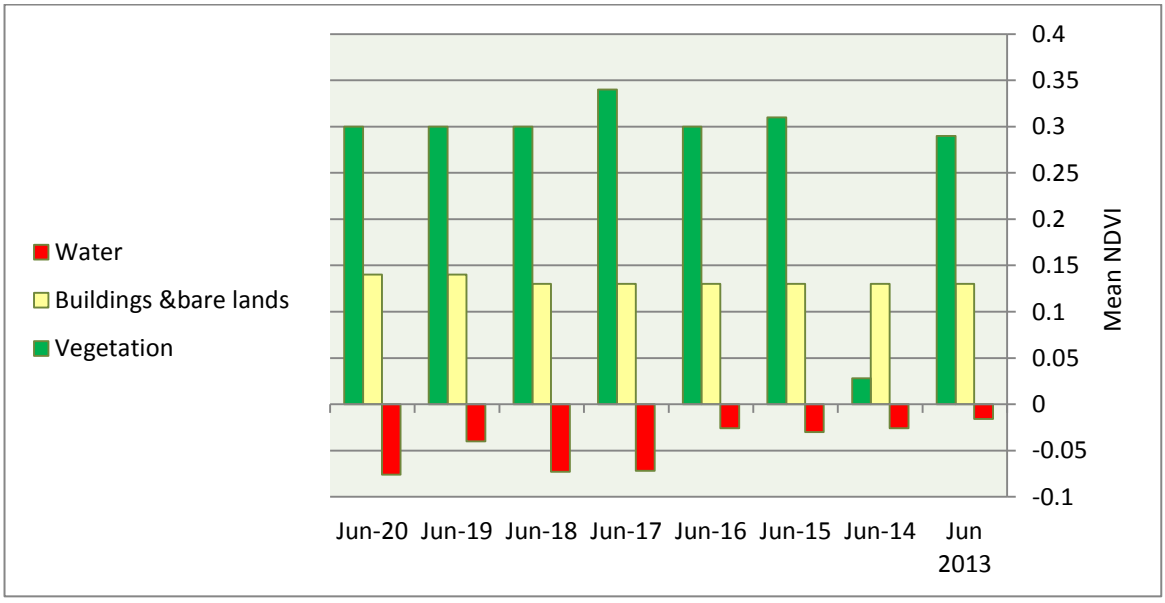

Fig. (4.10): Mean values of NDVI for each class of LULC in different years.

Table (4.2) shows the values of the high, middle and low temperatures for each year from 2013 to 2020. It also shows the mean NDVI values for each year for the same period.

Table (4.2): Mean, maximum (max), minimum (min) of LST values and Mean NDVI values.

Year	Dates	LST			NDVI
		Max	Mean	Min	Mean
2013	24 June	58	49	30	0.15
2014	27 June	61	50	31	0.16
2015	30 June	55	48	30	0.15
2016	2 July	55	48	31	0.16
2017	19 June	60	51	32	0.15
2018	22 June	52	45	30	0.16
2019	25 June	61	51	33	0.17
2020	27 June	62	51	32	0.17

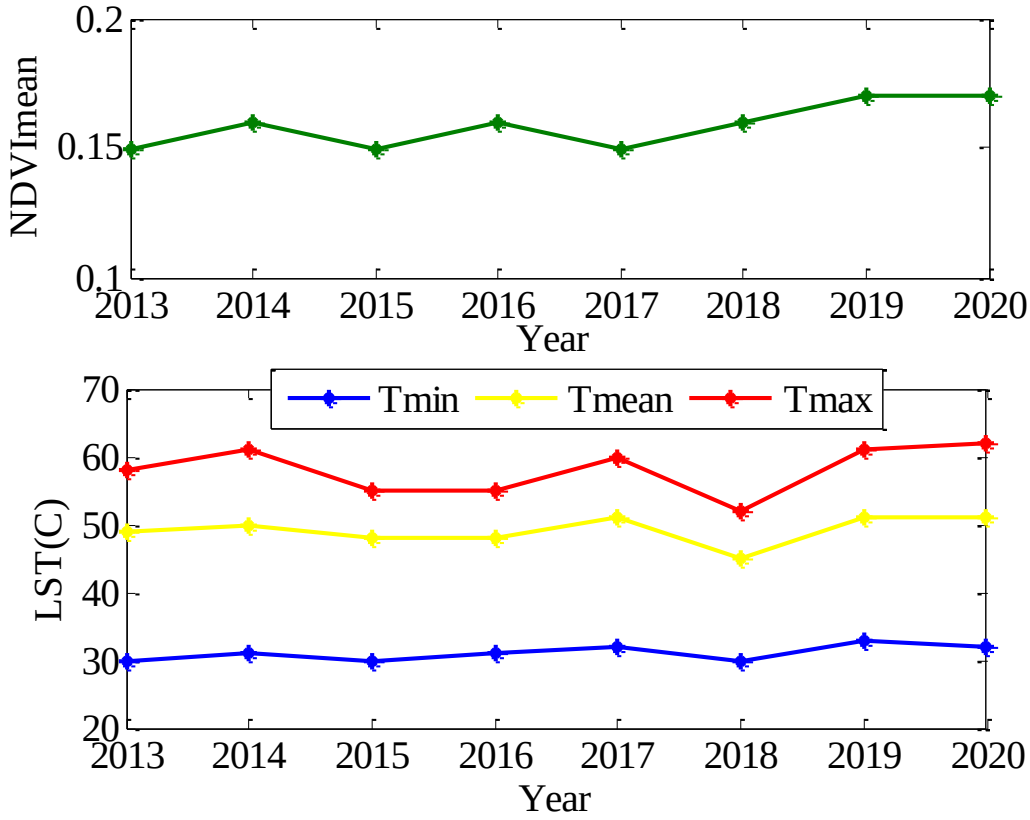

Fig (4.11): Temporal LST and NDVI change for Babylon Governorate from 2013 to 2020.

the values of mean NDVI range between 0.15 to 0.17. The years with the highest temperatures were 2013, 2014, 2017, 2019, and 2020, while the years with the lowest temperatures were 2015, 2016, and 2018, as shown in Figure (4.11).

4.3 Total spatial-temporal difference of LST for Babylon Governorate over years

Regional LST would reveal sensitive and visible shifts with the variations in time and space. In fact, annual change in LST has significant impacts on human growth. Babylon Governorate has a diverse climate and geological landscape, and its LST adjustments are of considerable scientific interest. Babylon's central region is a significant agriculture area.

Higher-quality data may aid in more precise monitoring and analysis of temporal and spatial changes in LST. Traditionally, field stations have been used to measure LST. With high precision and reliability, this type of data will reliably represent the LST near the stations. Furthermore, data from ground stations is less affected by fog and rain, resulting in comparatively high data integrity and a long time series protected (Yan et al., 2020).

Moreover, the total spatiotemporal changes of LST classes of Babylon Governorate between years were explored quantitatively in Table (4.3).

Table (4.3): LST area changes for Babylon Governorate polygon from 2013 to 2020.

Year intervals	**Area of increase temperature,Km^2**	**Area of decrease temperature, Km^2**	**Total area, Km^2**
2020 – 2019	1426	2134	3560
2019 – 2018	3407	153	3560
2018 – 2017	89	3471	3560
2017 – 2016	3381	179	3560
2016 – 2015	1955	1605	3560
2015 – 2014	631	2929	3560
2014 – 2013	2910	650	3560
2020 – 2013	2973	587	3560

The study also analyzed the LST changes in Babylon region from 2013 to 2020 as shown in Figure (4.12).

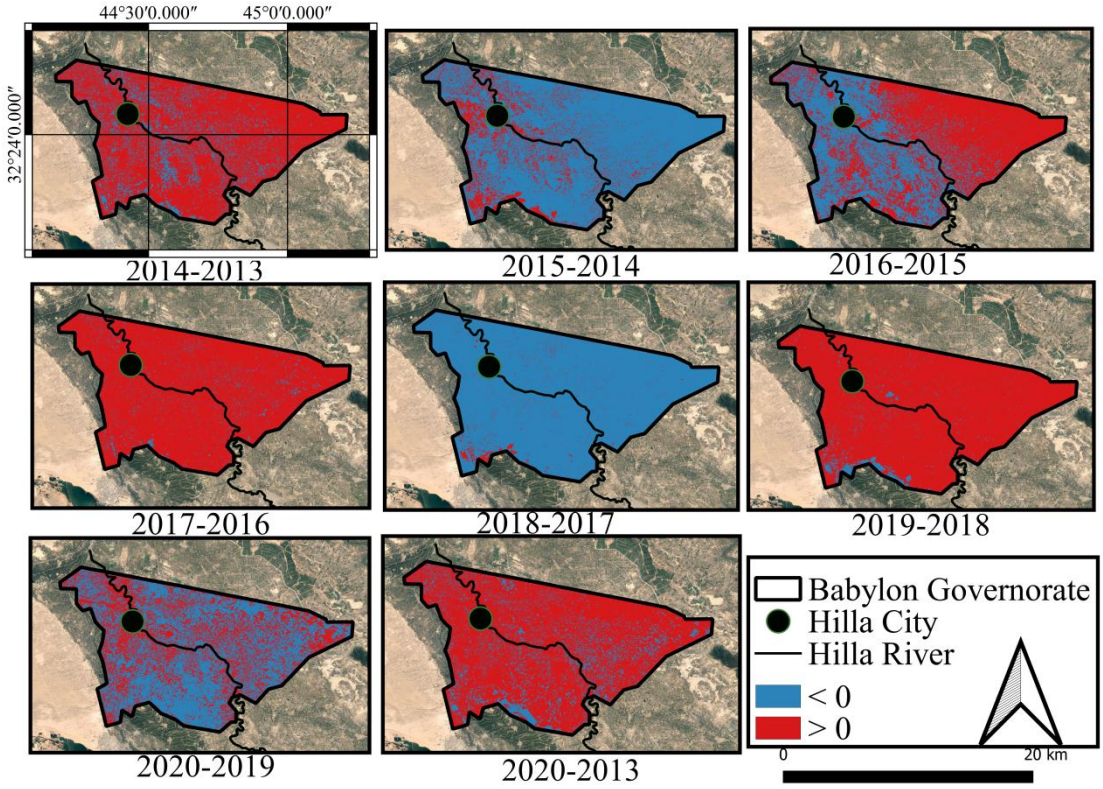

Fig. (4.12): changes of LST for Babylon Governorate over years.

The above figure shows the variation of LST by subtracting successive years to clear the change that occurred during the years in consecutively. Subtracting the map 2013 from the map of 2014 and the same for the other years by using raster calculator in QGIS program. The red part represents where LST becomes higher, while the blue part represents the LST decline.

The area of increase in temperature for the difference for the years 2020-2019 is greater than the area of the decrease, while for 2019-2018 the area of the increase in temperature is large compared to the area of the decrease, so the red color predominates. In 2018-2017 it is larger, so it

was shown in the blue color in 2016-2015, the areas are close, but the area of increase is more, so the red color appeared more. In 2015-2014, the area of decreased is high. In 2014-2013, the area of increase increased. The difference in years between 2020-2013, the temperature increased by a large percentage areas of increase in temperature appeared in red. Figure (4.13) shows the variation of LST by subtracting successive years to clear the change that occurred during the years in consecutively.

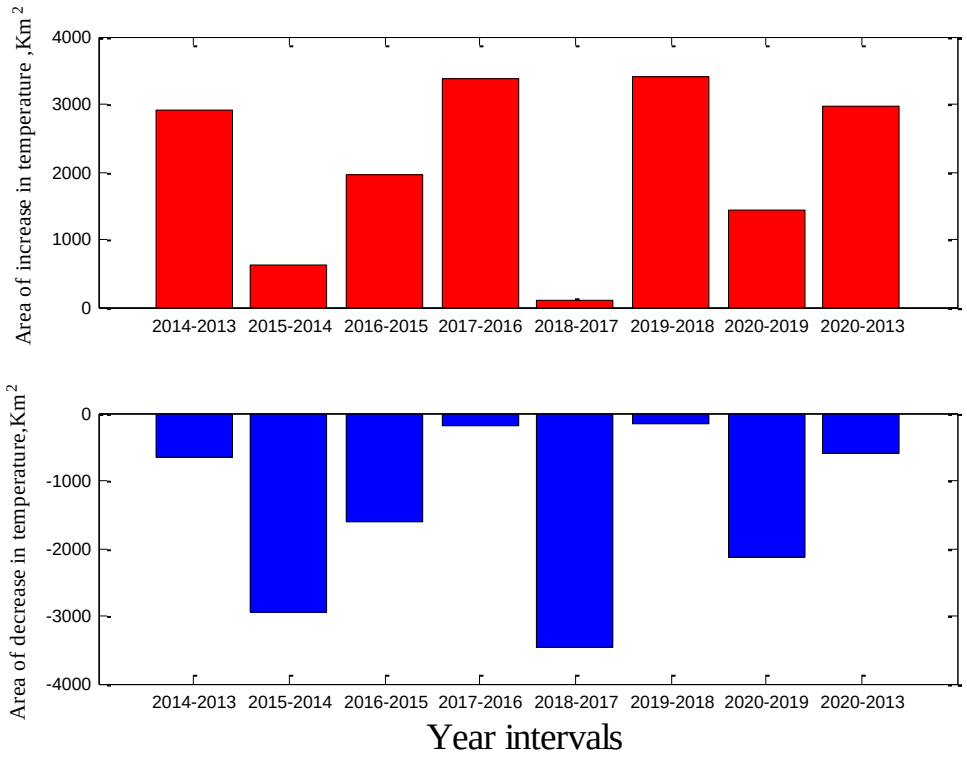

Fig. (4.13): LST area change between years for Babylon Governorate polygon.

4.4 Modeling of LST

To characterize the relationship between LST and the abundance of vegetation measured through NDVI for seven periods, a simple linear regression model was used (2013 to 2020). For the regression analysis

between the NDVI and the LST values, a randomly selected collection of 304 sample points was used in the study field. As the independent variable, NDVI is utilized, while the dependent variable is LST.

Samples were taken, covering the entire study area, about 304 points, by raster sampling tool in QGIS, as shown in Figure (4.14). Two hundred points were taken as training data to find a relationship between temperature and vegetation cover and to find a model for calculating temperature through vegetation values.

In this study, the selected information are used to investigate the performance of LST prediction QGIS, the models were fabricated utilizing Matlab software. The models designed in this study are used to investigate the temperature distribution. 200 points were used to build the models, and the remained points were used as the target for the examination phase. The LST, which are presented in Figure (4.15), were extracted using QGIS3.10.

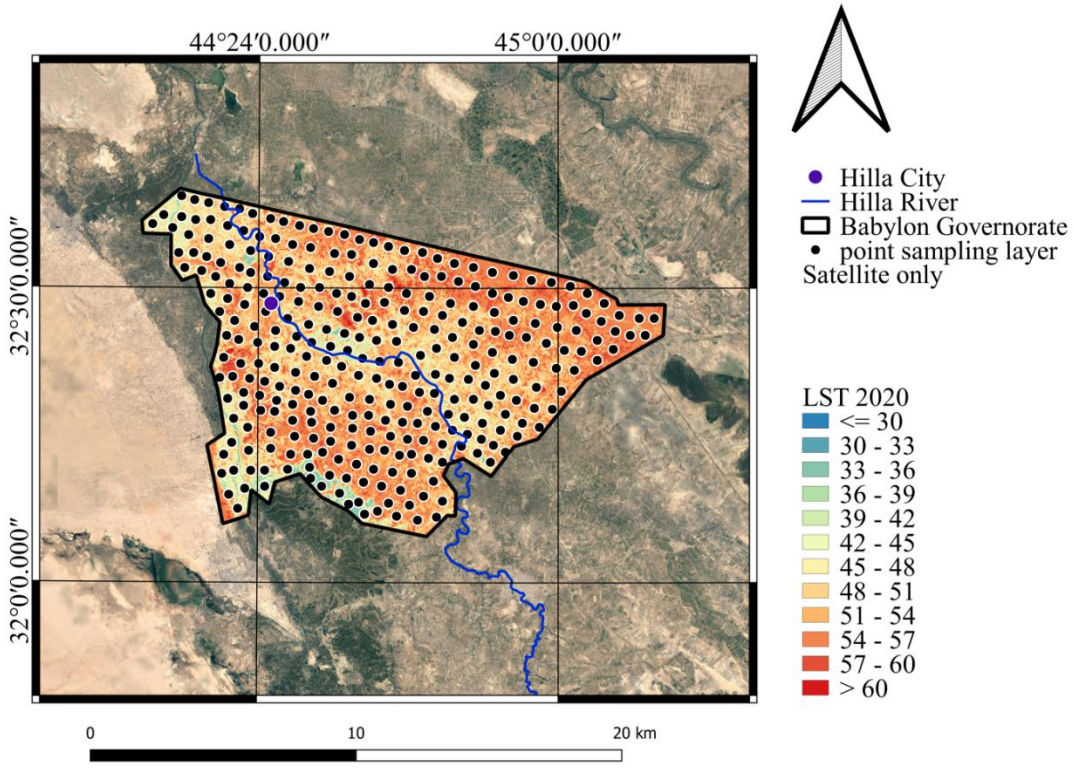

Fig. (4.14): Distribution of selection points for predicting LST.

In order to clarify the relationship between LSTs and vegetation, scatter plots of LST versus NDVI for the study period were drawn by Matlab software and a linear equation was found. The values of R-square and P-value for each year were calculated as shown in the scatter plots in Figure (4.16), and the regression lines showed an inverse correlation between LST and NDVI during the study periods. It indicates the importance of vegetation cover as a major land use factor in reducing LST in the study area. Indeed, the lack of interest in the study area in planting and expanding tree cover and landscapes would cause the city to suffer from the warm local climate.

As for the rest of the points, they were considered as test data to test the validity of the resulting model. A drawing was made for each year of research between the measured test temperature and the temperature

calculated from the model resulting from the training data. RMSE and MAE for each year were found (Figure 4.17).

In the north-east of Babylon, the hotspots are more focused. Babylon lands are associated with the greatest temperature particularly the north-east of the city.

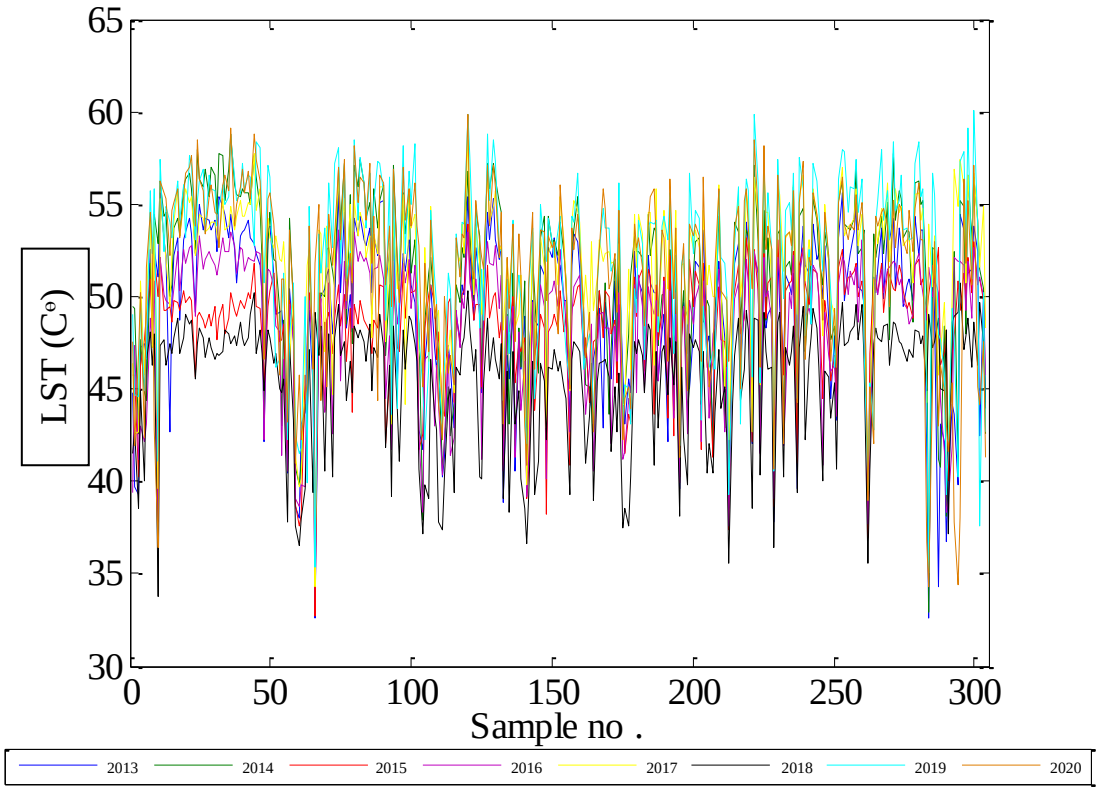

Fig. (4.15): LST for the month of July at the specified four years.

4.5 LST-NDVI relationship

In Babylon Governorate, LST and NDVI have a close relationship. NDVI is the independent variable, while LST is the dependent variable. Figure (4.16) shows the regression analysis result for the study area, and for all the years. The strength and kind of relationship between the independent and dependent variables is indicated based on the coefficient of each independent variables. For all years, the coefficients of the regression analysis results in the study area are negative indicating that

NDVI is inversely related to LST. This suggests that the LST decreases with an increase in vegetation richness. Generally, an accurate fit was indicated by the NDVI-LST regression. Lower R^2 values were recorded in the years 2013, 2017, 2018, 2019 and 2020 ($0.6 > R^2 < 0.4$), while higher ones were gained in 2014, 2015 and 2016 (> 0.6). The greatest R^2 was 0.645 and was recorded on 30 June 2015 and the lowest one was 0.458 (27June 2020). Hence, the outcomes of the regression analysis were very considerable ($p < 4.19$ E -28). A constant pattern was indicated for the urban area. Thus, NDVI can be utilized as an indicator for the variability presented in LST as shown in Figure (4.16).

Bare soils with no vegetation gave the lowest NDVI values. In areas where high LST values were observed, the NDVI diminished due to the variation in vegetation state or abundance. This is associated with alterations in the natural cycle of vegetation or diverse human activity. Bare soils and urbanized land showed the highest temperatures.

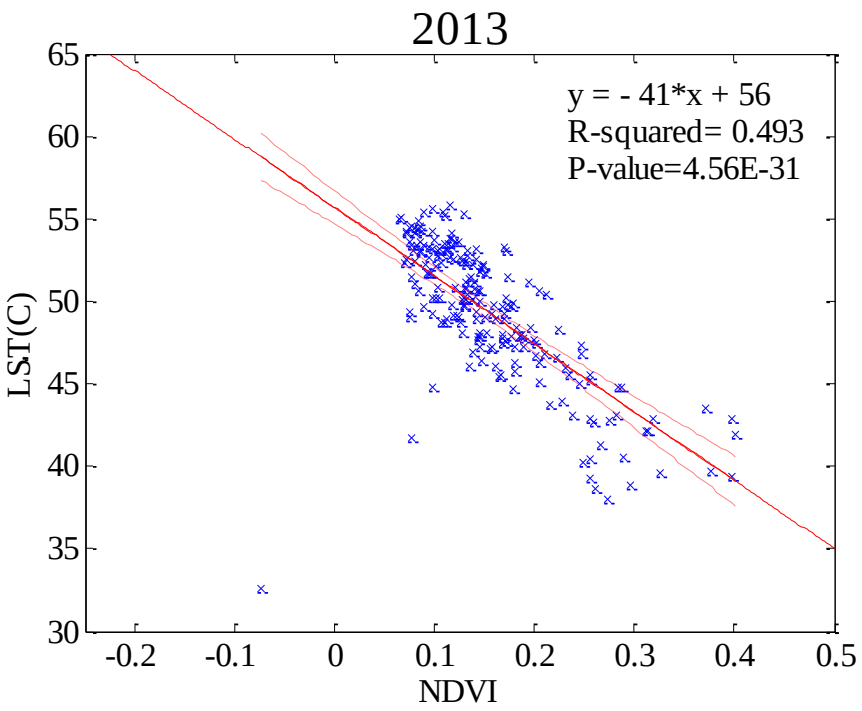
2013
y = - 41*x + 56
R-squared= 0.493
P-value=4.56E-31
LST(C)
NDVI
65
60
55
50
45
40
35
30
-0.2
-0.1
0
0.1
0.2
0.3
0.4
0.5

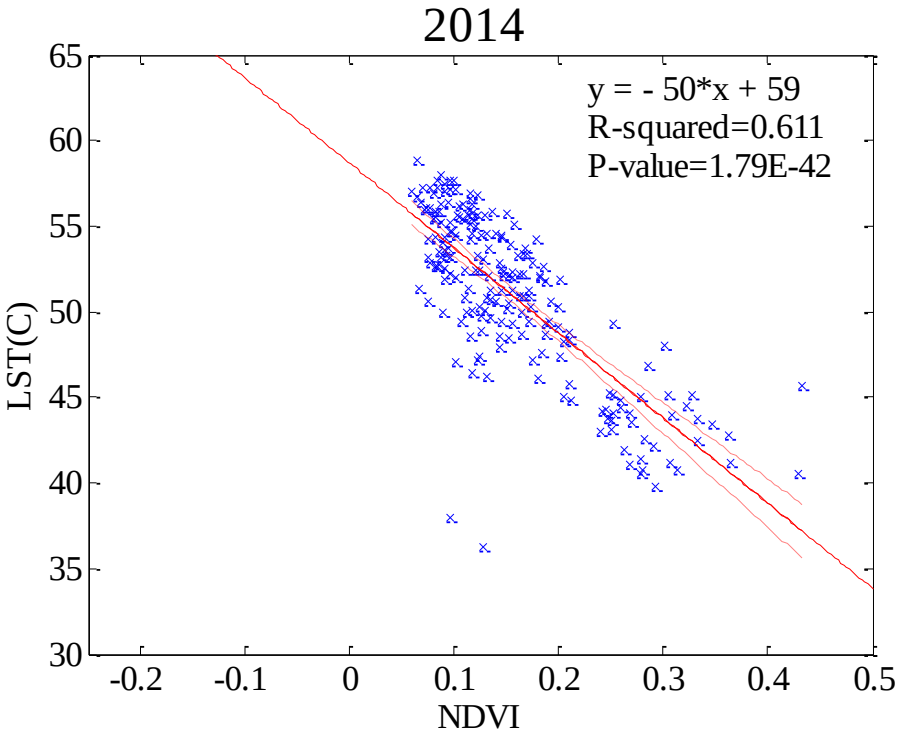
2014
y = - 50*x + 59
R-squared=0.611
P-value=1.79E-42
LST(C)
NDVI
65
60
55
50
45
40
35
30
-0.2
-0.1
0
0.1
0.2
0.3
0.4
0.5

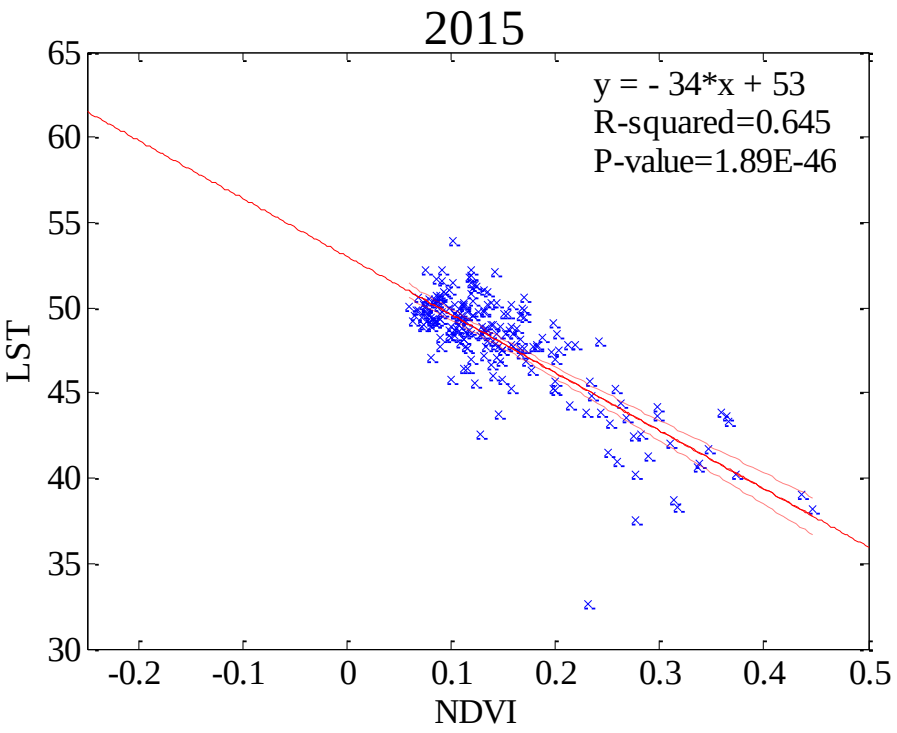
2015
y = - 34*x + 53
R-squared=0.645
P-value=1.89E-46
LST
NDVI
65
60
55
50
45
40
35
30
-0.2
-0.1
0
0.1
0.2
0.3
0.4
0.5

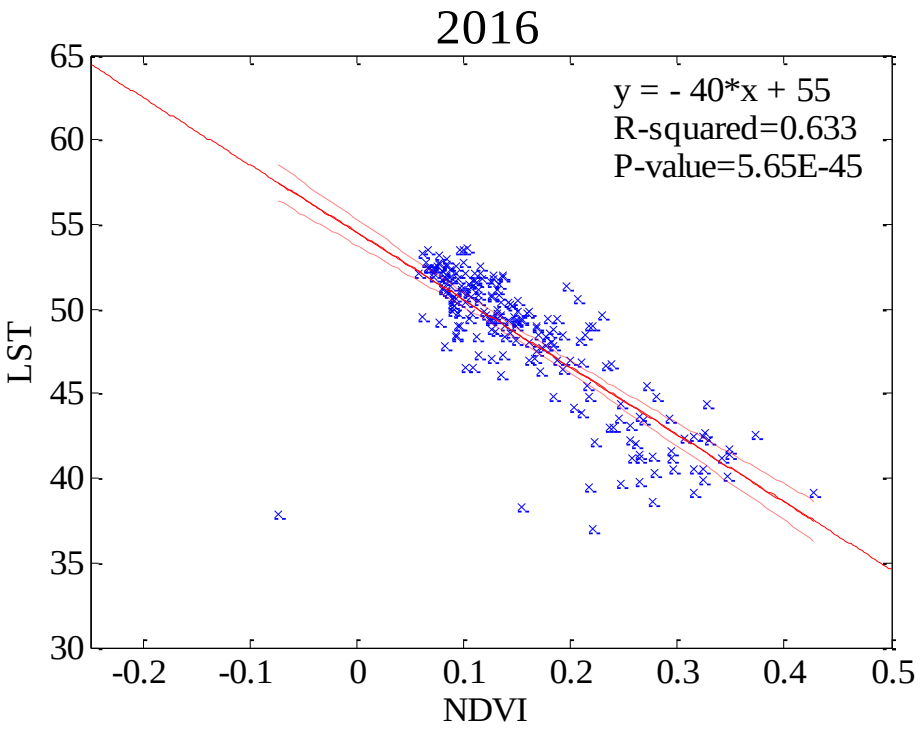
2016
y = - 40*x + 55
R-squared=0.633
P-value=5.65E-45
LST
NDVI
65
60
55
50
45
40
35
30
-0.2
-0.1
0
0.1
0.2
0.3
0.4
0.5

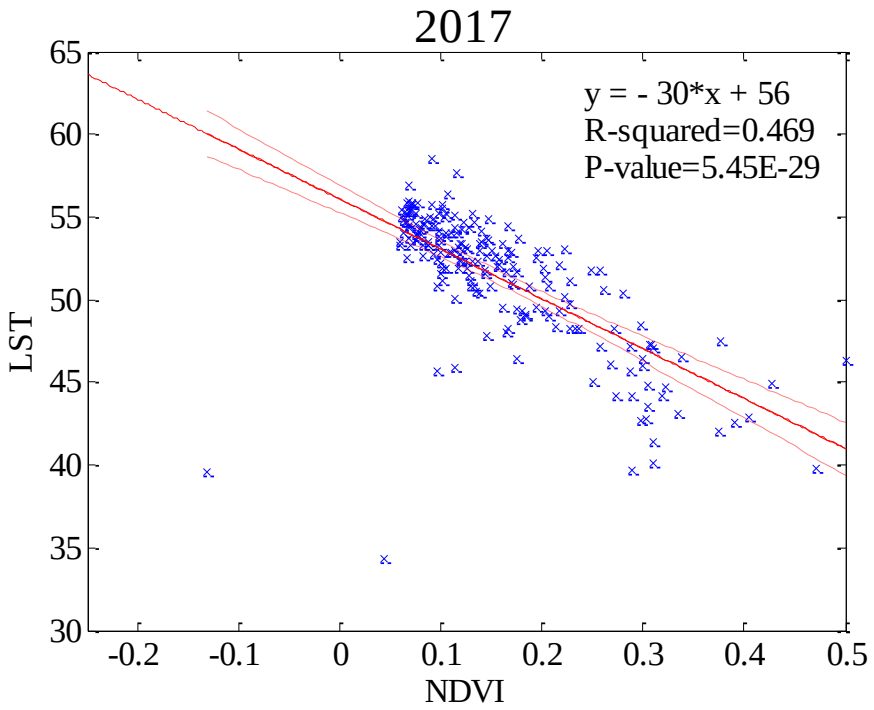
2017
y = - 30*x + 56
R-squared=0.469
P-value=5.45E-29
LST
NDVI
65
60
55
50
45
40
35
30
-0.2
-0.1
0
0.1
0.2
0.3
0.4
0.5

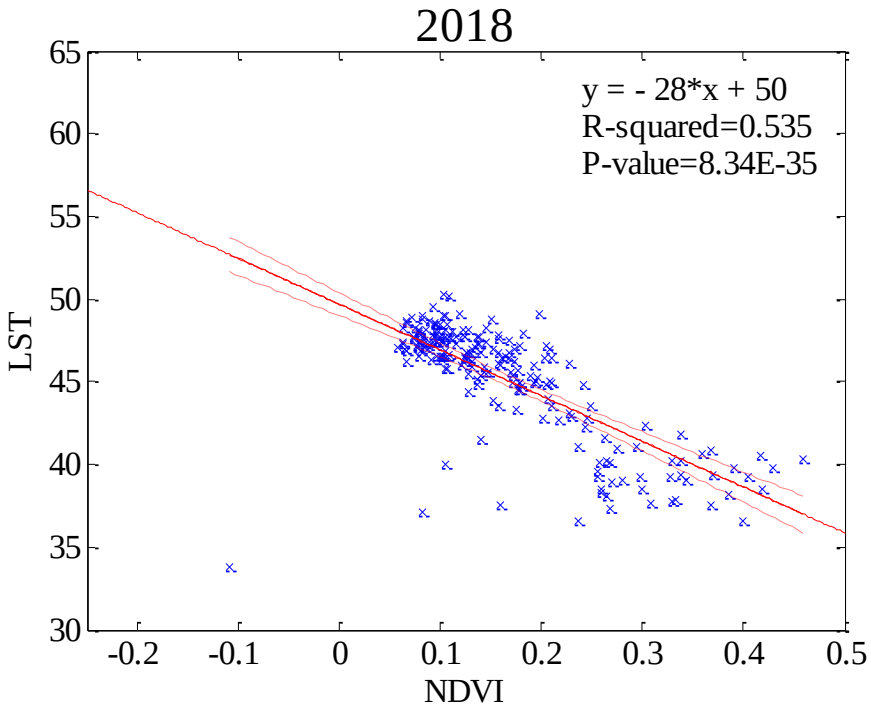
2018
y = - 28*x + 50
R-squared=0.535
P-value=8.34E-35
LST
NDVI
65
60
55
50
45
40
35
30
-0.2
-0.1
0
0.1
0.2
0.3
0.4
0.5

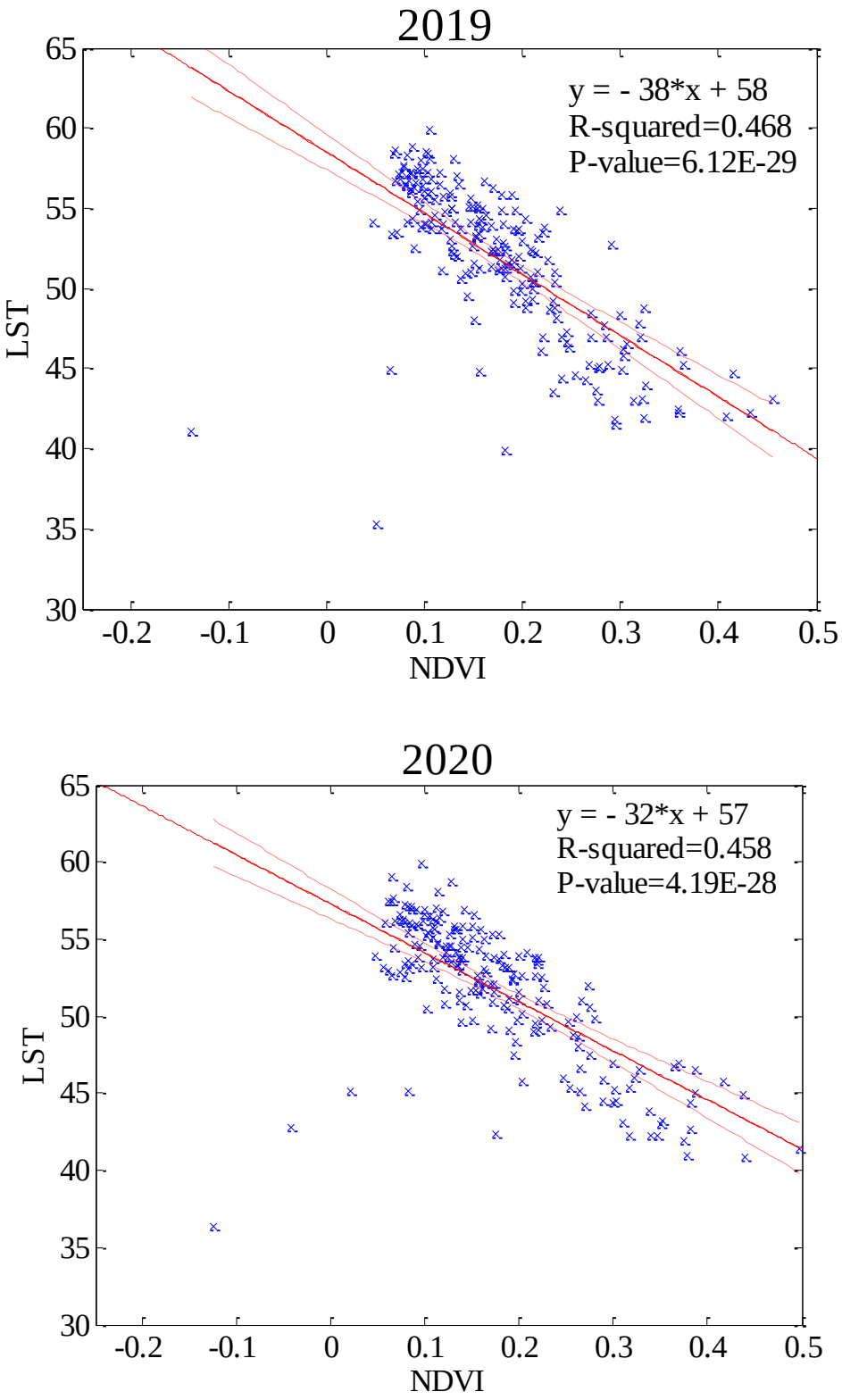

Fig. (4.16): Scatterplots of LST against NDVI.

Indexes assessment indicated that the models were capable of simulating and forecasting LST values over the upcoming year in a satisfying way due to the very close predict and observed values of LST. Scatter graphs and plots of LST (2013, 2014, 2015, 2016, 2017, 2018, 2019 and 2020) observed and predicted as depicted in Figure (4.17) indicate very good agreement. Mean square error (MSE) quantitative and RMSE values of observed and predicted LST in 2018 were 1.4 and 1.7 C^{o} showing how strong is the correlation between the predicted and observed LST.

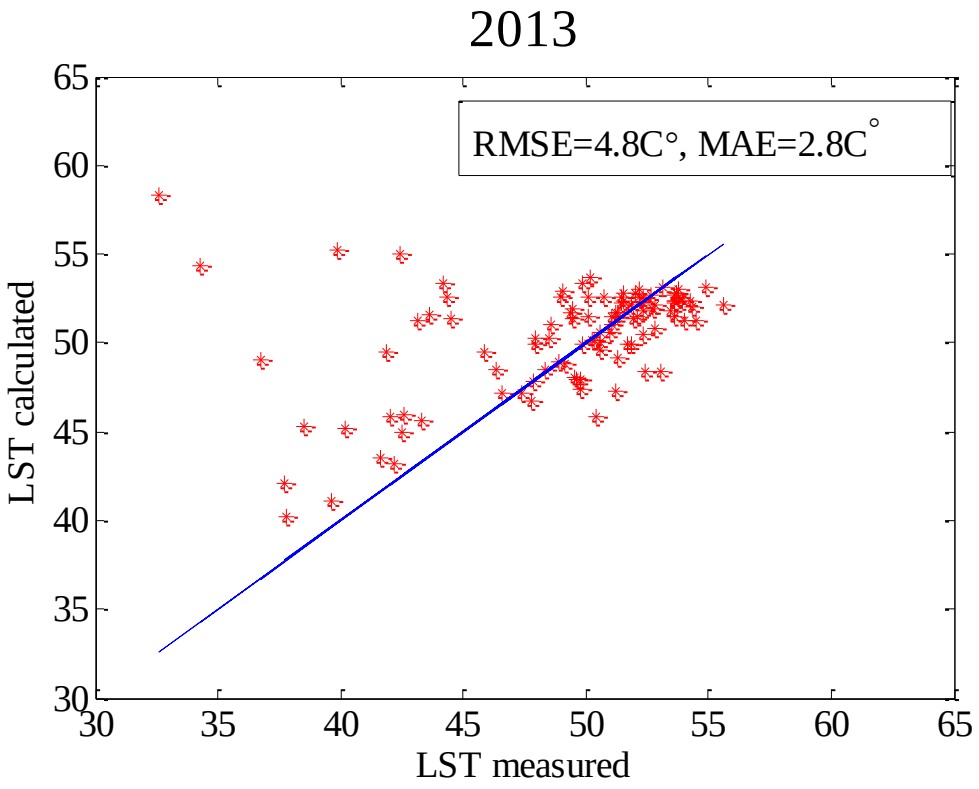
2013
RMSE=4.8C°, MAE=2.8C°
LST calculated
LST measured
65
60
55
50
45
40
35
30
30
35
40
45
50
55
60
65

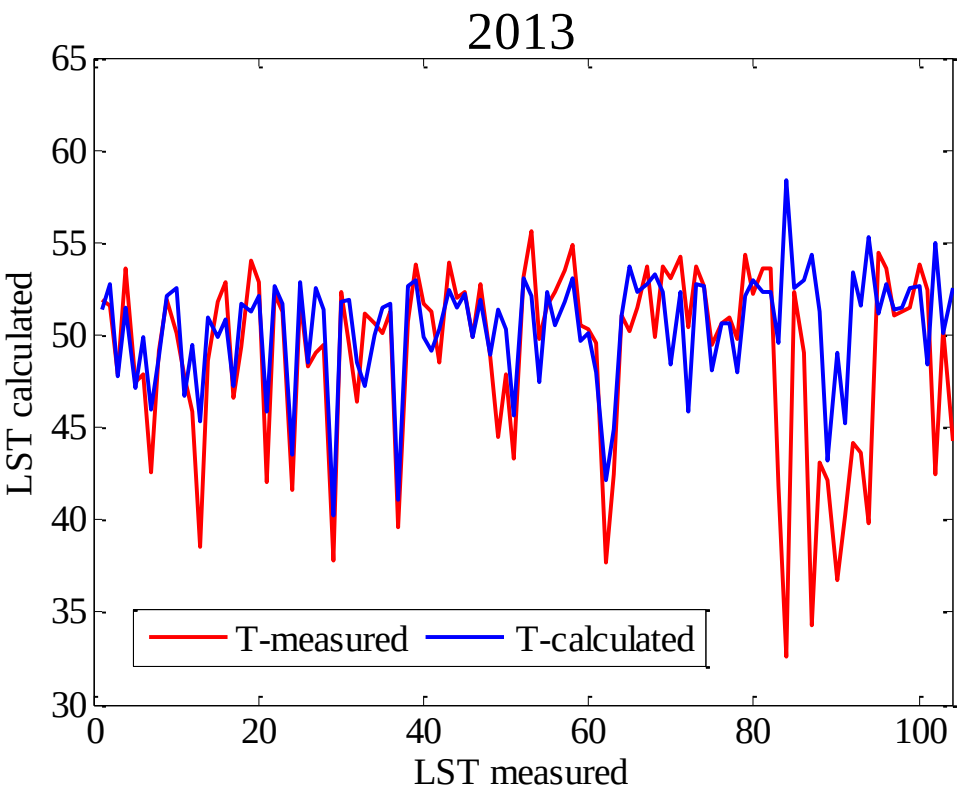
2013
T-measured
T-calculated
LST calculated
LST measured
65
60
55
50
45
40
35
30
0
20
40
60
80
100

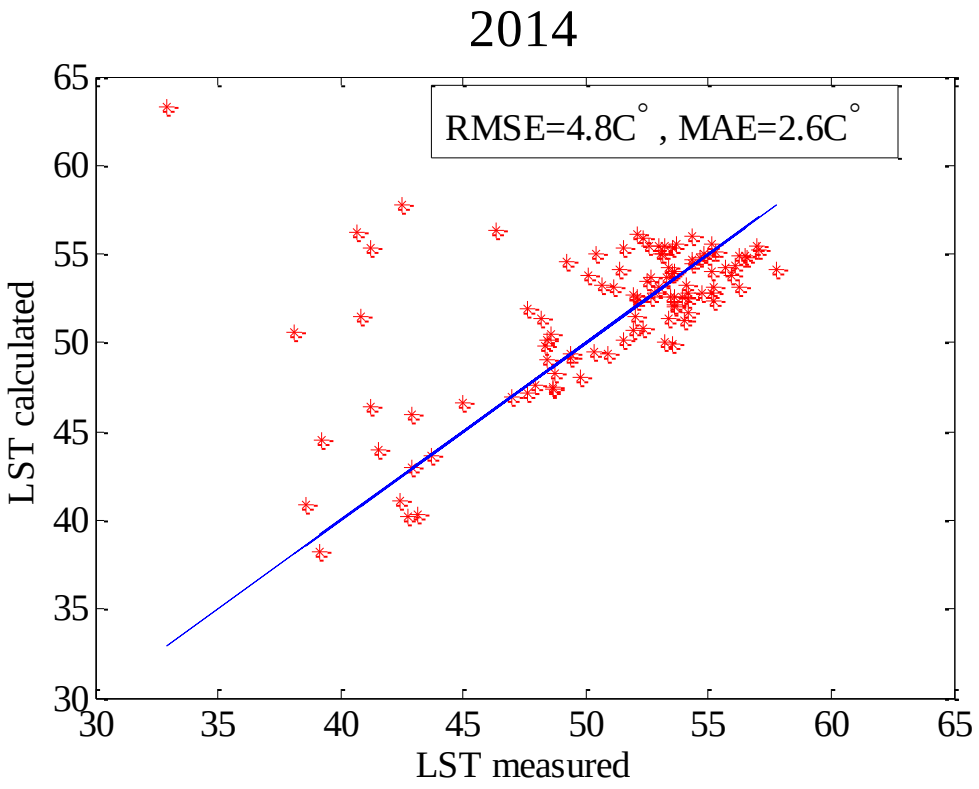
2014
RMSE=4.8C° , MAE=2.6C°
LST calculated
LST measured
65
60
55
50
45
40
35
30
30
35
40
45
50
55
60
65

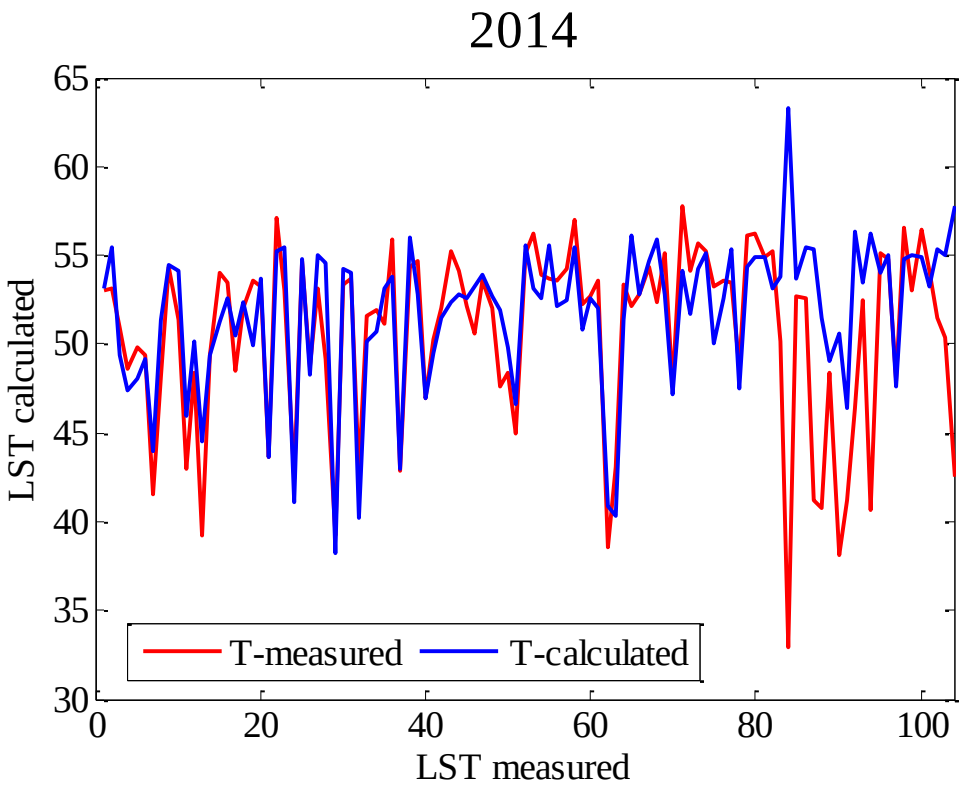
2014
T-measured
T-calculated
LST calculated
LST measured
65
60
55
50
45
40
35
30
0
20
40
60
80
100

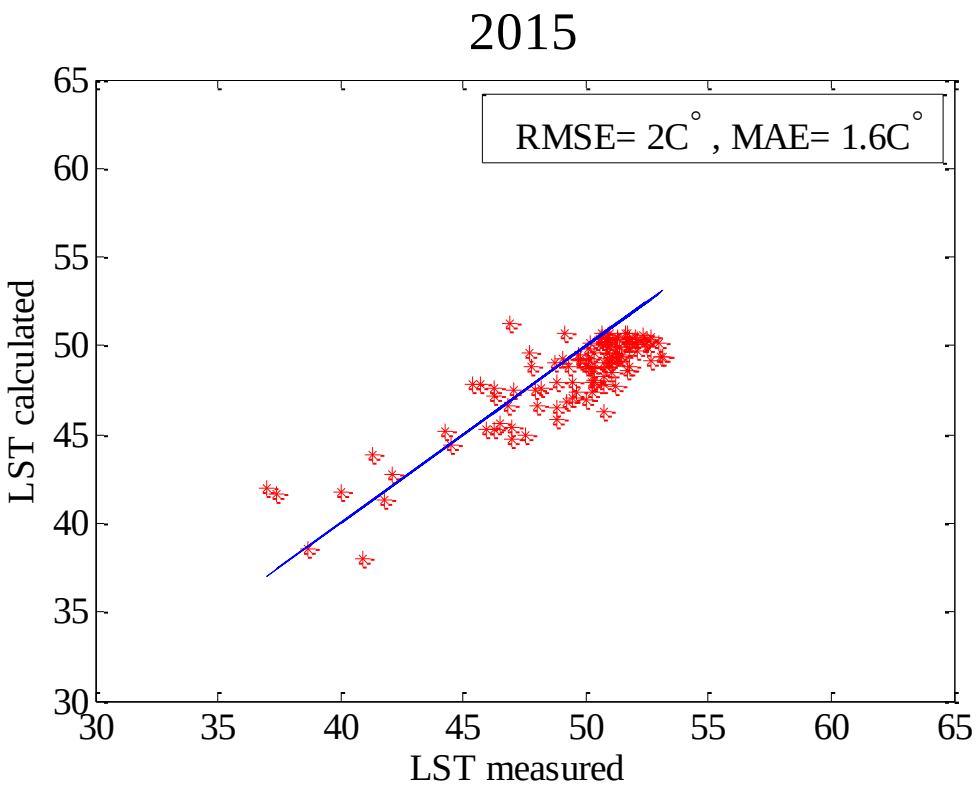
2015
RMSE= 2C° , MAE= 1.6C°
LST calculated
LST measured
65
60
55
50
45
40
35
30
30
35
40
45
50
55
60
65

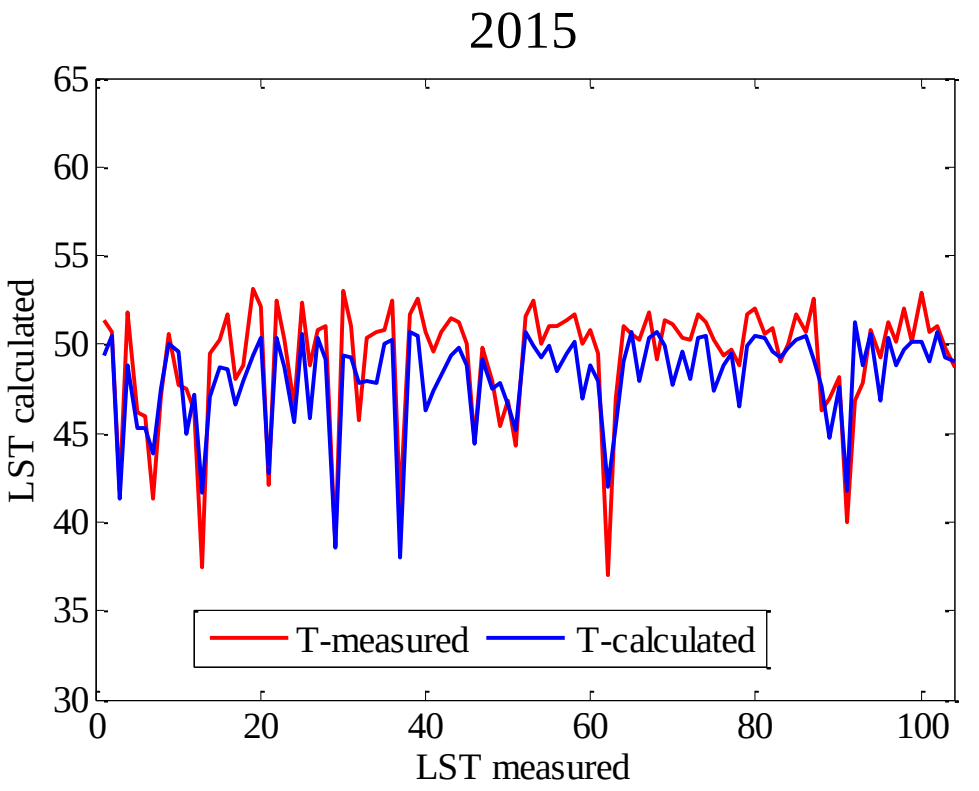
2015
LST calculated
LST measured
T-measured
T-calculated
65
60
55
50
45
40
35
30
0
20
40
60
80
100

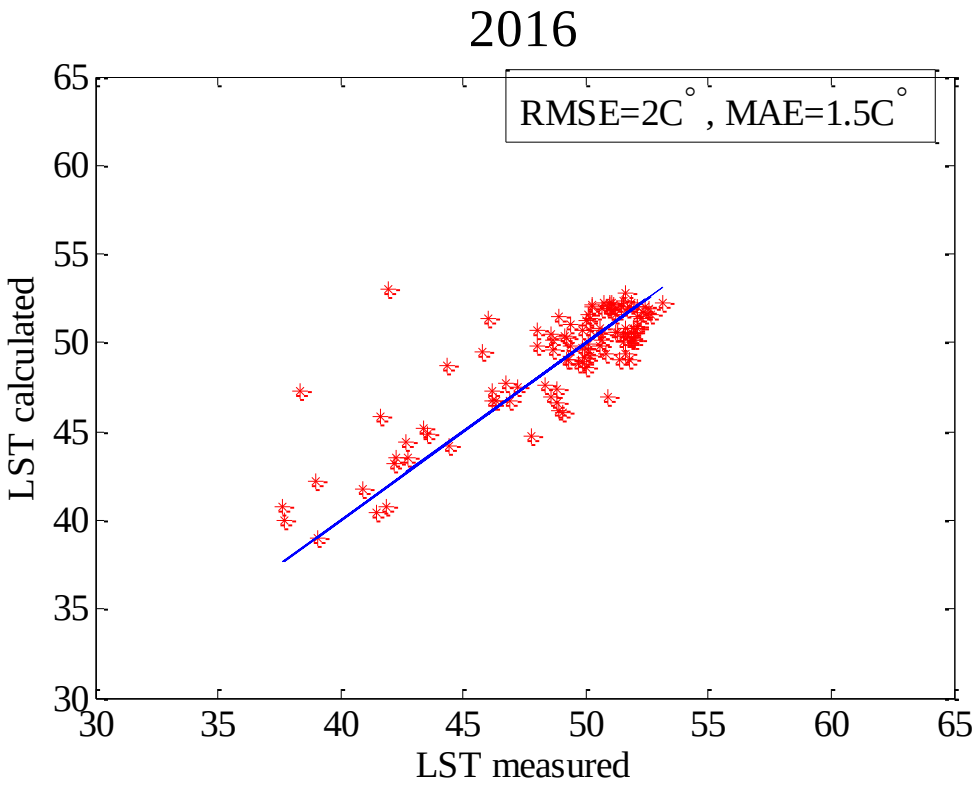
2016
RMSE=2C° , MAE=1.5C°
LST calculated
LST measured
65
60
55
50
45
40
35
30
30
35
40
45
50
55
60
65

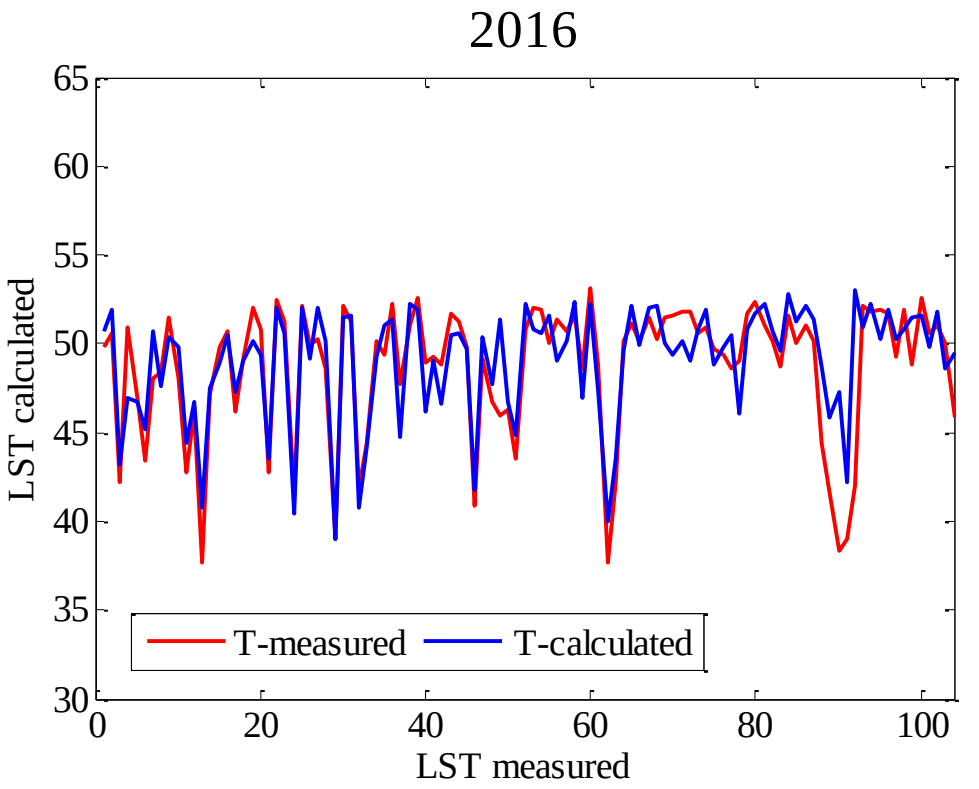
2016
LST calculated
LST measured
T-measured
T-calculated
65
60
55
50
45
40
35
30
0
20
40
60
80
100

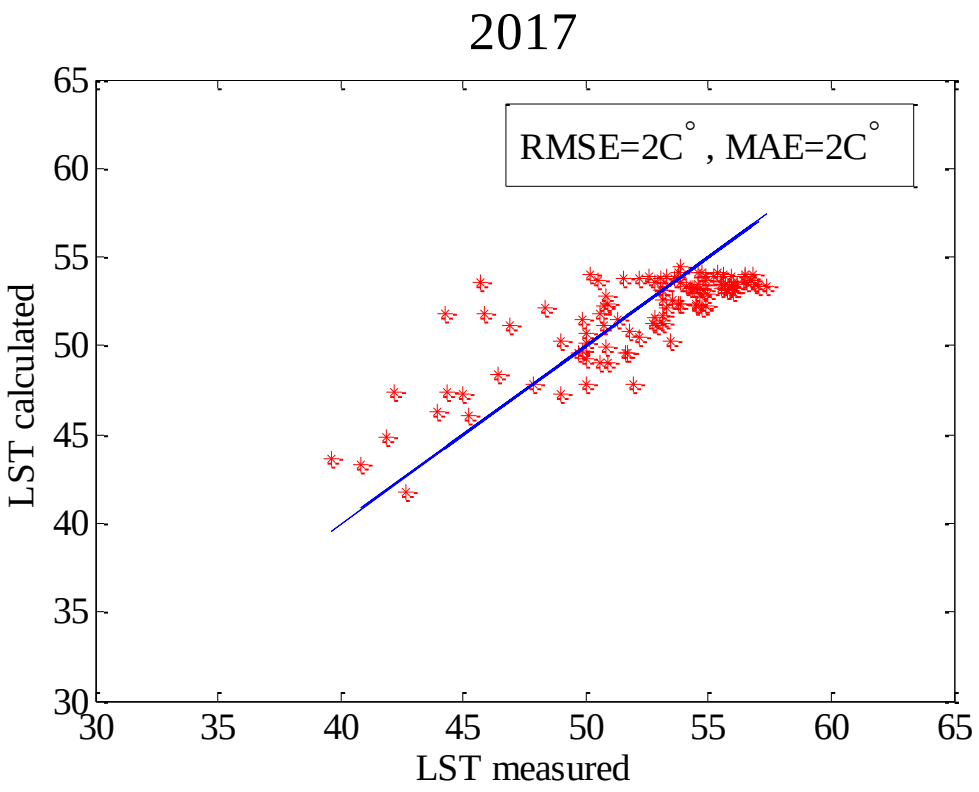
2017
RMSE=2C° , MAE=2C°
LST calculated
LST measured
65
60
55
50
45
40
35
30
30
35
40
45
50
55
60
65

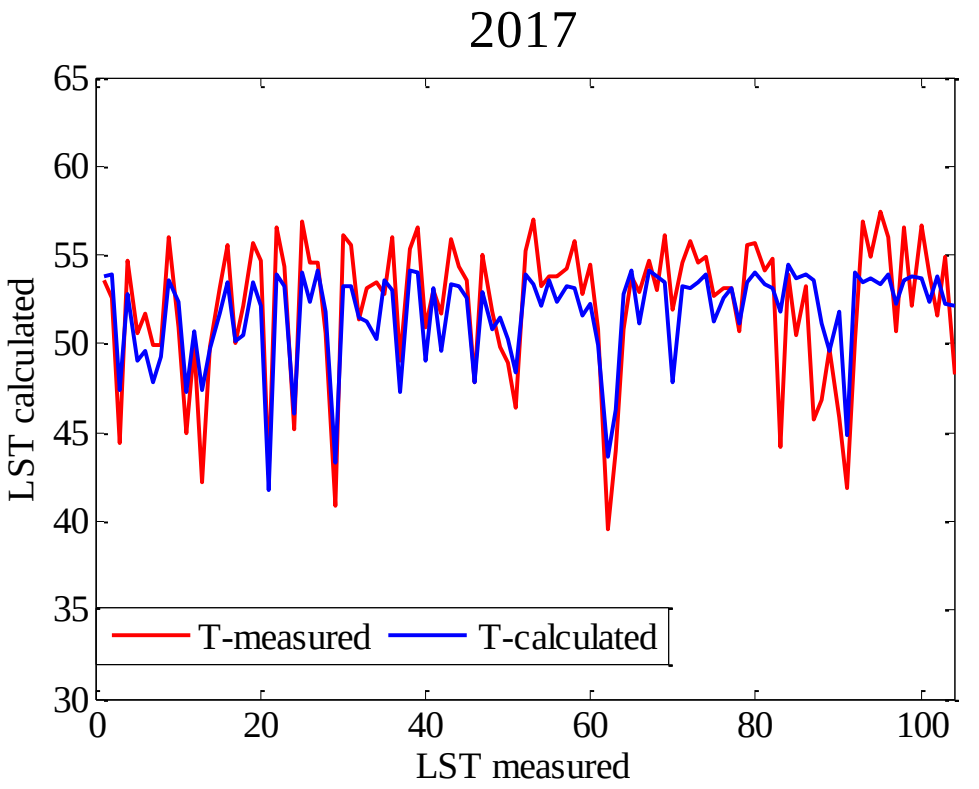
2017
T-measured
T-calculated
LST calculated
LST measured
65
60
55
50
45
40
35
30
0
20
40
60
80
100

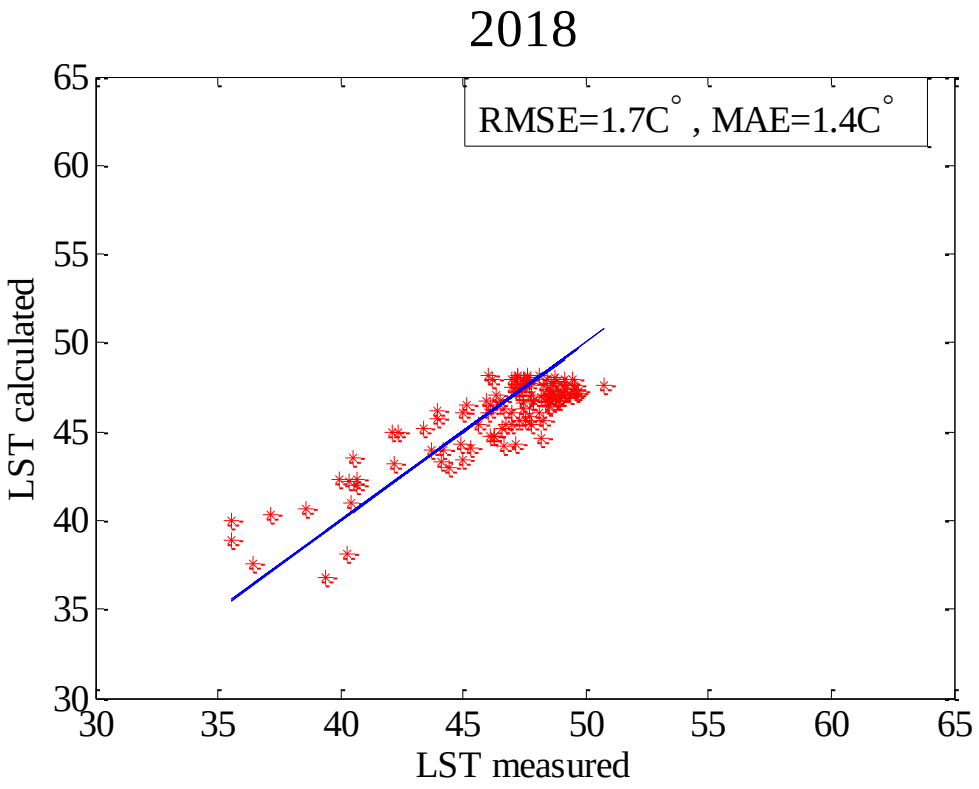
2018
RMSE=1.7C° , MAE=1.4C°
LST calculated
LST measured
65
60
55
50
45
40
35
30
30
35
40
45
50
55
60
65

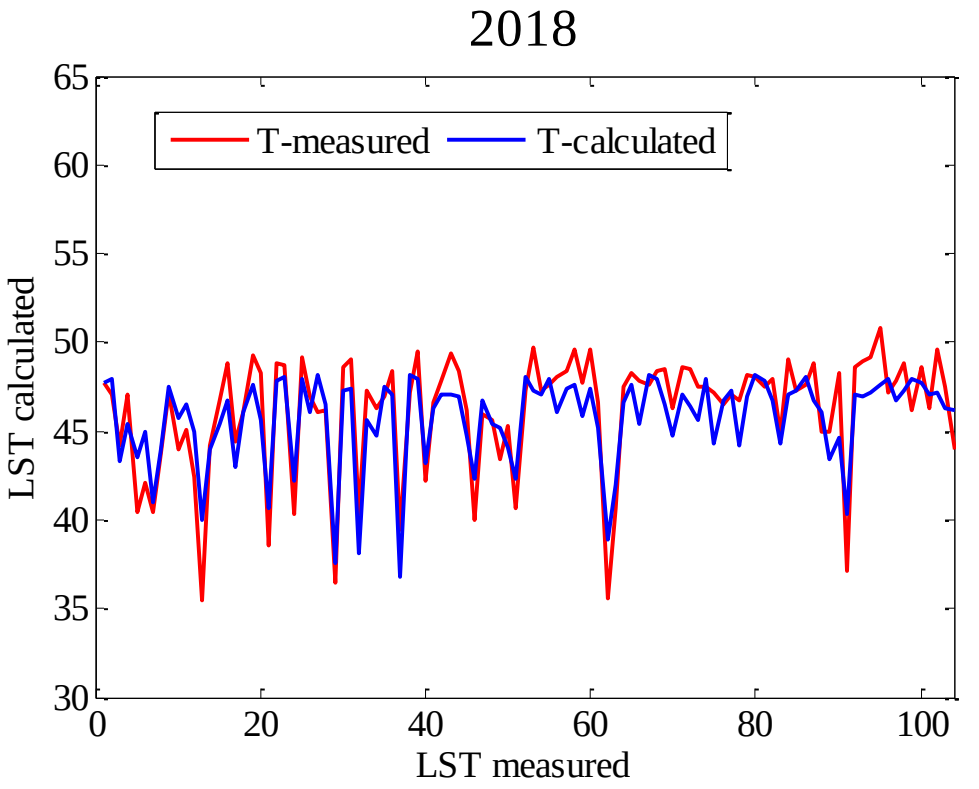
2018
T-measured
T-calculated
LST calculated
LST measured
65
60
55
50
45
40
35
30
0
20
40
60
80
100

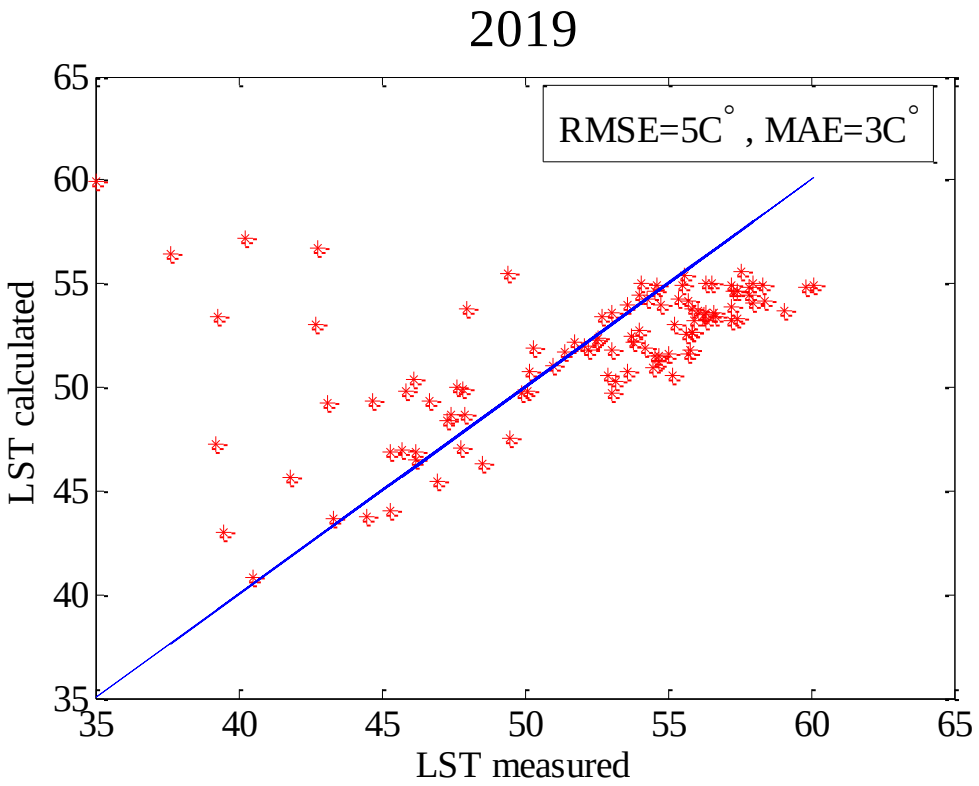
2019
RMSE=5C° , MAE=3C°
LST calculated
LST measured
65
60
55
50
45
40
35
35
40
45
50
55
60
65

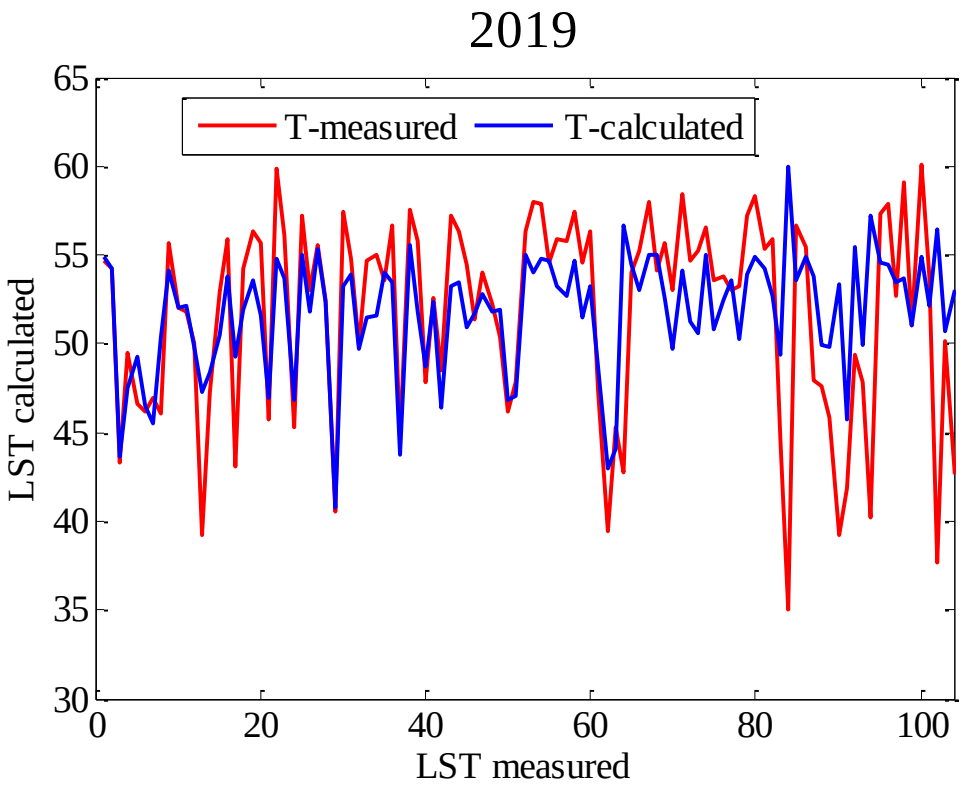
2019
T-measured
T-calculated
LST calculated
LST measured
65
60
55
50
45
40
35
30
0
20
40
60
80
100

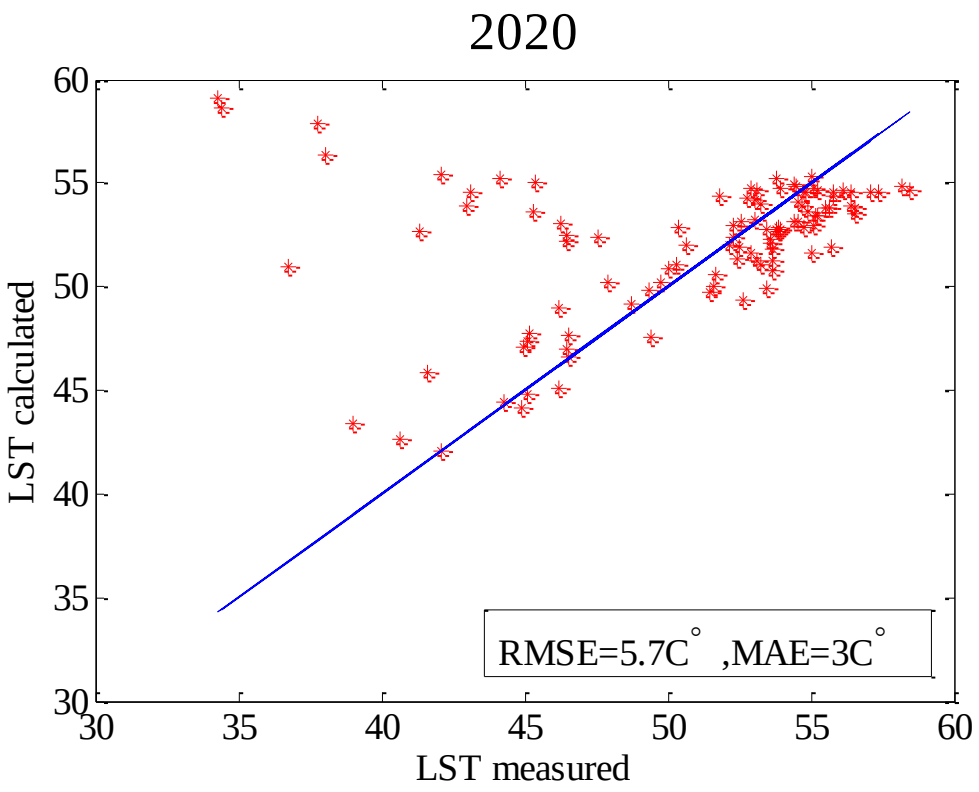

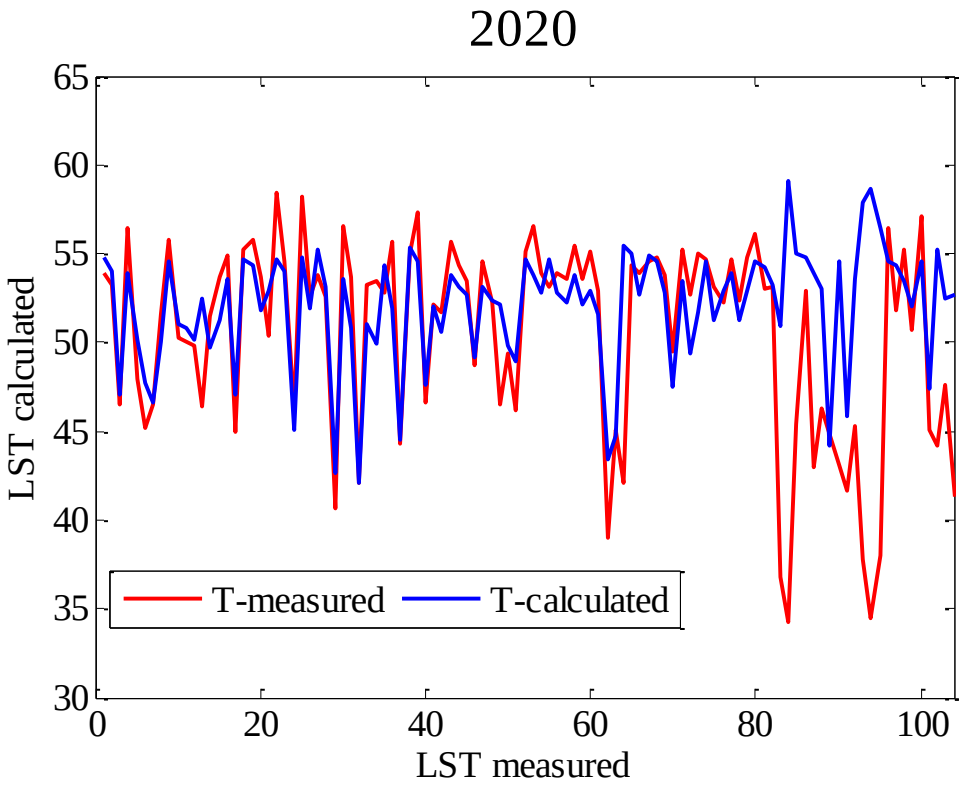

Fig. (4.17): The relationship between the observed data and the estimated data for Land Surface Temperature.

4.6 The comparison between LST calculated and air temperature measured from meteorological stations.

The following item indicates the comparison results of LST from Landsat 8 which is the monthly mean values with monthly measured from Hilla Meteorological Station for July from 2013 to 2019. The results gained from Landsat 8 thermal band can be measured as the hot weather in Iraq in that session. Hence, temperatures that generated in the range between 38.3 and 47 C^{o} were credible. Nevertheless, to assess the accuracy of the results, they need to be compared with the measurements of Hilla climate gained from monitoring station at that land. The accuracy with average of 3 ^{0}C RMSE was reliable since Landsat TIRS gave temperatures greater than the real ones. This is due to the fact that TIRS does not determine the air as the station does (Sameen, et al., 2014). Table (4.4) shows the comparison between the air temperature (Observed) and land surface temperature (Estimated) in Hilla Meteorological Station. Figure (4.18) shows the plot of the relationship between air temperature and LST.

Table (4.4): A comparison between the observed and the retrieved surface temperature data for Hilla Meteorological Station.

Year		Air Temperature measured (C^{o})	Land Surface Temperature calculated(C^{o})
2013	July	43.3	47
2014		43.8	42.5
2015		45.6	47
2016		44.7	42
2017		45.9	42.2
2018		43.6	38.3
2019		43.7	42.6

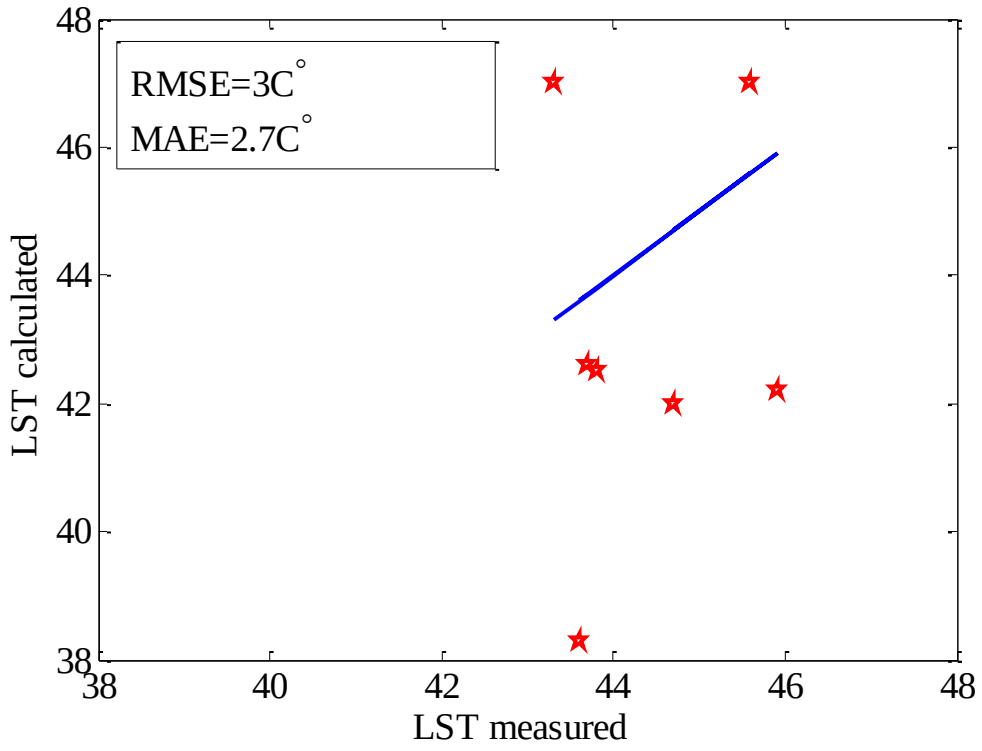

Fig (4.18): The relationship between the observed data and the estimated data for selected meteorological station.

LST needs verification in order to ensure the accuracy of the results. Thus, air temperature data was gained from the Meteorological Department of Baghdad City for Hilla Station.

Air temperature data for Hilla Station was acquired from the Meteorological Department in Baghdad City. Table (4.4) displays the mean data for every year in correspondence with the Landsat satellite data period. The greatest temperature recorded was 45.9 ^{0}C while the lowest one was 43.3 C, according to the data obtained from the meteorological station.

Compared to the reported temperature, a negative difference signifies a higher LST estimate, while a positive variation implies a minimal

appreciation in compared with the recorded one. In urban area, the air temperature varies significantly because of the urban heat index (UHI).

In the years 2013 and 2015 for example, higher temperature was recorded because the radiation released by vegetation, pavement surface, water, urban land and soil was at its maximum value. Nevertheless, checking the accuracy of the results is achieved by comparing them with the calculations obtained from Iraqi weather monitoring station at that region.

(Al-Anbari et al. , 2019) proposed a model to estimate high resolution air temperature for different regions. Based on climate data sets calculated by the Iraqi Agrometeorological Network daily air temperature and ground surface temperature derived from thermal bands of Landsat 8 images over part of Babylon governorate as a case study. For the year 2017, observations from four weather stations in the governorate of Babylon for four months from (6-9) were used for air temperature modeling and accuracy assessment. LST validation models are through measurements near-surface air temperature. The comparison was made with air temperature, which is different and can sometimes result in big differences since the resolution of Landsat 8 for the used bands is 100 m for the thermal band and 30 m for the red and NIR bands. The LST was calculated and taken for the pixel in which the meteorological station fell. Sometimes, the differences can be very big depending on the weather condition. It should also be taken into consideration that there is 1.1 to 2 meters difference between the LST and the air temperature, which means that differences in the temperatures are normal and expected.

4.7 Polygon of Hilla River basin temperature

The NDVI layer was used to separate water from green areas and buildings by using the raster calculator in the QGIS program using the code NDVI layer <= 0 to generate layer as shown in Figure (4.19).

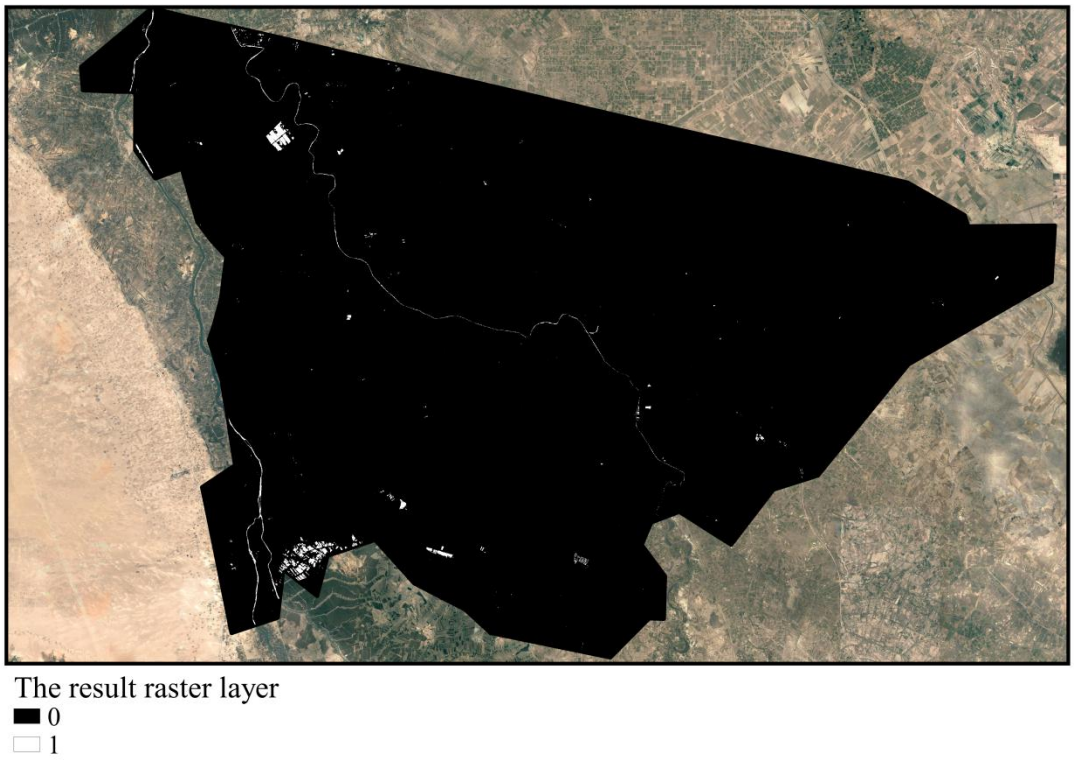

Fig. (4.19): Raster generated for Hilla River extraction.

After that, a polygon was made for Hilla River area and the resulting raster was cut on the basis of this polygon as shown in Figures (4.20 and 4.21). The Hilla River basin was cut by polygon to study the change in temperature in this area.

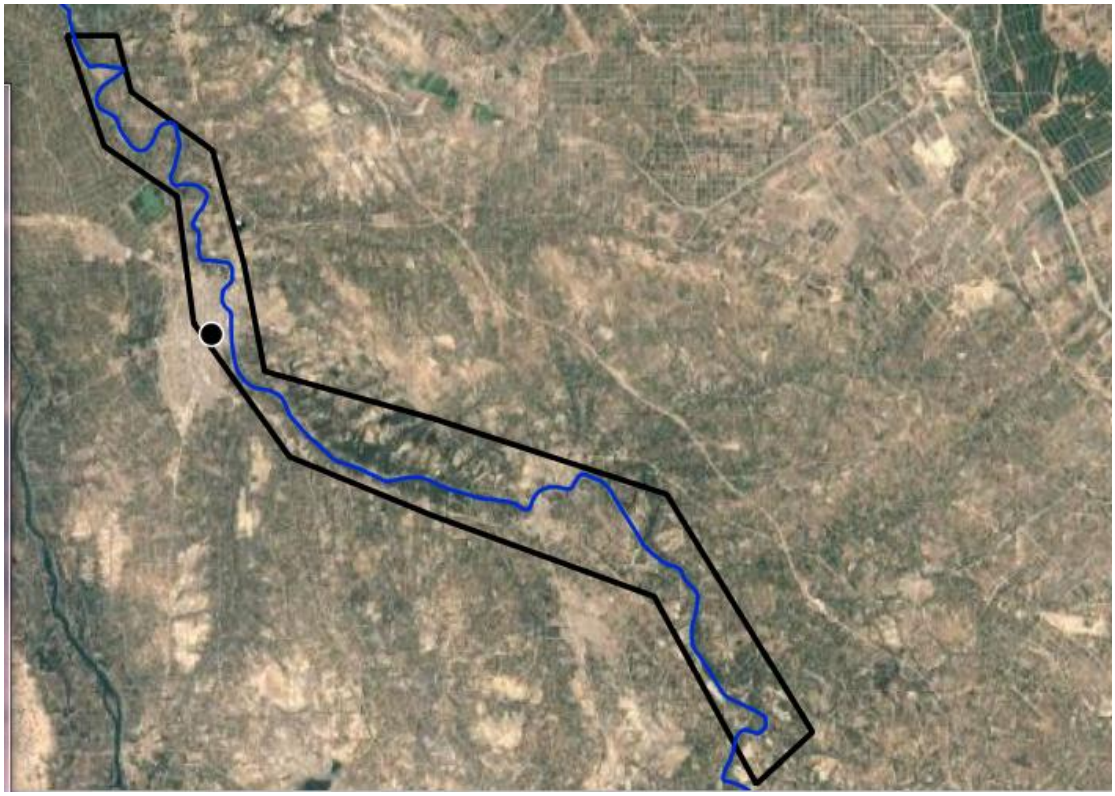

Fig. (4.20): Polygon of Hilla River basin.

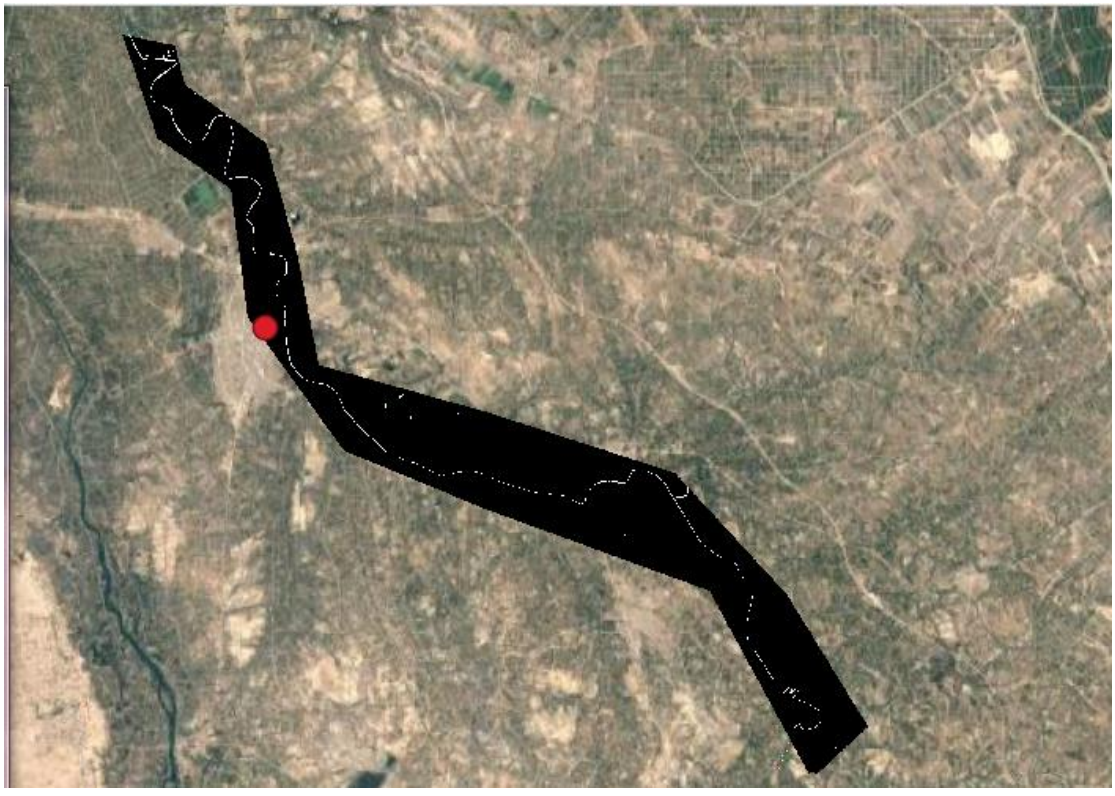

Fig. (4.21): Clip of raster based on polygon.

The layer resulting from the cutting is converted into a vector for cutting layers at the temperature based on it (Figure 4.22).

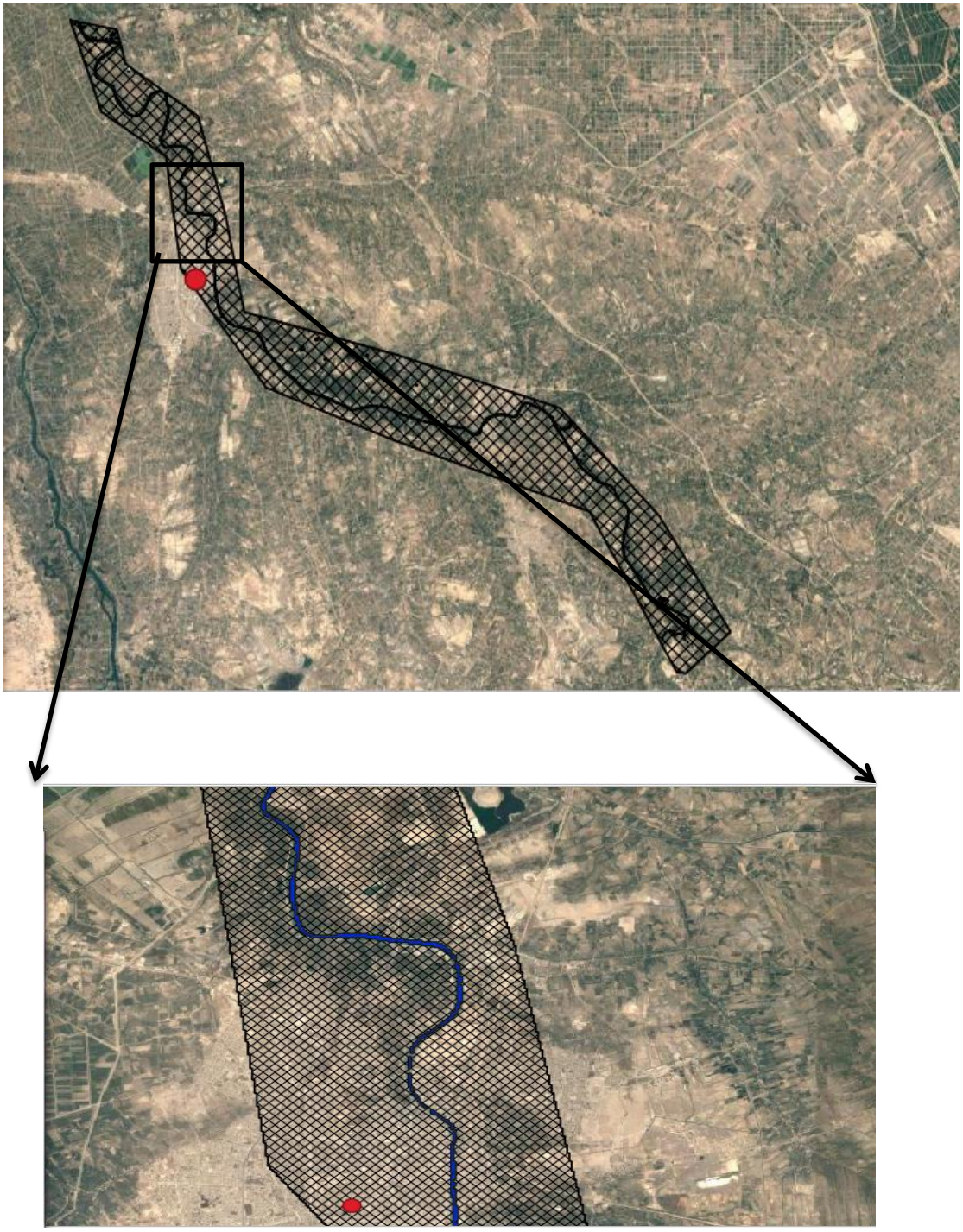

Fig. (4.22): Vector of polygon.

The Hilla River Basin in Babylon Governorate is a well-known local environment. Nevertheless, Hilla River Basin suffered of deterioration in its eco-environment in the last years. To supervise the alteration in temperature as well as land cover/land use in this region, the region was divided into three land cover types which are water body, farming region and urban region. A monitored classifier is applied to the nearby Landsat scene in order to cover the whole basin of Hilla River in the city of Babylon. The classification images were generated in 2013 to 2020 respectively. Analyzing the dynamic alterations of these three categories in term of LULC in the period from 2013 to 2020 utilizing post-classification technique leads to obtain several conclusions. Farmland suffers of declination this associated with increase in the urban lands and various rates during the last years. These trends can be attributed to the expansion of the urbanized areas and other factors. Thus, higher temperatures were recorded in middle of the study region in compared with the other parts of the region as shown in Figure (4.23).

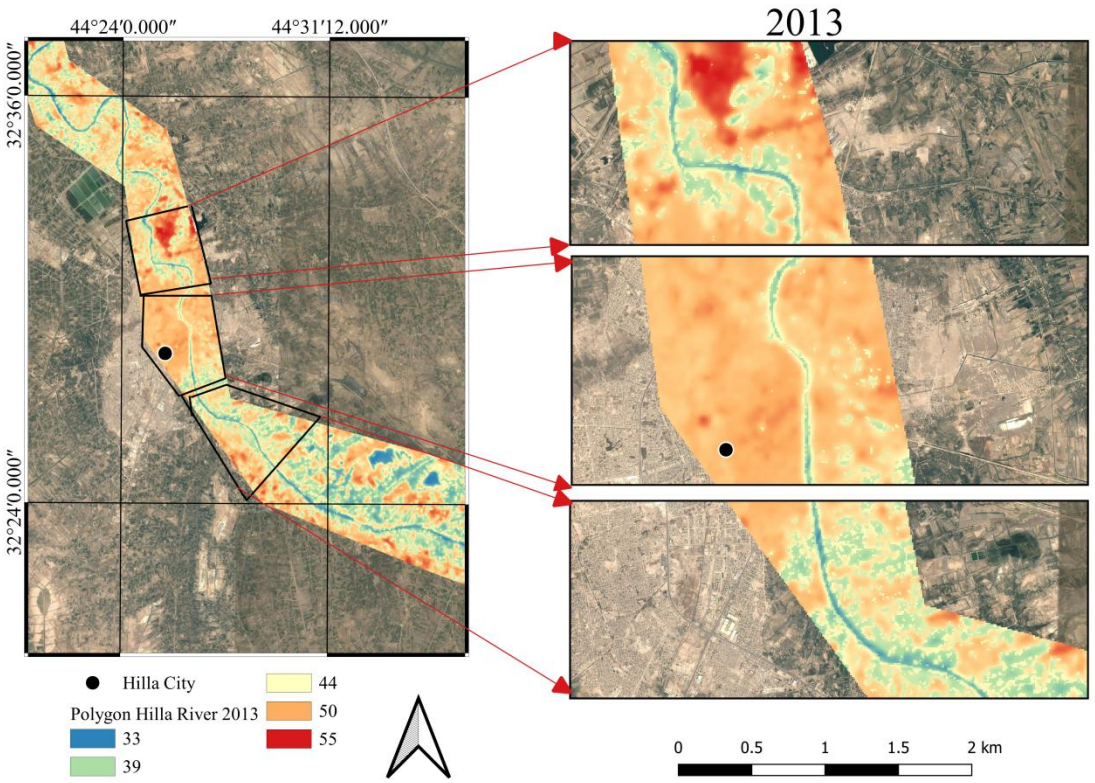
2013
44°24'0.000"
44°31'12.000"
32°36'0.000"
32°24'0.000"
Hilla City
Polygon Hilla River 2013
33
39
44
50
55
0
0.5
1
1.5
2 km

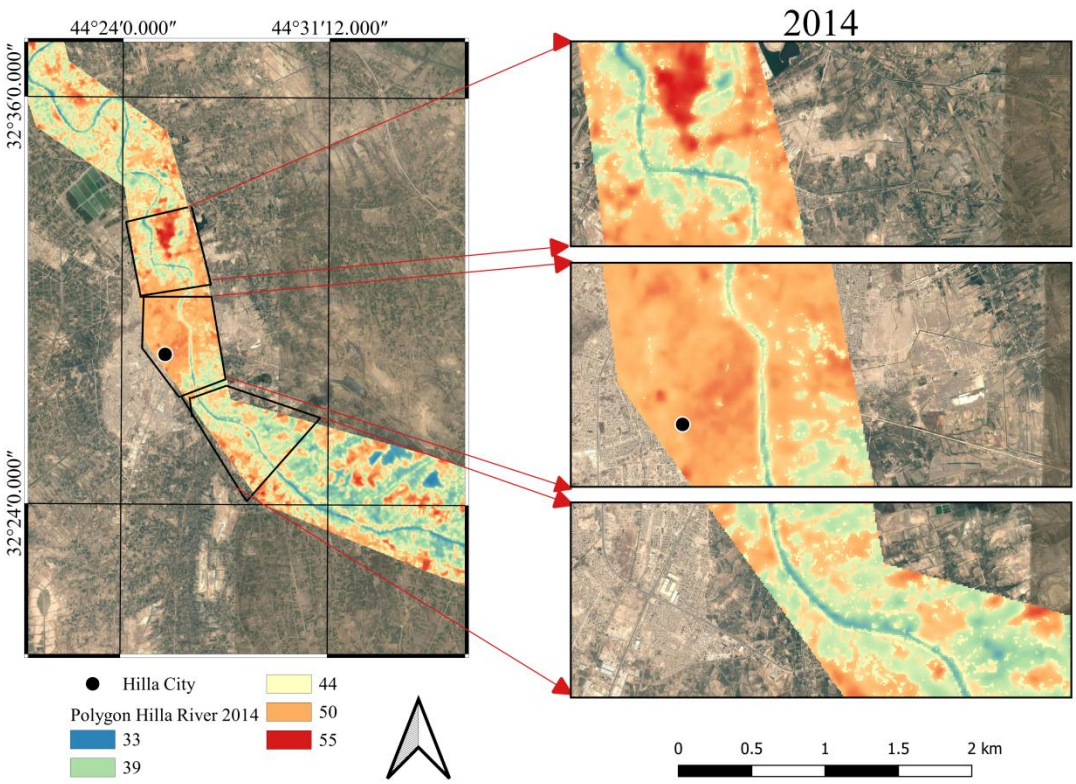
2014
44°24'0.000"
44°31'12.000"
32°36'0.000"
32°24'0.000"
Hilla City
Polygon Hilla River 2014
33
39
44
50
55
0
0.5
1
1.5
2 km

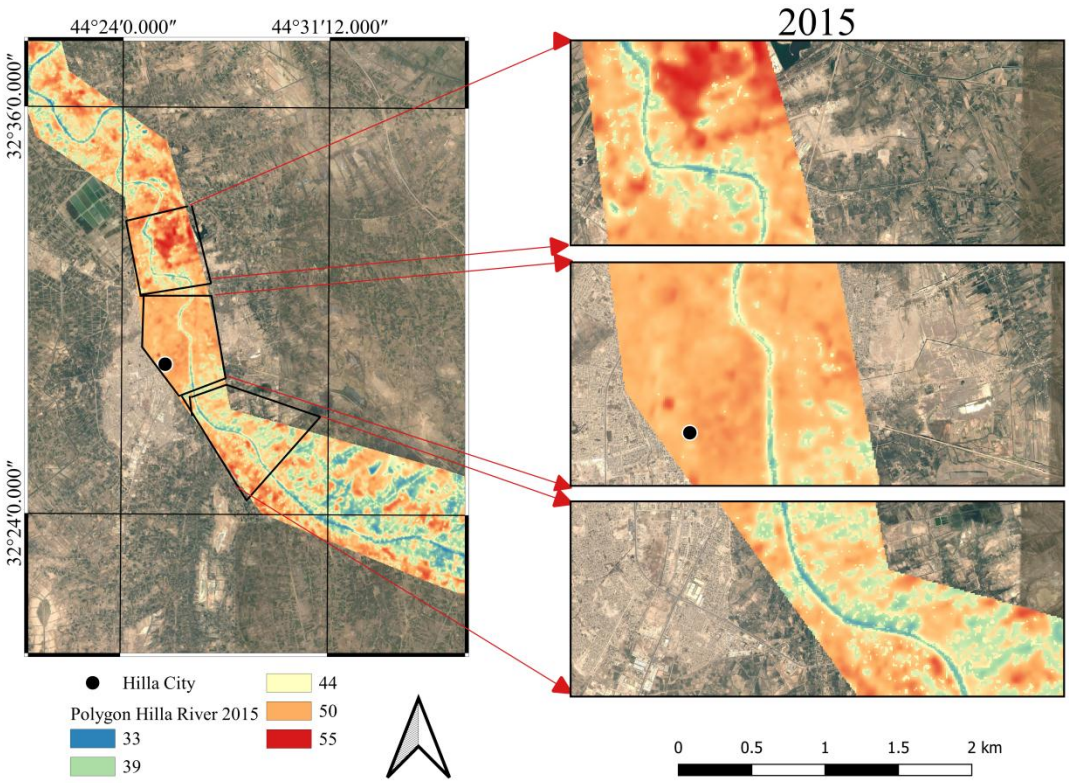
2015
44°24'0.000"
44°31'12.000"
32°36'0.000"
32°24'0.000"
Hilla City
Polygon Hilla River 2015
33
39
44
50
55
0
0.5
1
1.5
2 km

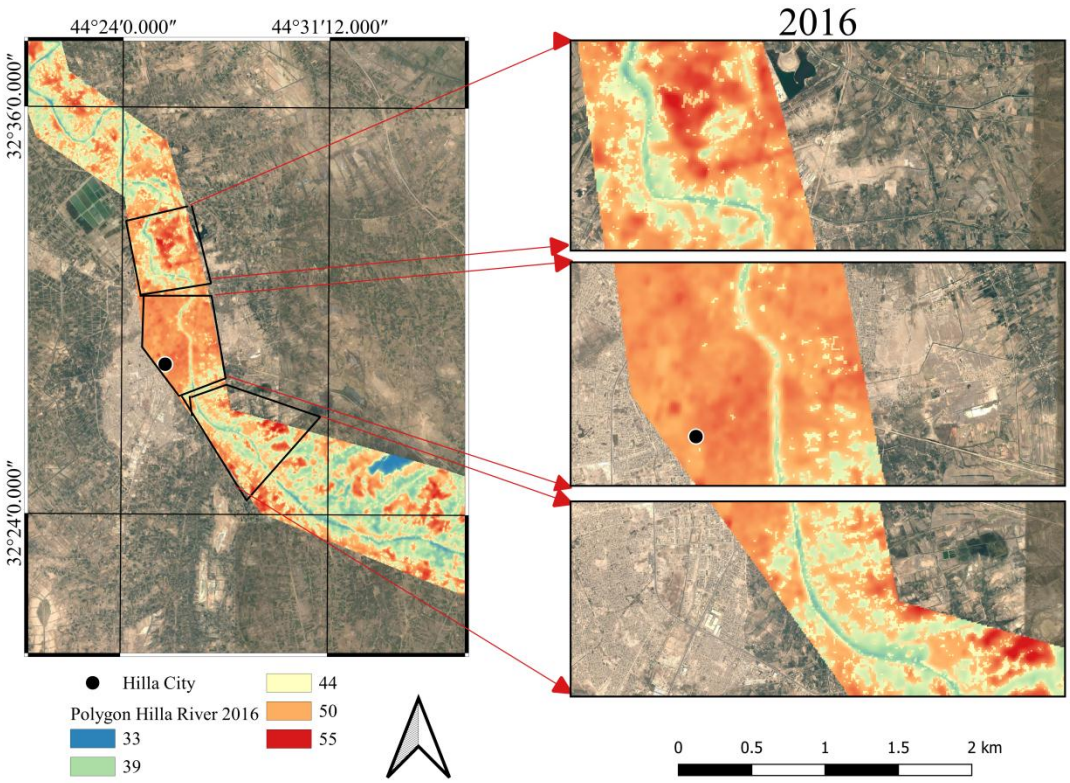
2016
44°24'0.000"
44°31'12.000"
32°36'0.000"
32°24'0.000"
Hilla City
Polygon Hilla River 2016
33
39
44
50
55
0
0.5
1
1.5
2 km

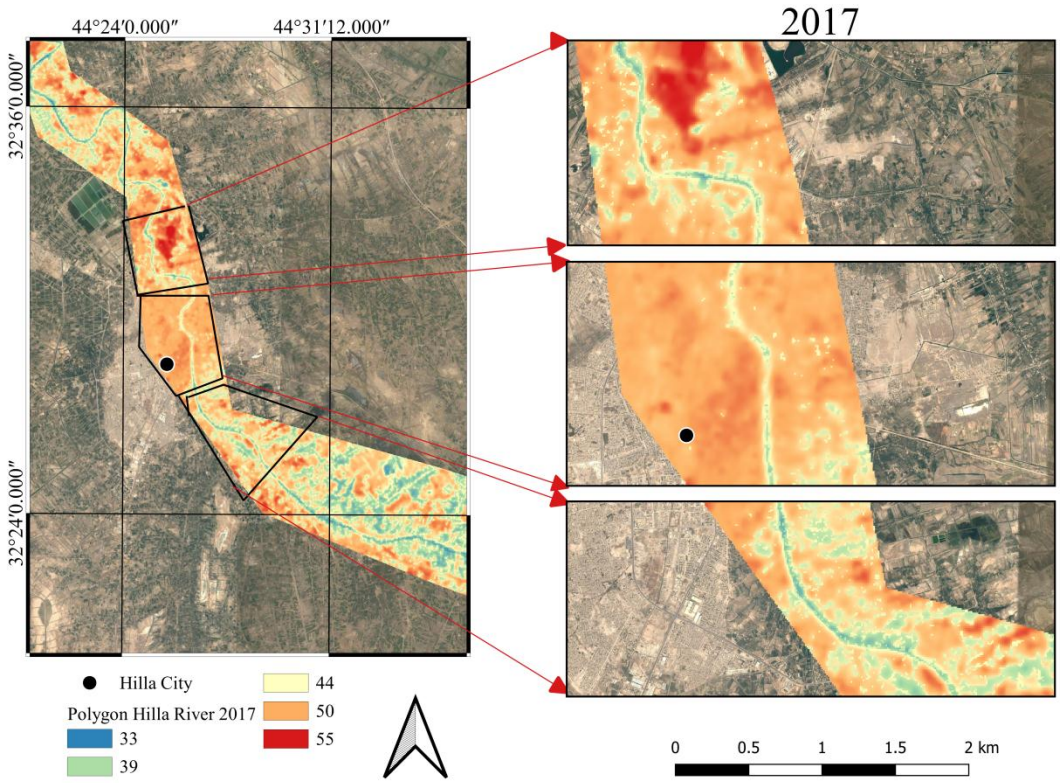
2017
44°24′0.000″
44°31′12.000″
32°36′0.000″
32°24′0.000″
Hilla City
Polygon Hilla River 2017
33
39
44
50
55
0
0.5
1
1.5
2 km

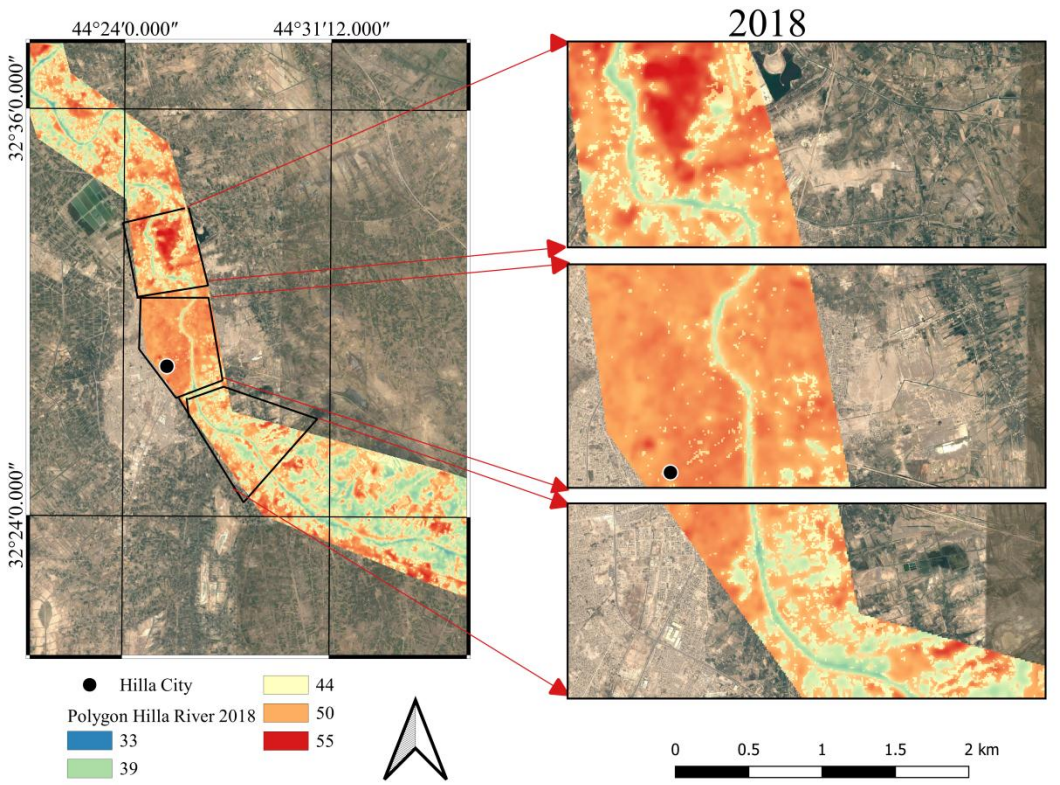
2018
44°24′0.000″
44°31′12.000″
32°36′0.000″
32°24′0.000″
Hilla City
Polygon Hilla River 2018
33
39
44
50
55
0
0.5
1
1.5
2 km

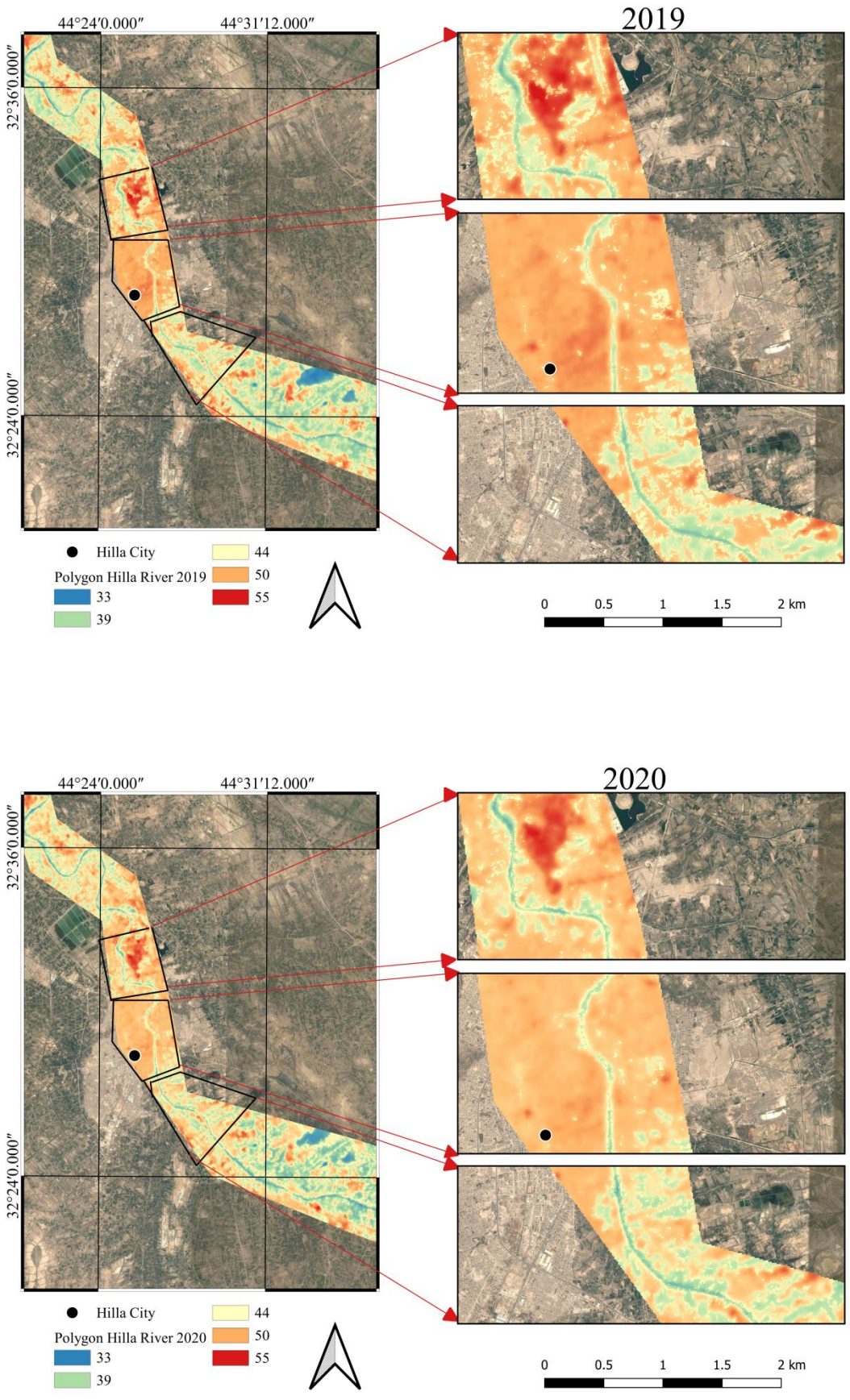

Fig. (4.23): Polygon of Hilla River basin temperature change.

As it is evident from the figure above, the temperature of the river basin began to rise with time. In the year 2013, the temperature is average and began to rise gradually in 2014 and 2015, and the temperature raised significantly in 2016, 2017, 2018 and 2019, but in 2020 the temperature droped slightly compared to last years.

4.8 Urbanization and river temperature

Zero values are omitted from the attribute table of the resulting polygon to obtain only the river and the remaining areas are discarded to study the change in river temperature as shown in Figures (4.24 and 4.25).

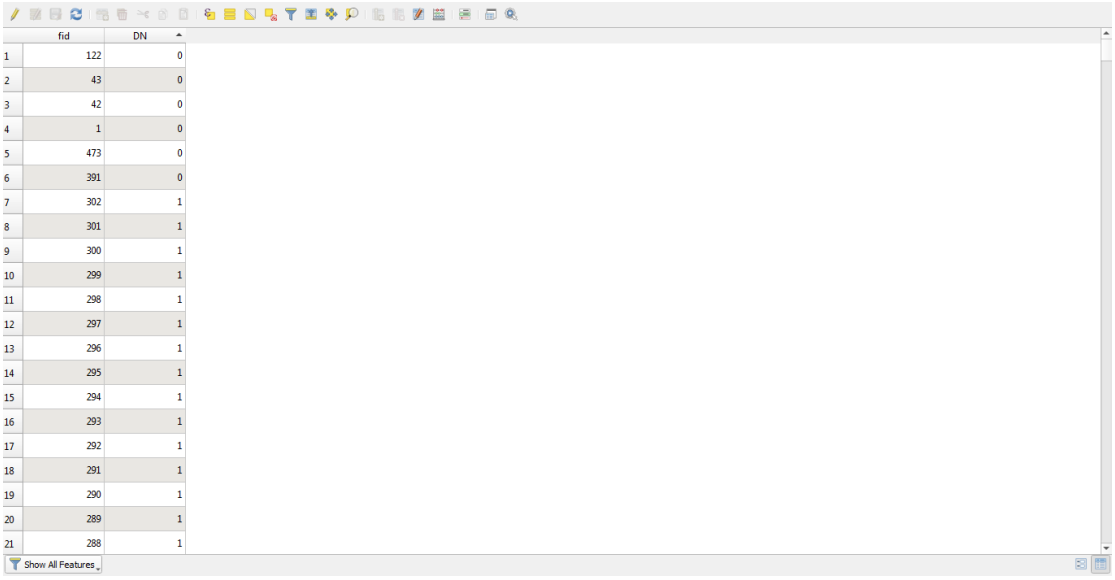

	fid	DN
1	122	0
2	43	0
3	42	0
4	1	0
5	473	0
6	391	0
7	302	1
8	301	1
9	300	1
10	299	1
11	298	1
12	297	1
13	296	1
14	295	1
15	294	1
16	293	1
17	292	1
18	291	1
19	290	1
20	289	1
21	288	1

Show All Features

Fig. (4.24): Window of attribute table.

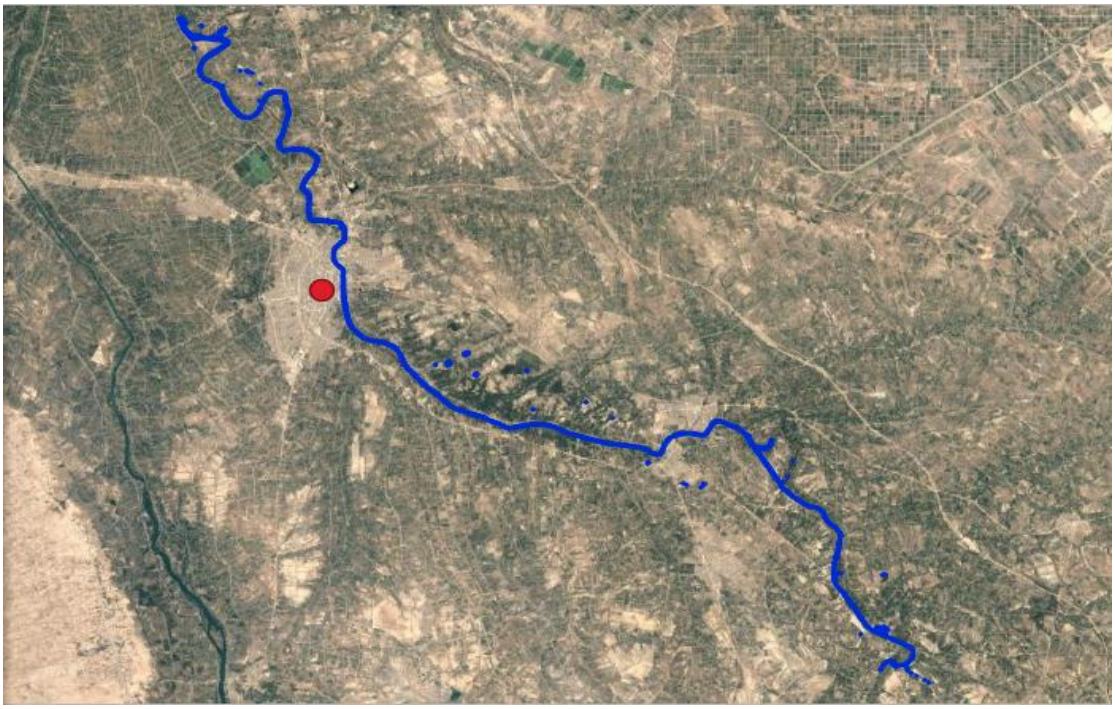

Fig. (4.25): Hilla River.

Increased river temperatures are a common consequence of urbanization, particularly in the summer because of the production of isolated heat storage or urban heat island near cities. Many other facets of urbanization will lead to stream warming as well, including: Riparian changes will minimize canopy cover and shading, allowing more sunlight to enter the water's surface.

Storm water runoff from warm impervious surfaces will heat surface waters and minimize colder groundwater inputs by reducing infiltration.Wastewater inputs can result in direct discharge of warmer effluents into rivers.

One of the water quality parameters affected by urbanization is river temperature. River temperature is an important physical characteristic of water quality. Usually, the presence of water bodies reduces LST. Cities alter the thermal regime of urban rivers in very variable ways for Hilla River basin. Alteration in river temperature has significant influence on

human and environment. This section gives a new idea about the subject by assessing alterations in temperature of river for the city of Babylon for the period ranged from 2013 to 2020 as shown in Figure (4.26). The knowledge available about space-time variability is very limited. Historical evidence about the increase in the temperature of Hilla river in the last years is available. Nevertheless, the attribution of alterations gain low acceptance due to the complexity of river temperature, and the dynamic response to hydrological and climate pattern influenced by anthropogenic effects and basin characteristics.

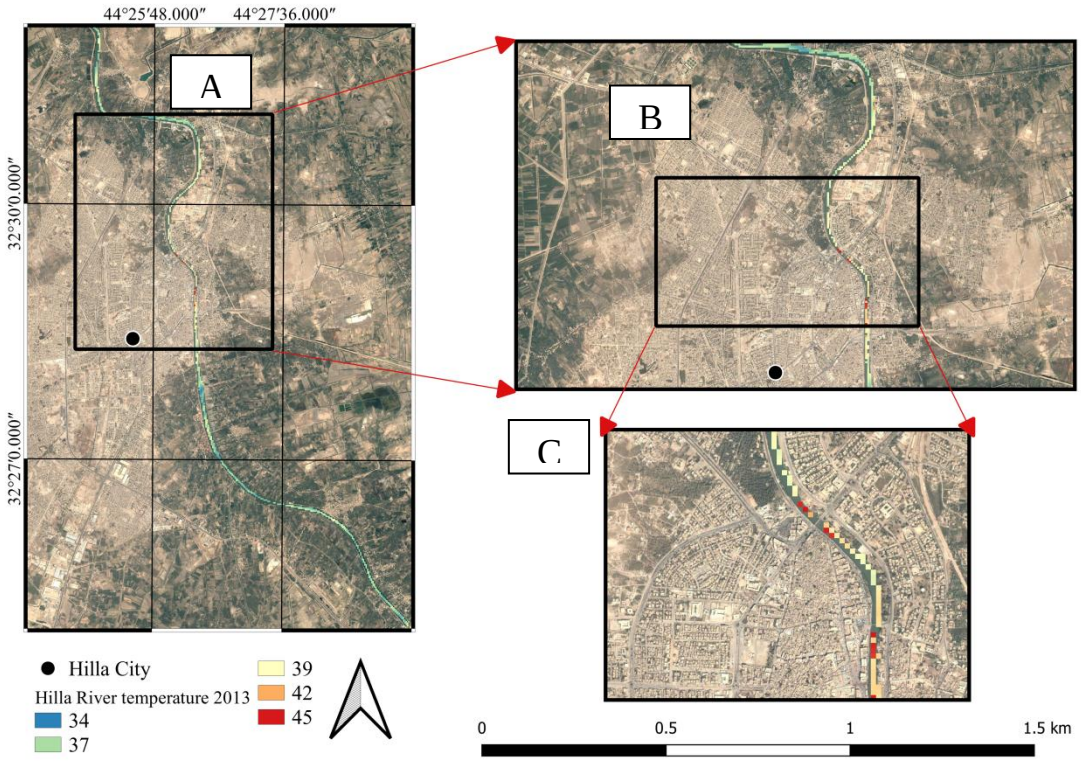

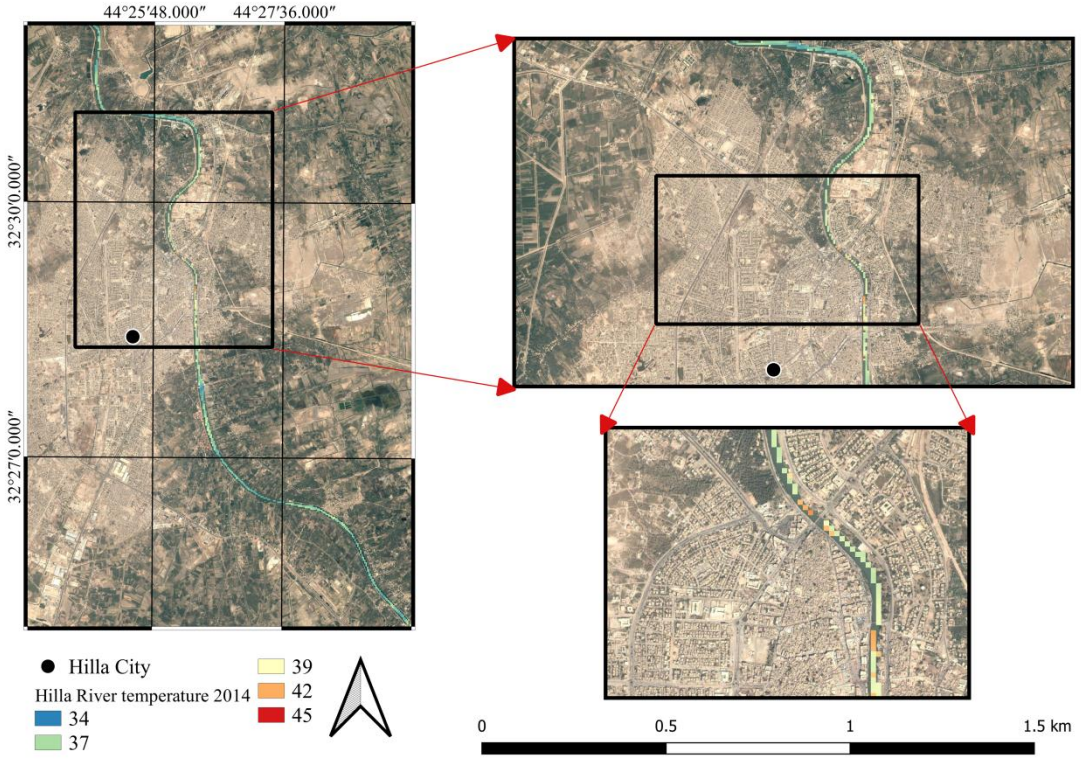
44°25'48.000"
44°27'36.000"
32°30'0.000"
32°27'0.000"
Hilla City
Hilla River temperature 2014
34
37
39
42
45
0
0.5
1
1.5 km

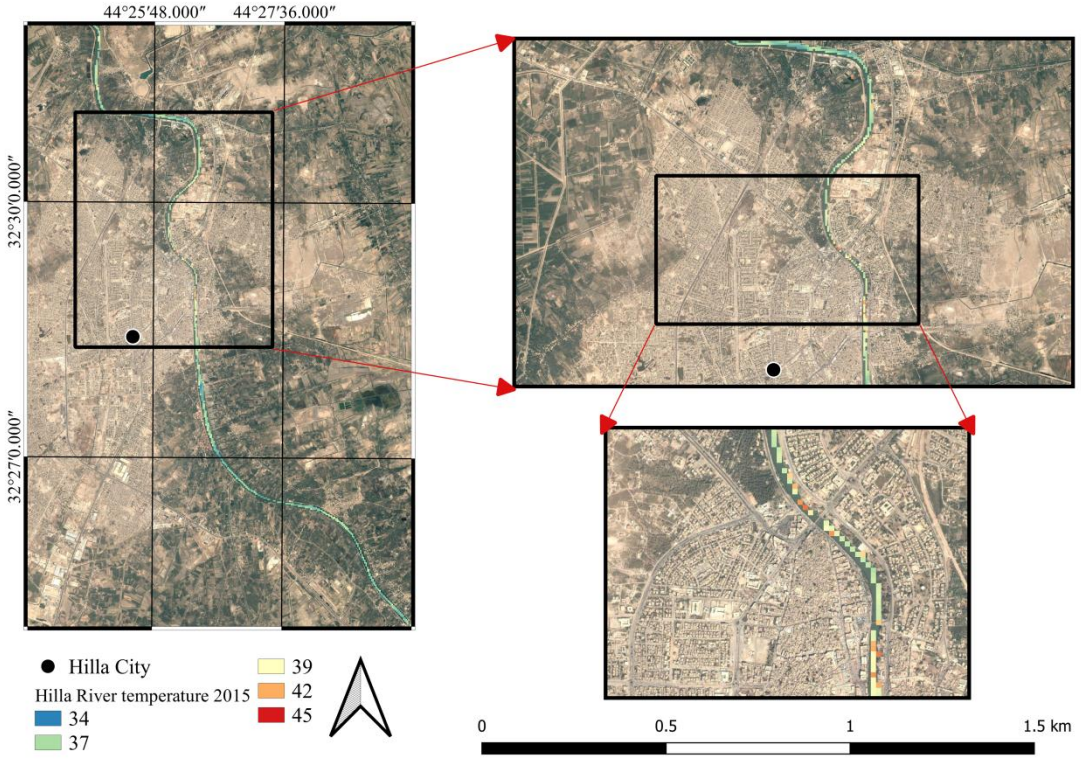
44°25'48.000"
44°27'36.000"
32°30'0.000"
32°27'0.000"
Hilla City
Hilla River temperature 2015
34
37
39
42
45
0
0.5
1
1.5 km

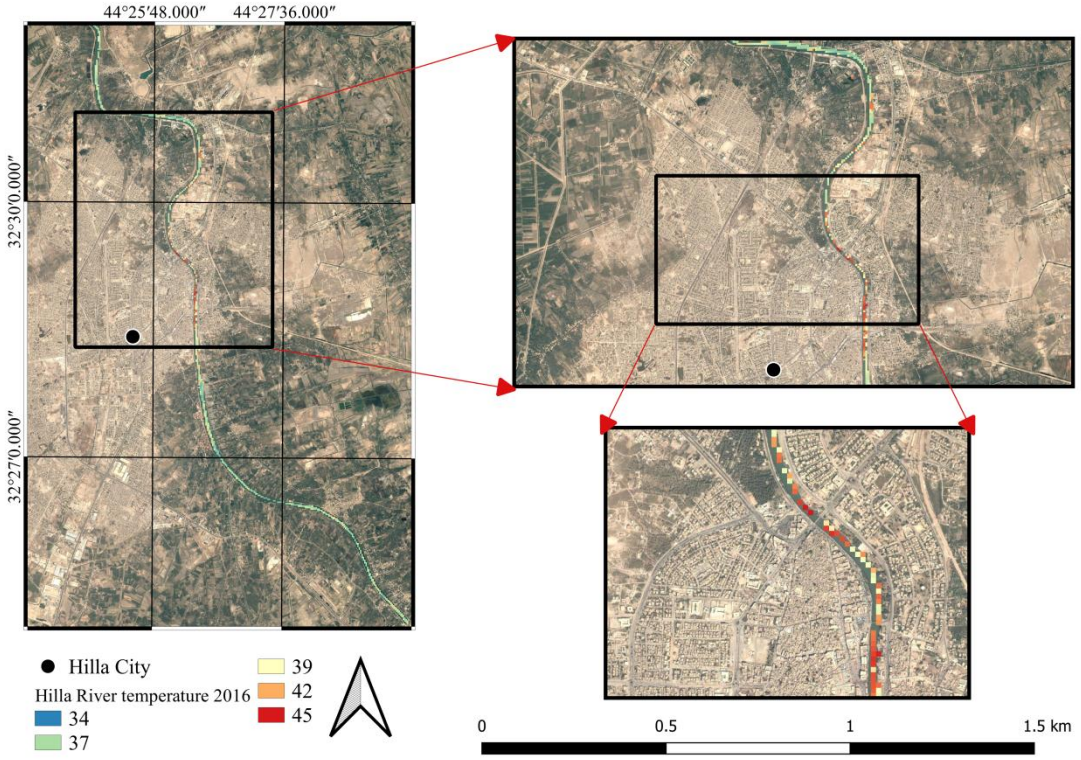
44°25'48.000"
44°27'36.000"
32°30'0.000"
32°27'0.000"
Hilla City
Hilla River temperature 2016
34
37
39
42
45
0
0.5
1
1.5 km

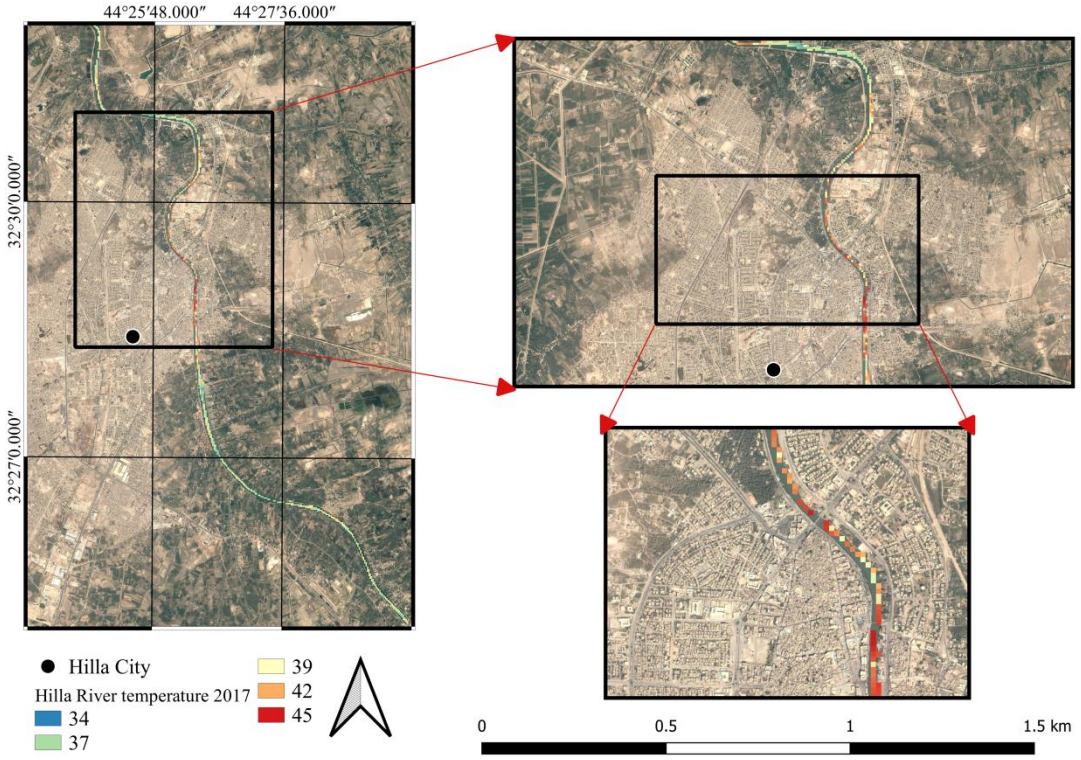
44°25'48.000"
44°27'36.000"
32°30'0.000"
32°27'0.000"
Hilla City
Hilla River temperature 2017
34
37
39
42
45
0
0.5
1
1.5 km

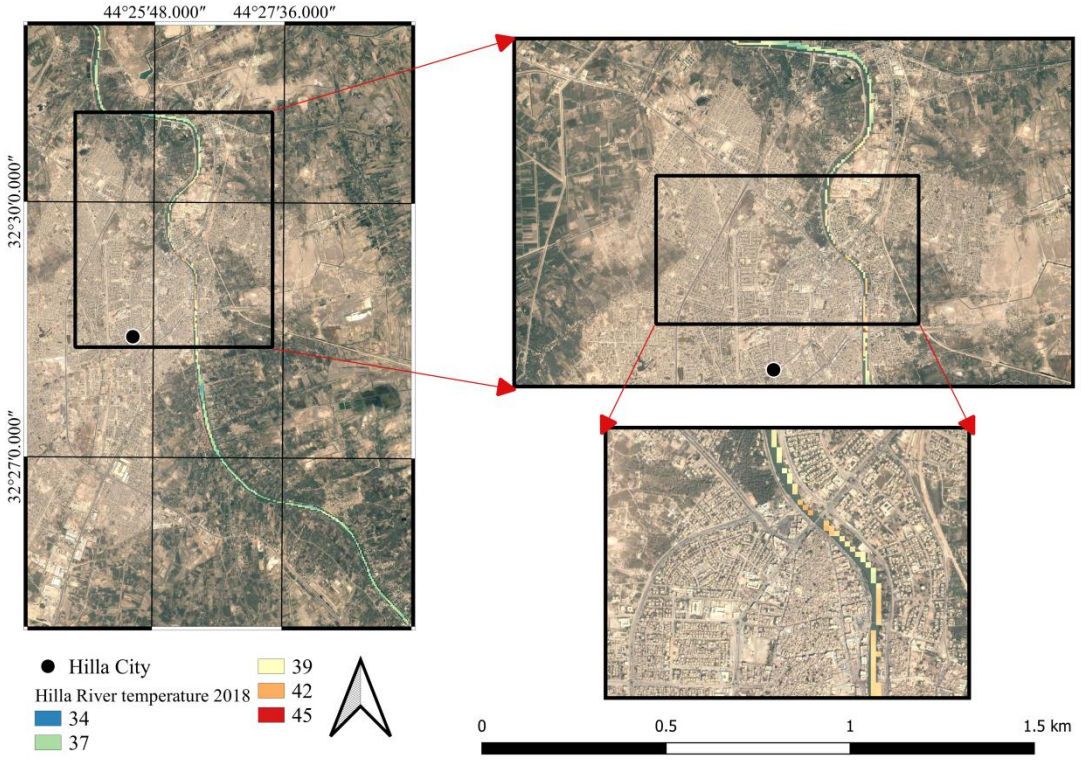
44°25'48.000"
44°27'36.000"
32°30'0.000"
32°27'0.000"
Hilla City
Hilla River temperature 2018
34
37
39
42
45
0
0.5
1
1.5 km

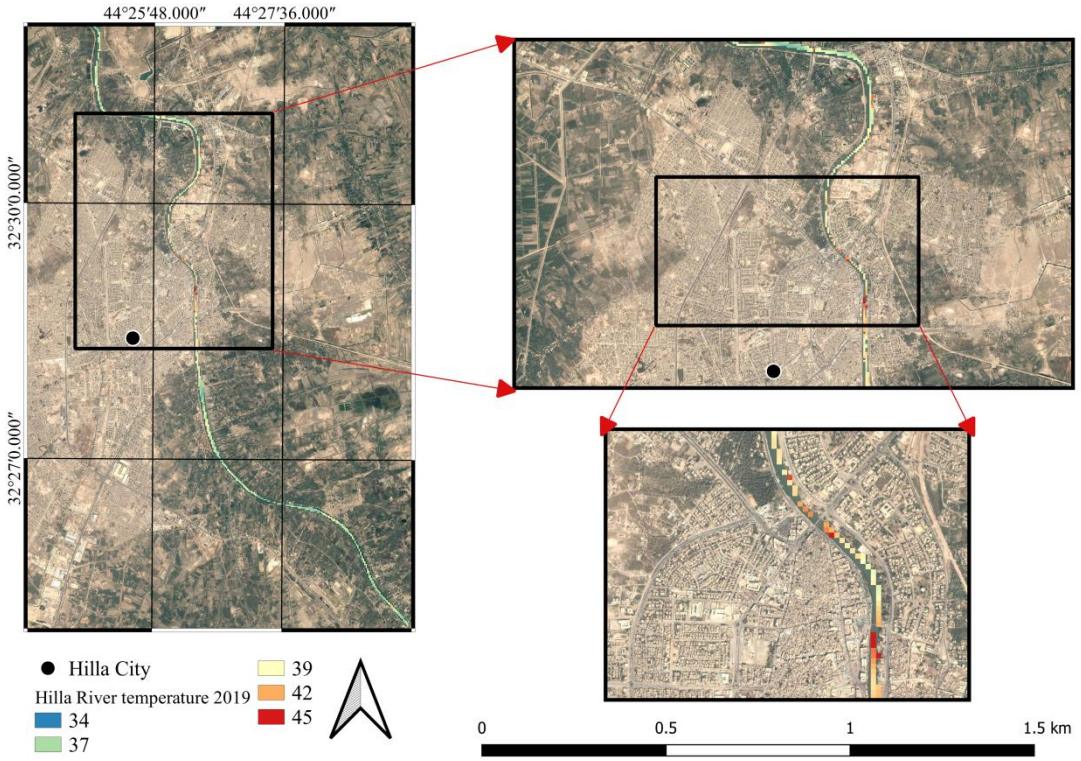
44°25'48.000"
44°27'36.000"
32°30'0.000"
32°27'0.000"
Hilla City
Hilla River temperature 2019
34
37
39
42
45
0
0.5
1
1.5 km

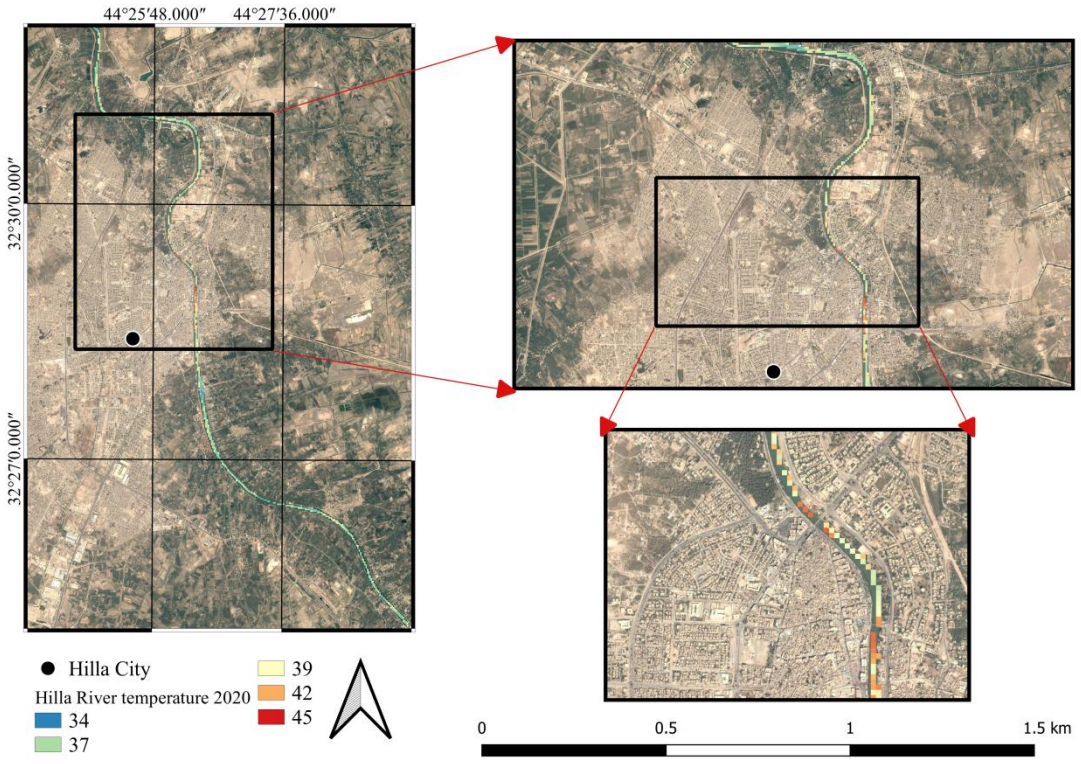

Fig. (4.26): Hilla River temperature change for the period of (2013 to 2020).

Water temperature can be altered by many processes such as disposing hot water from thermal plants in the rivers, rise and fall in water levels, loss of riparian planting, release of water from rivers or lakes.

Water temperature considerably influences the development, the biological activity, water chemistry, quantity of water and kinds of species presented in the water.

The temperature of water decides the kind and numbers of plants, and animals lived in the water bodies.

Temperatures in a stream, river, or lake vary with the seasons, and water is normally warmer on the surface because of higher air temperature and cooler at the bottom because of groundwater input (U.S. Geological Survey and School, 2018)

Most plants and species living in our water bodies have a favorable temperature in order to grow and reproduce, hence the adjustment of the temperatures make them severely harmed.

4.9 Changes for Alsiha District in 2013 and 2020

● LULC area changes for Alsiha District in 2013 and 2020

One of the most dynamic aspects of the climate is Land Use Land Cover (LULC) which have changed dramatically at different scales since the industrial revolution. Land cover of the District of Alsiha was studied exclusively during 2013 and 2020 using satellite scenes, as Landsat OLI 8 satellite images were used. The land has been classified into three subclasses: crop, built-up and water bodies according to the characteristics of the land cover by using the QGIS to show the change of vegetation due to environmental factors and human influences. The years 2013 and 2020 has been highlighted because of its privacy in changing the land cover of the District of Alsiha in which built-up lands have been expanded over the vegitiation. The results indicate to an increase in the bare and built-up area in the last eight years from 2.6 km^2 in 2013 to 2.8 km^2 in 2020. Meanwhile, vegetation and crops have been reduced from 0.31 in 2013 to 0.18 km^2 in 2020. Water bodies have also declined in the same period from 0.11 km^2 to 0.06 km^2.

Moreover, decrease has been observed in water body from 0.11 in 2013 to 0.06 km^2. This item indicated that the main alteration in Alsiha District land occurred in a negative trend in terms of environment concerns (Figures 4.27 and 4.28).

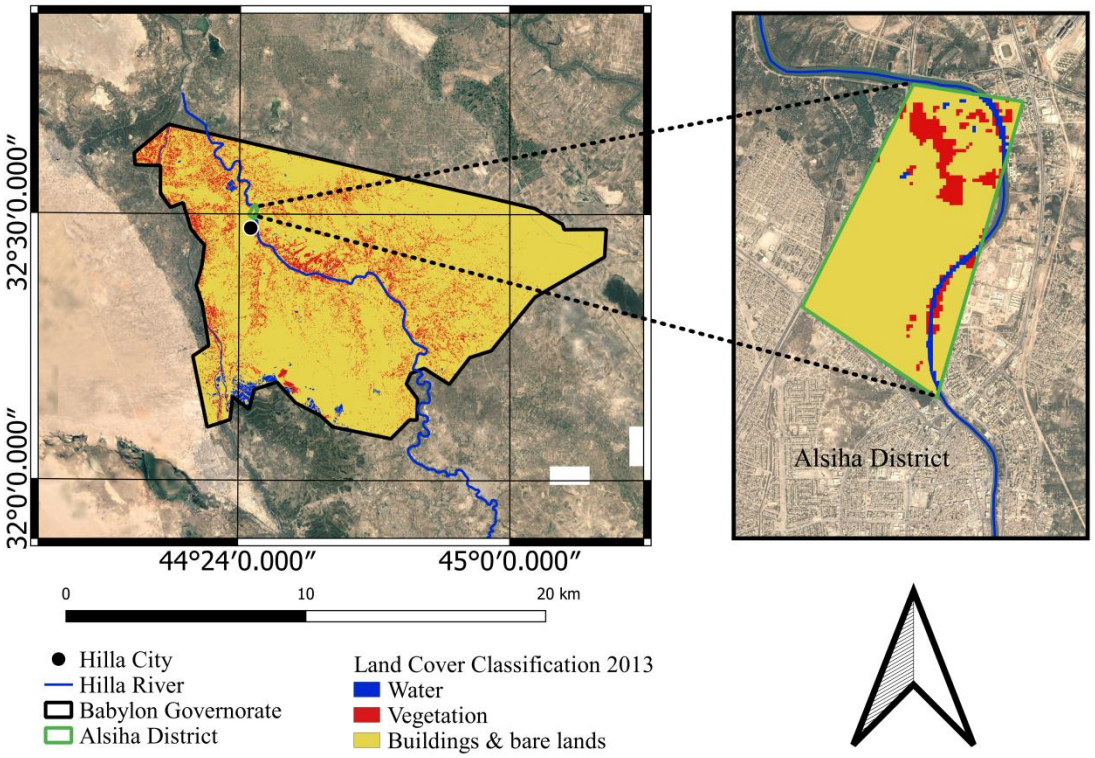

Fig. (4.27): LULC change for Alsiha District in 2013.

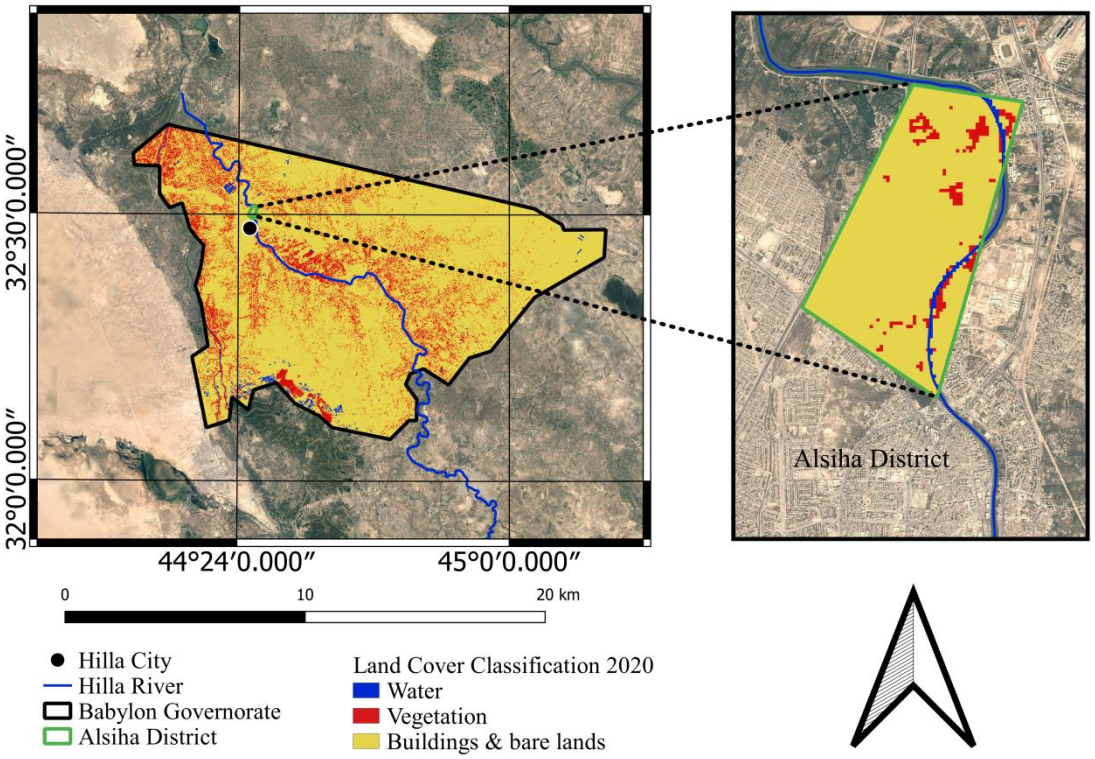

Fig. (4.28): LULC change for Alsiha District in 2020.

This study extends to incorporate the results of modeling LULC by observing the alteration taken place in 2013 and 2020 in Alsiha District and predicting LULC for these years. The comparison between the LULC map of 2013 and that of 2020 showed remarkable decline in vegetation land by about 0.13 km^2 which needs be organized to protect of green environment. Moreover, results showed an increase in the urban land by about 0.2 km^2 which need to be watched to maintain development and limit eco-environment degradation. This results help show how to use Geographic Information System (GIS), Remote Sensing (RS), and QGIS in studying LULC alteration.

Throughout the world, there is remarkable increase in urbanized areas. In the developing counties, the rate of urbanization is considerably high such as in Iraq (Alkaradaghi et al., 2019). This study showed the improvement in the urbanized region in Alsiha District in Babylon Governorate from 2013 and 2020 using different Landsat imagery. However, alteration in land use land cover in the region were determined for 2013 till 2020. In the Change Detection Analysis, an explosive demographic shift in the urban region was occurred, in 2013 water percentage was about 4 % , vegetation was about 10 %, and buildings and bare lands were about 86 % as shown in Figure (4.29).

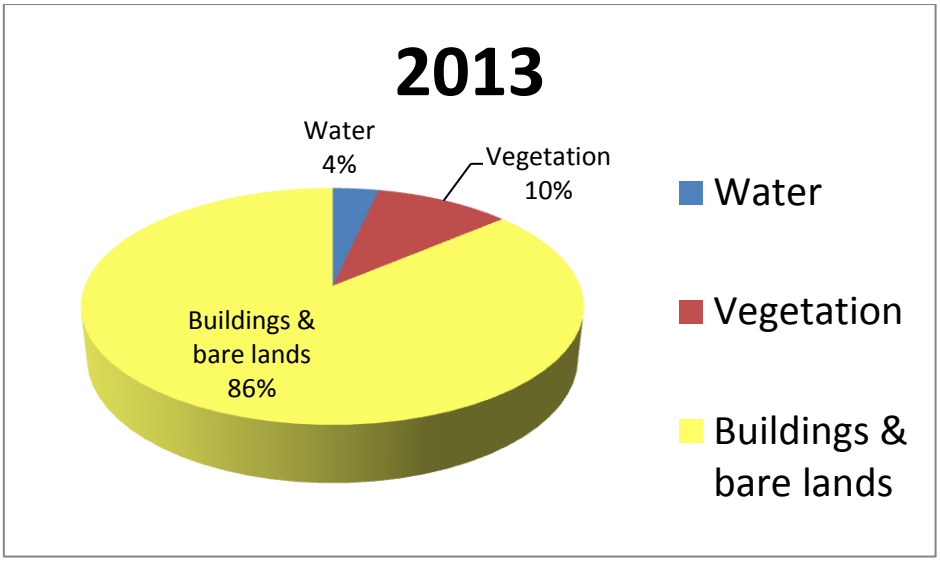

Fig. (4.29): Percentage of LULC categories for Alsiha District in 2013 ; water, vegetation and buildings & bare lands.

On the other hand, in 2020 , water percentage was about 2 %, vegetation was about 6 %, and buildings and bare lands were about 92 %. This work would give the urban planners a great assistance in developing the city in the future by understanding the alteration and developing green sustainability for it (Figure 4.30).

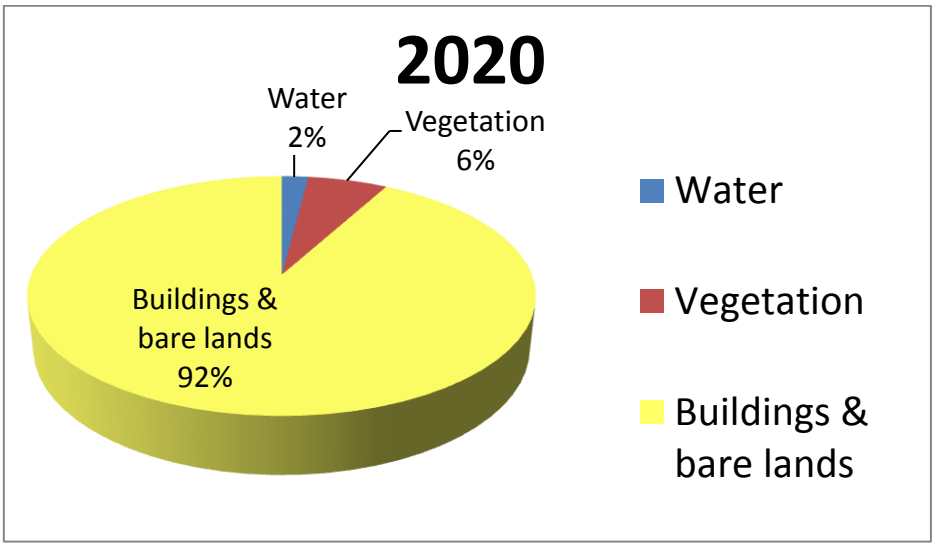

Fig. (4.30): Percentage of LULC categories for Alsiha District in 2020 ; water, vegetation and buildings & bare lands.

● LST changes for Alsiha District in 2013 and 2020 .

The results gathered for the section have been used to draw a map of the Alsiha District's absolute LST. Figures (4.31 and 4.32) show the computed value of LST map. LST value was between 36-50 ^{0}C in 2013, while it was 40-54.6 ^{0}C in 2020. This indicated that the maximum LST value for the entire land increased by 4.6 ^{0}C from 2013 to 2020, the minimum temperature increased by 4 ^{0}C from 36 ^{0}C to 40 ^{0}C. This increase can be attributed to the urbanization and replacement of vegetation with buildings.

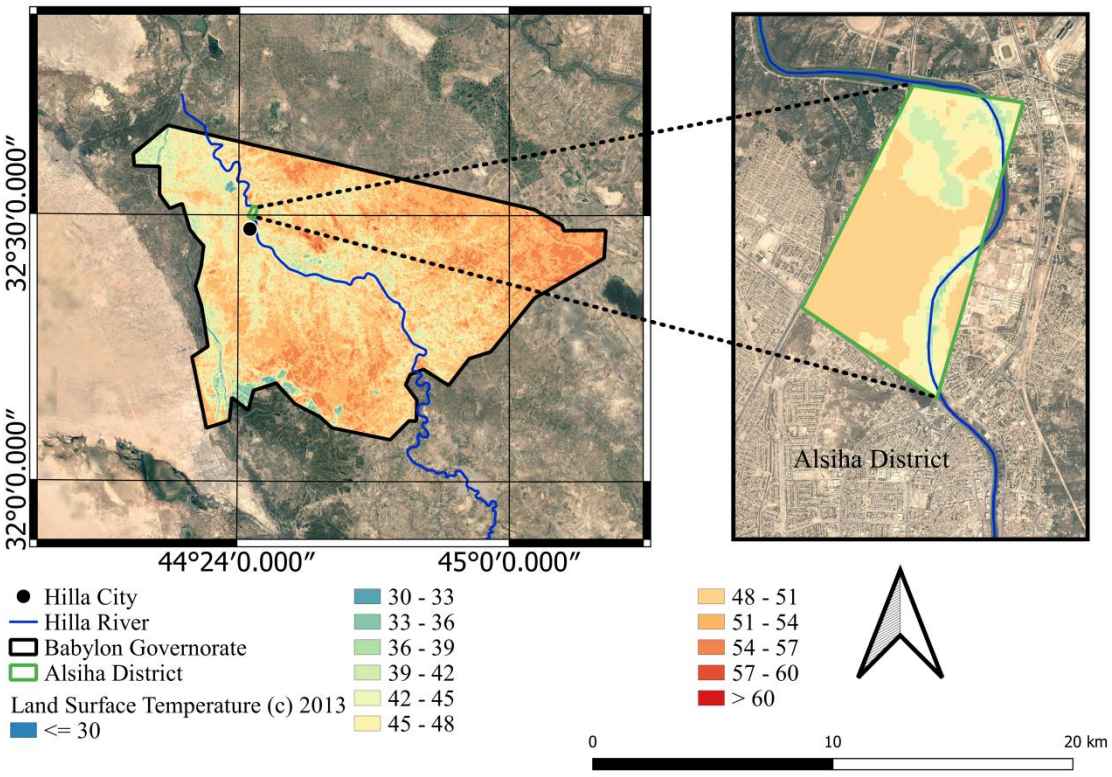

Fig. (4.31): LST changes for Alsiha District in 2013.

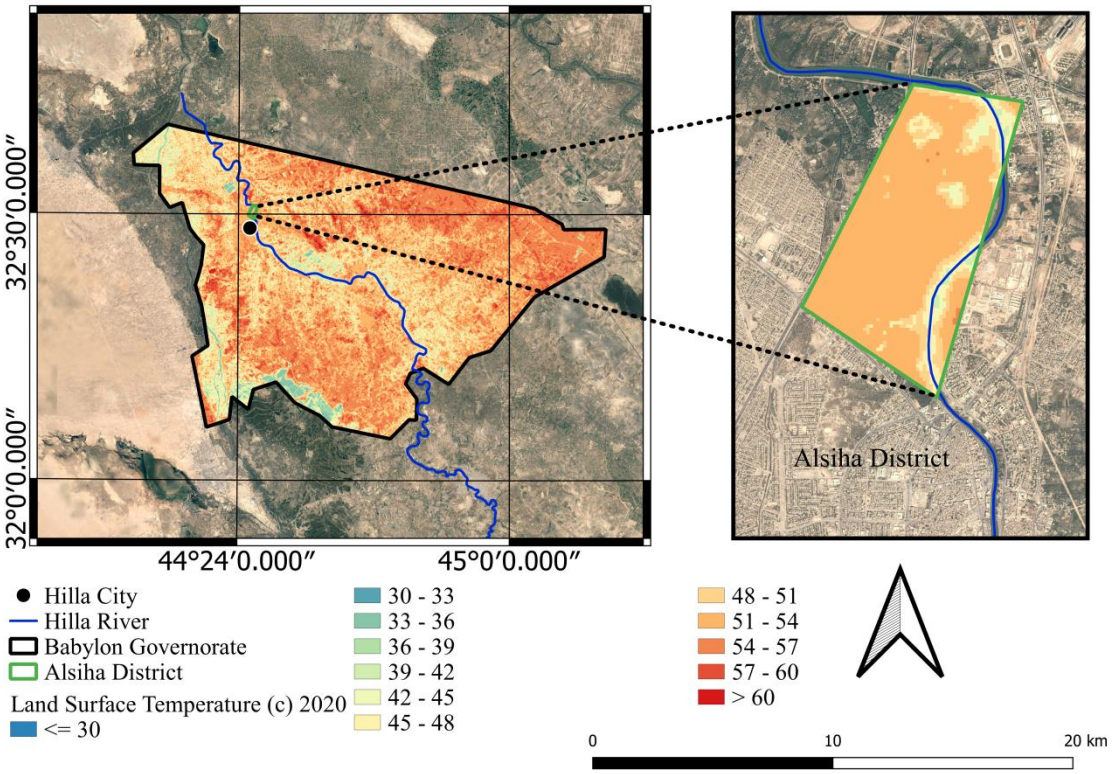

Fig. (4.32): LST changes for Alsiha District in 2020.

4.10 Comparison between temperature data download from NASA site and temperature calculated in QGIS

In this comparison, temperature data was downloaded from the NASA website. Points were taken with specific coordinates, including a water body, plants, buildings, and barren lands. Data for those points were presented from the NASA website regarding temperature data and an excel file was downloaded for each location. The temperature of those locators was calculated using the QGIS program and a comparison was made between them. The results were plotted in Matlab. Finally, RMSE and MAE results were extracted for each drawing as shown in Figure (4.33).

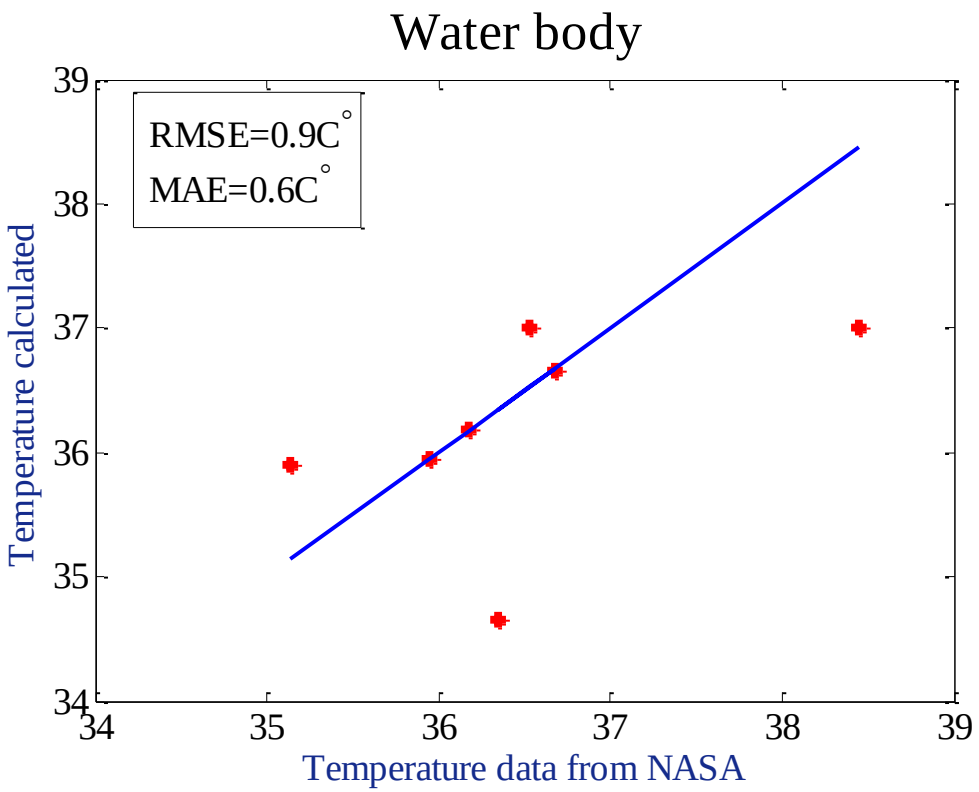
Water body
RMSE=0.9C°
MAE=0.6C°
Temperature calculated
Temperature data from NASA
34
35
36
37
38
39

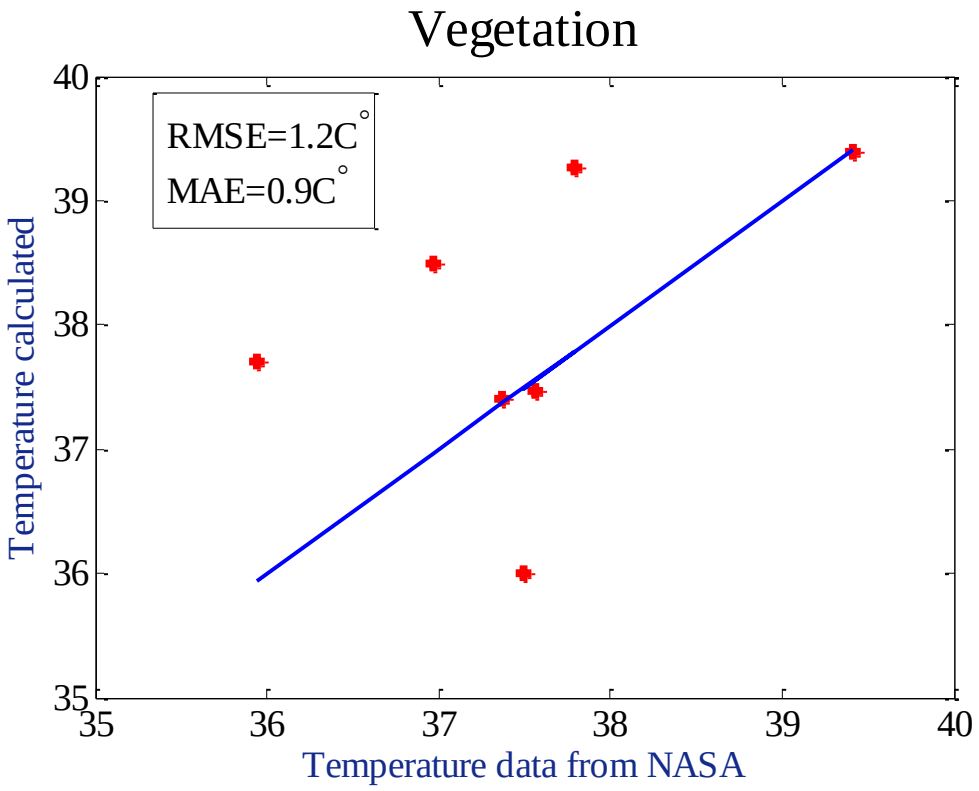
Vegetation
RMSE=1.2C°
MAE=0.9C°
Temperature calculated
Temperature data from NASA
35
36
37
38
39
40

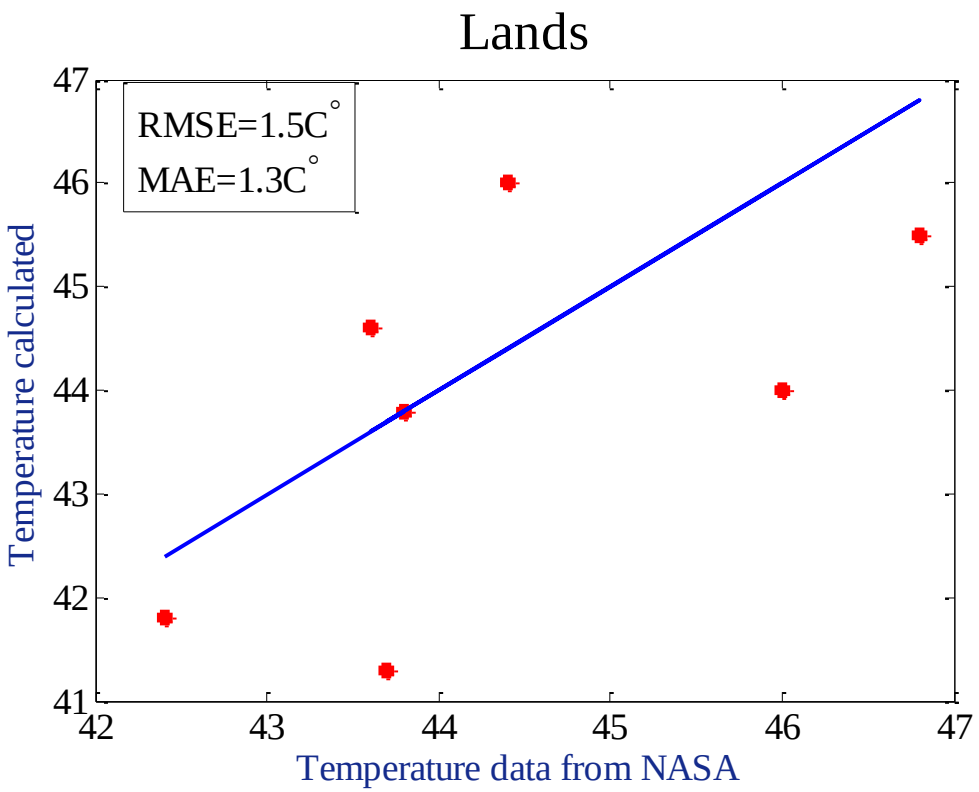

Fig. (4.33): Graphics showing the relationship between the temperature load data from NASA and the calculated temperature.

There is evident from the graphic above. The temperature data loaded from the NASA site were very close to the temperature calculated in the program regarding the water body. For vegetation and lands, RMSE and MAE were found to be low. The RMSE for water bodies is 0.9 and for plants is 1.2, while for lands it equals 1.5. The MAE values were 0.6 and 0.9 for water and plants, respectively, while its value was 1.3 for lands.

CHAPTER FIVE

CONCLUSIONS AND RECOMMENDATIONS

CHAPTER FIVE

CONCLUSIONS AND RECOMMENDATIONS

5.1. Conclusions

The findings of this study are:

1. In Babylon Governorate, lands such as built-up areas and bare regions and vegetation coverage form the main part of land use land cover, controlling the spatial distribution of LSTs.
2. The urban development was the forcing factor that has been changing the temperature distribution spatially and temporally along the study period.
3. The increase in barren lands and built-up areas has widened LSTs distribution and raised temperature in the study area, leading to a warmer local climate conditions.
4. Land covers (water, vegetation, and built-up/bare areas) fluctuated from low to medium to high temperature values, respectively.
5. A valid inverse linear models were found between LST and NDVI. Thus, LSTs can be determined depending on NDVI values only.
6. Air temperature data can be used as an indicator of land surface temperature.
7. Polygon was made for the the Hilla River basin to cut it, and it was observed that temperature within the basin increased with time.
8. Clip of Alsiha District was made, the outcomes showed that build-up and bare land had been increased in the last eight years from 2.6 km^2 in 2013 to 2.8 km^2 in 2020. Vegetation and crops have been decreased from 0.31 in 2013 to 0.18 km^2 in 2020. Moreover, decrease has been observed in water body from 0.11 in 2013 to 0.06 km^2, and the temperature increased in the years 2013 and 2020. LST values showed ranges between thirty five to fifty Celsius in 2013 and forty to fifty four Celsius in 2020.

9. The results of temperature data loaded from the NASA site showed that it was very close to the temperature calculated in thid study regarding to the water body, plants, buildings and barren lands.

5.2 Recommendations

1. The thermal band of the ETM+ sensor on the Landsat 7 satellite may be used to determine land surface temperature. The thermal pictures are transformed to thematic maps that depict land surface temperatures using ERDAS 8.4 software.
2. Selecting night TIR imagery to have a comprehensive thought about the surface temperature properties, further studies on the surface temperature at night are needed. The new researches could utilize the thermal images taken at daytime and nighttime at different seasons to understand seasonal and diurnal alterations in the relationship between the kind of urban buildings and LST.
3. The variation in the temporal and spatial LST can be revealed by various dated satellite photos of Landsat 4, 7 and 8. Also, To determine the LST parameters, ERDAS 2014 software may be utilized.
4. In this research, surface temperature was determined utilizing band 10. Bands 10 and 11 could also be used to find it.
5. There another way to calculate the surface temperature through NDVI can be used.

6- In this research, NDVI was calculated using the level 1 data from Landsat 8, and the NDVI can be calculated using level 2 data from Landsat 8 and compared the results.

7- In this research, maps were produced and results were obtained through the QGIS program, and the results can also be obtained through other programs such as ArcGIS.
8- The surface temperature has been linked to NDVI and can also be linked to other parameters such as NDBI, NDWI.
9- LSTs can be linked with SAVI, MSAVI, DVI, EVI, CL green, ARVI, and MSI.

References

References

Al Ajmi, Dhari, and Saif ud din. 2009. “Remote Sensing: Fundamentals, Types and Monitoring Applications of Environmental Consequences of War.” *Handbook of Environmental Chemistry, Volume 3: Anthropogenic Compounds* 3 U:41–123. doi: 10.1007/978-3-540-87963-3_3.

Al-Anbari, Riyad H., Oday Z. Jasim, and Zainab T. Mohammed. 2019. “Estimation High Resolution Air Temperature Based on Landsat8 Images and Climate Datasets.” *IOP Conference Series: Materials Science and Engineering* 518(2). doi: 10.1088/1757-899X/518/2/022033.

Al-ansari, Nadhir, and Ali Chabuk. 2021. “4/23/2021 (PDF) Soil Characteristics in Selected Landfill Sites in the Babylon Governorate, Iraq.” 2021:1–9. doi: 10.17265/1934-7359/2017.04.005.

Al-Timimi, Yaseen K., Ali M. Al-Salihi, and Alaa M. Al-lami. 2014. “Estimation of Land Surface Temperature for Different Regions in Iraq Using Remote Sensing Technique (ETM+).” *Engineering and Technology Journal* 32(6 Part (B) Scientific).

Ali, Dr. Abdulrahman K. 2010. “Remote Sensing.” *Department of Applied Sciences University of Technology*.

Ali, Jasim M., Stuart H. Marsh, and Martin J. Smith. 2017. “A Comparison between London and Baghdad Surface Urban Heat Islands and Possible Engineering Mitigation Solutions.” *Sustainable Cities and Society* 29:159–68. doi: 10.1016/j.scs.2016.12.010.

Ali, Mr Ershad. 2020. “Geographic Information System (GIS):

Definition, Development, Applications & Components." doi: https://www.researchgate.net/publication/340182760.

Alkaradaghi, Karwan, Salahalddin S. Ali, Nadhir Al-Ansari, and Jan Laue. 2019. "Land Use Classification and Change Detection Using Multi-Temporal Landsat Imagery in Sulaimaniyah Governorate, Iraq." 117–20. doi: 10.1007/978-3-030-01440-7_28.

Anandababu, D., B. M. Purushothaman, and B. S. Suresh. 2018. "Estimation of Land Surface Temperature Using Landsat 8 Data." *International Journal of Advance Research* 4(2):177–86.

Anderson, James Richard. 1976. *A Land Use and Land Cover Classification System for Use with Remote Sensor Data*. Vol. 964. US Government Printing Office.

Avdan, Ugur, and Gordana Jovanovska. 2016. "Algorithm for Automated Mapping of Land Surface Temperature Using LANDSAT 8 Satellite Data." *Journal of Sensors* 2016. doi: 10.1155/2016/1480307.

Beg, Ayad. 2018. "Assessment of Land Surface Temperature Variation over Rusafa Side of Baghdad City, Iraq." *MATEC Web of Conferences* 162(2018):1–7. doi: 10.1051/matecconf/201816203032.

Bentuk, Reka, Pemantauan Kesihatan, and Tanaman Lada. 2021. "Design of NDVI Plant Health Monitoring for Pepper Vines." 2(1):46–50.

Bobrinskaya, Maria. 2012. "Remote Sensing for Analysis of Rela-Tionships between Land Cover and Land Surface Temperature in Ten Megacities." (December).

Congedo, Luca. 2016. "Semi-Automatic Classification Plugin Documentation." *Release* 4(0.1):29.

Dev Acharya, Tri, and Intae Yang. 2015. "Exploring Landsat 8." *International Journal of IT, Engineering and Applied Sciences Research* 4(4):4–10.

Dissanayake, DMSLB, Takehiro Morimoto, Manjula Ranagalage, and Yuji Murayama. 2019. "Land-Use/Land-Cover Changes and Their Impact on Surface Urban Heat Islands: Case Study of Kandy City, Sri Lanka." *Climate* 7(8):99.

Dynamics, Drone. 2015. "NDVI – Normalized Difference Vegetation Index Explained NDVI - Normalized Difference Vegetation Index." 19–21.

Earth Observing System. 2020. "Crop Monitoring." 1–9.

Erasu, D. 2017. "Remote Sensing-Based Urban Land Use/Land Cover Change Detection and Monitoring." *Journal of Remote Sensing & GIS* 6(2):5.

Gosteva, Anna A., Aleksandra K. Matuzko, and Oleg E. Yakubailik. 2019. "Search of Changes in the Temperature of Urban Environment with Use of Satellite Data on the Example of the Krasnoyarsk."

Hashim, Haslina, Zulkiflee Abd Latif, and Nor Aizam Adnan. 2019. "Urban Vegetation Classification with NDVI Thresold Value Method with Very High Resolution (VHR) PLEIADES Imagery." *Int. Arch. Photogramm. Remote Sens. Spat. Inf. Sci* 237–40.

Hunter, Assoc Prof G., and Assoc Prof I. Bishop. 2013. "Introduction to GIS Definition of GIS." *Introduction to GIS* 1–13.

Hussain, Sajjad, Muhammad Mubeen, Waseem Akram, Ashfaq Ahmad, Muhammad Habib-ur-Rahman, Abdul Ghaffar, Asad Amin, Muhammad Awais, Hafiz Umar Farid, and Amjad Farooq. 2020. "Study of Land Cover/Land Use Changes Using RS and GIS: A Case Study of Multan District, Pakistan." *Environmental Monitoring and Assessment* 192(1):1–15.

Ibrahim, Gaylan Rasul Faqe. 2017. "Urban Land Use Land Cover Changes and Their Effect on Land Surface Temperature: Case Study Using Dohuk City in the Kurdistan Region of Iraq." *Climate* 5(1). doi: 10.3390/cli5010013.

Ilayaraja, K., Wasi Reza, Vivek Kumar, Sourov Paul, and Ravindra Chowdhary. 2016. "Estimation of Land Surface Temperature of Chennai Metropolitan Area Using Landsat Images." *Journal of Chemical and Pharmaceutical Sciences* 9(2):E219–22.

Irons, James, Michael Taylor, and Laura Rocchio. 2013. "Landsat Science." *Nasa* 1.

Jeevalakshmi, D., S. Narayana Reddy, and B. Manikiam. 2017. "Land Surface Temperature Retrieval from LANDSAT Data Using Emissivity Estimation." *International Journal of Applied Engineering Research* 12(20):9679–87.

Jenner, L. 2019. "Landsat Overview." *National Aeronautics and Space Administration* 2:2–5.

Jiang, Jing, and Guangjin Tian. 2010. "Analysis of the Impact of Land Use/Land Cover Change on Land Surface Temperature with Remote Sensing." *Procedia Environmental Sciences* 2:571–75.

Kaplan, Gordana, and Ugur Avdan. 2018. "Monthly Analysis of

Wetlands Dynamics Using Remote Sensing Data." *ISPRS International Journal of Geo-Information* 7(10). doi: 10.3390/ijgi7100411.

Luman. 2021. "Featured Maps! Land Use, Land Cover and Vegetation." 2–7.

Mahmou, Reham Riyadh, Rabab Hadi Abood, and Kadhim Naief Kadhim. 2021. "STUDYING THE RELATIONSHIP BETWEEN LAND COVER LST UTILIZING LANDSAT 8 DATA IN KARBALA GOVERNORATE."

Mårtensson, Ulrik. 2011. "Introduction to Remote Sensing and Geographical Information Systems."

MohanRajan, Sam Navin, Agilandeeswari Loganathan, and Prabukumar Manoharan. 2020. "Survey on Land Use/Land Cover (LU/LC) Change Analysis in Remote Sensing and GIS Environment: Techniques and Challenges." *Environmental Science and Pollution Research* 27(24):29900–926. doi: 10.1007/s11356-020-09091-7.

Morais, Caitlin Dempsey. 2000. "GIS Data Explored – Vector and Raster Data." *GIS Lounge* 1–17.

Moran, M. Susan, Ray D. Jackson, Philip N. Slater, and Philippe M. Teillet. 1992. "Evaluation of Simplified Procedures for Retrieval of Land Surface Reflectance Factors from Satellite Sensor Output." *Remote Sensing of Environment* 41(2–3):169–84.

NASA. 2013. "A Landsat Timeline." *Landsat Science* 1.

Naughton, Joseph, and Walter McDonald. 2019. "Evaluating the Variability of Urban Land Surface Temperatures Using Drone

Observations.” *Remote Sensing* 11(14):1722.

Njoku, Elijah Akwarandu. 2019. “Analysis of Spatial-Temporal Pattern of Land Surface Temperature (LST) Due to NDVI and Elevation in Ilorin , Nigeria.” (106).

Packard, Victoria Lynn. 2018. “The International Encyclopedia of Geography: People, the Earth, Environment and Technology.” *Reference Reviews* 32(1):31–32. doi: 10.1108/rr-07-2017-0174.

Pavlovic, Danijela, Bogdan Nikolic, Sanja Djurovic, Hadi Waisi, Ana Andjelkovic, and Dragana Marisavljevic. 2015. “Chlorophyll as a Measure of Plant Health: Agroecological Aspects.”

Rolf, A., and R. A. de By. 2001. “Principles of Geographic Information Systems.” *The International Institute for Aerospace Survey and Earth Sciences (ITC), Hengelosestraat* 99.

Saied, Pakiza. 2015. *The Impact of Urban Expansion on Land Surface Temperatures in Sulaymaniyah City*. GRIN Verlag.

Sameen, Maher Ibrahim, and Mohammed Ahmed Al Kubaisy. 2014. “Automatic Surface Temperature Mapping in Arcgis Using Landsat-8 Tirs and Envi Tools, Case Study: Al Habbaniyah Lake.” *J. Environ. Earth Sci* 4(12):12–17.

Sekertekin, Aliihsan, and Stefania Bonafoni. 2020. “Land Surface Temperature Retrieval from Landsat 5, 7, and 8 over Rural Areas: Assessment of Different Retrieval Algorithms and Emissivity Models and Toolbox Implementation.” *Remote Sensing* 12(2):1–14. doi: 10.3390/rs12020294.

Tan, Jie, De Yu, Qiang Li, Xuelan Tan, and Weijun Zhou. 2020.

"Spatial Relationship between Land-Use/Land-Cover Change and Land Surface Temperature in the Dongting Lake Area, China." *Scientific Reports* 10(1):1–14. doi: 10.1038/s41598-020-66168-6.

Thapa, Sushil. 2017. "Exploring the Impact of Urban Growth on Land Surface Temperature of Kathmandu Valley."

U.S. Geological Survey, and Water Science School. 2018. "Temperature and Water Water Properties Information by Topic." 2–3.

Ullah, Siddique, Adnan Ahmad Tahir, Tahir Ali Akbar, Quazi K. Hassan, Ashraf Dewan, Asim Jahangir Khan, and Mudassir Khan. 2019. "Remote Sensing-Based Quantification of the Relationships between Land Use Land Cover Changes and Surface Temperature over the Lower Himalayan Region." *Sustainability (Switzerland)* 11(19). doi: 10.3390/su11195492.

Weih Jr, Robert C., and D. White Jr. 2008. "Land-Use/Land-Cover Characterization Using an Object-Based Classifier for the Buffalo River Sub-Basin in North-Central Arkansas." *Journal of the Arkansas Academy of Science* 62(1):125–32.

Weng, Qihao, Dengsheng Lu, and Jacquelyn Schubring. 2004. "Estimation of Land Surface Temperature–Vegetation Abundance Relationship for Urban Heat Island Studies." *Remote Sensing of Environment* 89(4):467–83.

Yan, Yibo, Kebiao Mao, Jiancheng Shi, Shilong Piao, Xinyi Shen, Jeff Dozier, Yungang Liu, Hong li Ren, and Qing Bao. 2020. "Driving Forces of Land Surface Temperature Anomalous Changes in North America in 2002–2018." *Scientific Reports* 10(1):1–38. doi:

10.1038/s41598-020-63701-5.

Yang, Haibo, Chaofan Xi, Xincan Zhao, Penglei Mao, Zongmin Wang Yong Shi, Tian He, and Zhenhong Li. 2020. “Measuring the Urban Land Surface Temperature Variations Under Zhengzhou City Expansion Using Landsat-Like Data.” *Remote Sensing* 12(5):801.

Young, Nicholas E., Ryan S. Anderson, Stephen M. Chignell, Anthony G. Vorster, Rick Lawrence, and Paul H. Evangelista. 2017. “A Survival Guide to Landsat Preprocessing.” *Ecology* 98(4):920–32. doi: 10.1002/ecy.1730.

ZANTER, KAREN. 2019. “LANDSAT 8 (L8) DATA USERS HANDBOOK Version 4.0 April 2019.” 8(April).

Zhibin, Ren, Zheng Haifeng, He Xingyuan, Zhang Dan, and Yu Xingyang. 2015. “Estimation of the Relationship between Urban Vegetation Configuration and Land Surface Temperature with Remote Sensing.” *Journal of the Indian Society of Remote Sensing* 43(1):89–100.

Appendix A

Histograms of LST Rasters

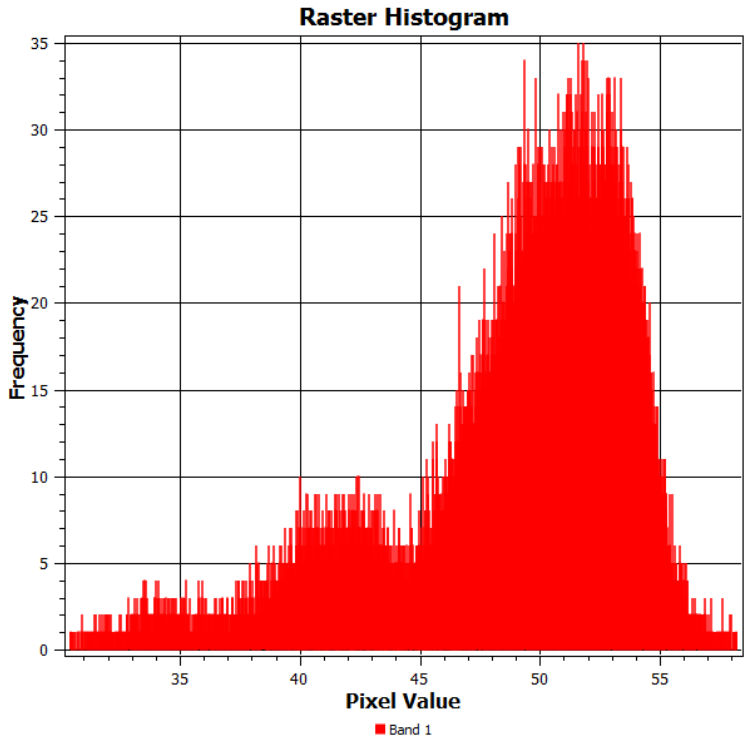
Raster Histogram
Frequency
Pixel Value
Band 1
0
5
10
15
20
25
30
35
35
40
45
50
55

2013

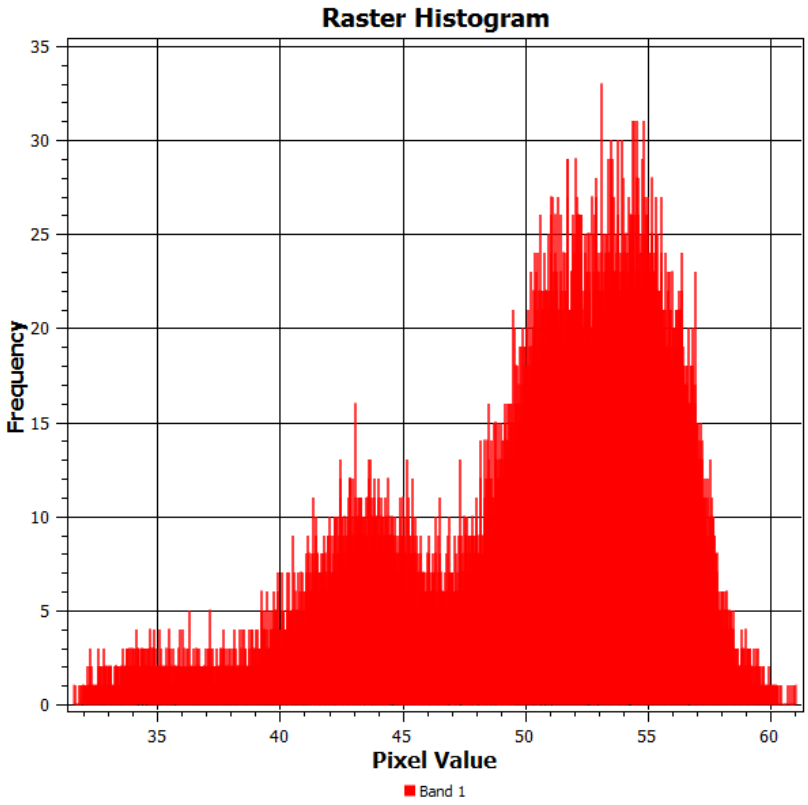
Raster Histogram
Frequency
Pixel Value
Band 1
0
5
10
15
20
25
30
35
35
40
45
50
55
60

2014

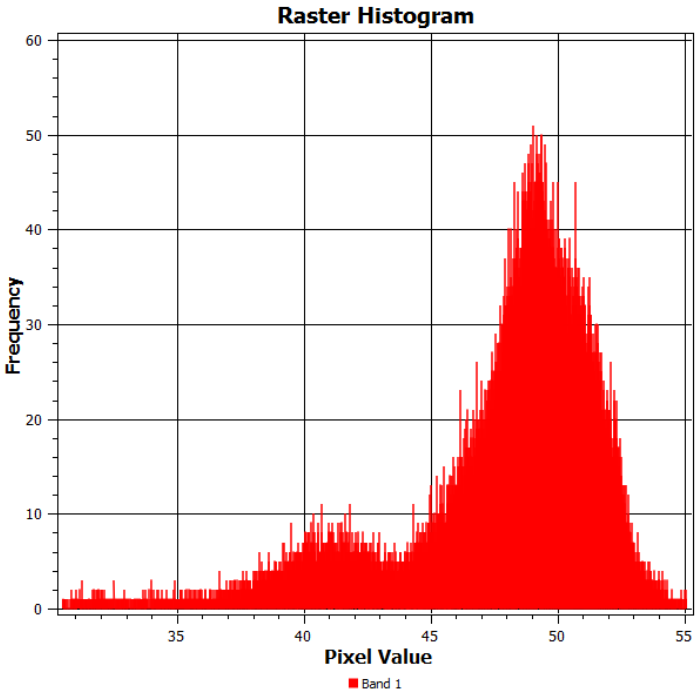
Raster Histogram
Frequency
Pixel Value
Band 1

2015

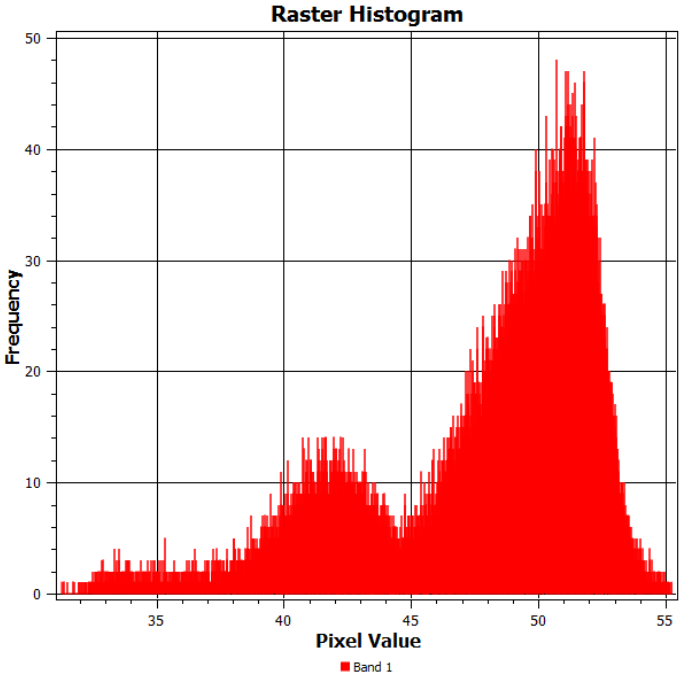
Raster Histogram
Frequency
Pixel Value
Band 1

2016

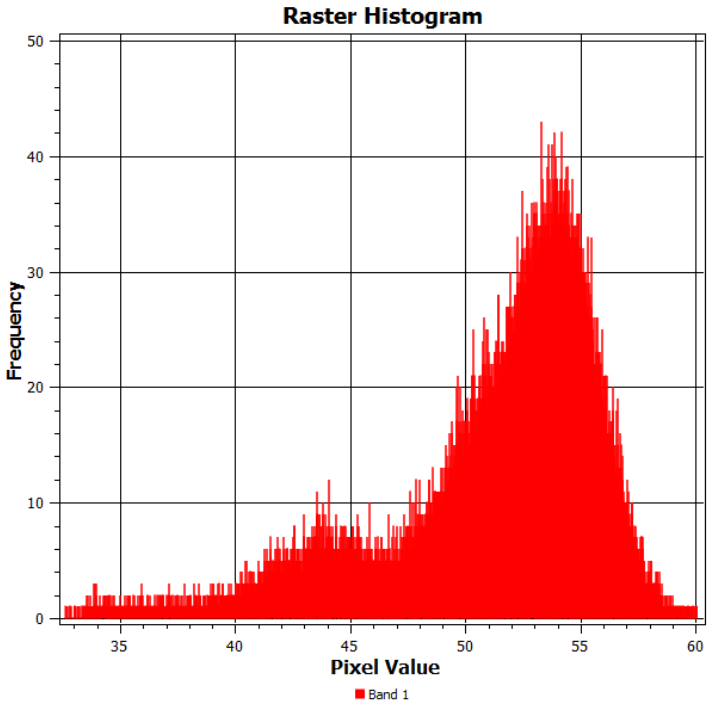
Raster Histogram
Frequency
Pixel Value
Band 1
0
10
20
30
40
50
35
40
45
50
55
60

2017

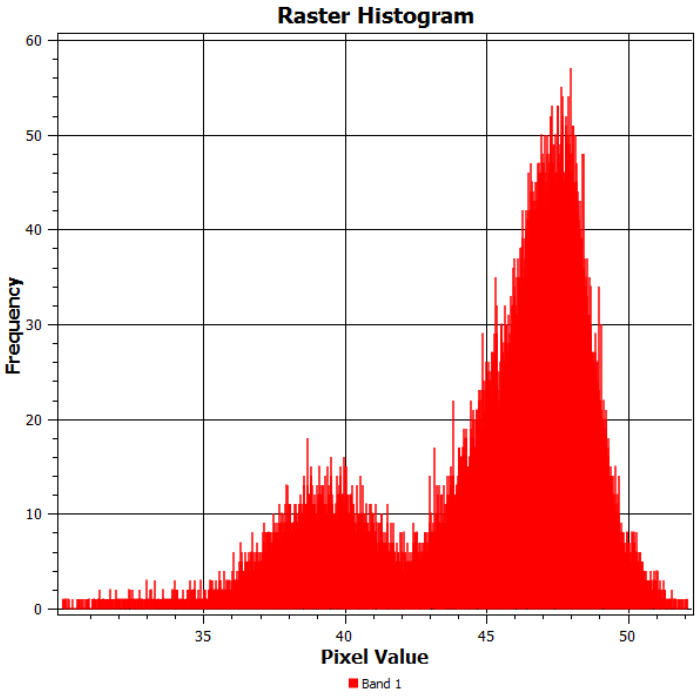
Raster Histogram
Frequency
Pixel Value
Band 1
0
10
20
30
40
50
60
35
40
45
50

2018

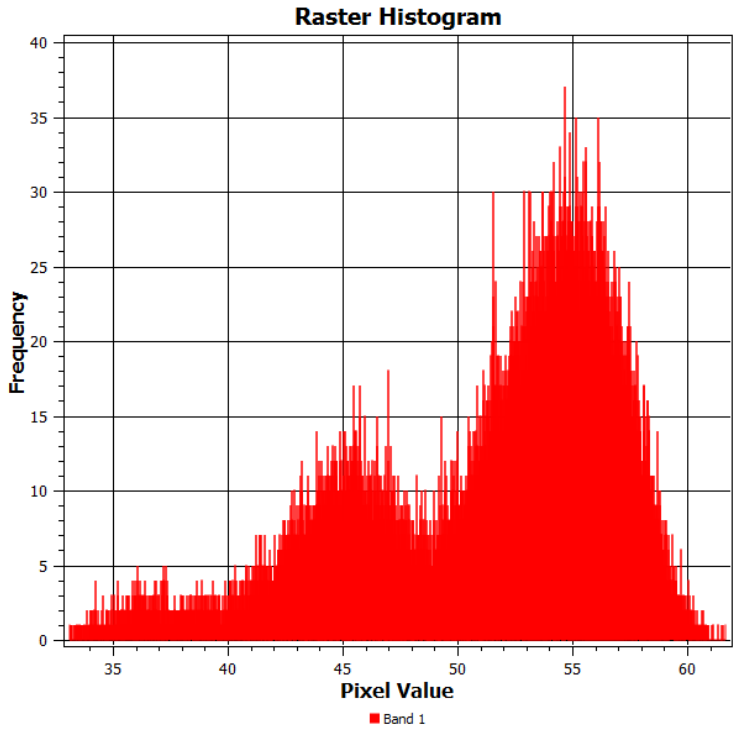
Raster Histogram
Frequency
Pixel Value
Band 1

2019

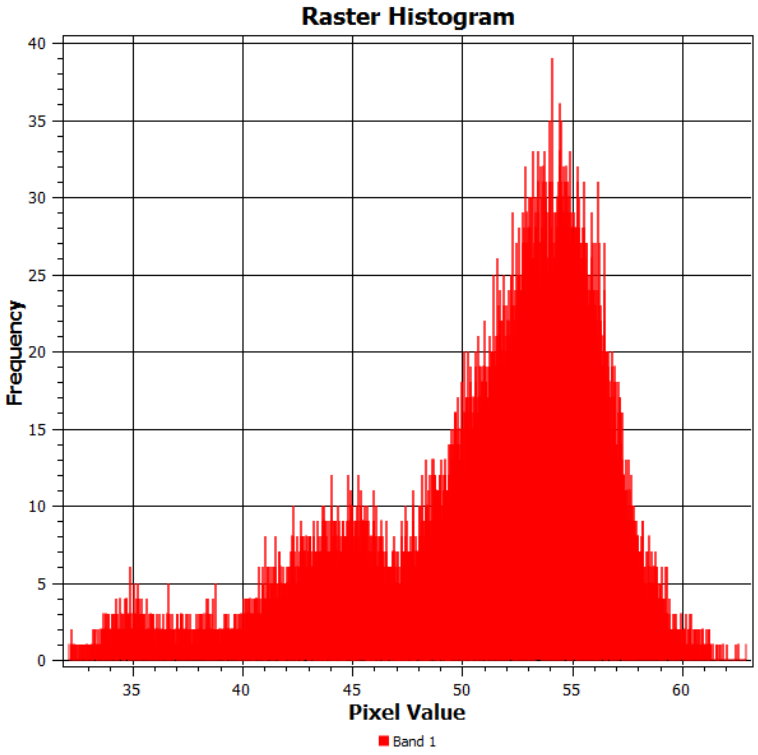
Raster Histogram
Frequency
Pixel Value
Band 1

2020

Appendix B

Land Surface Temperature

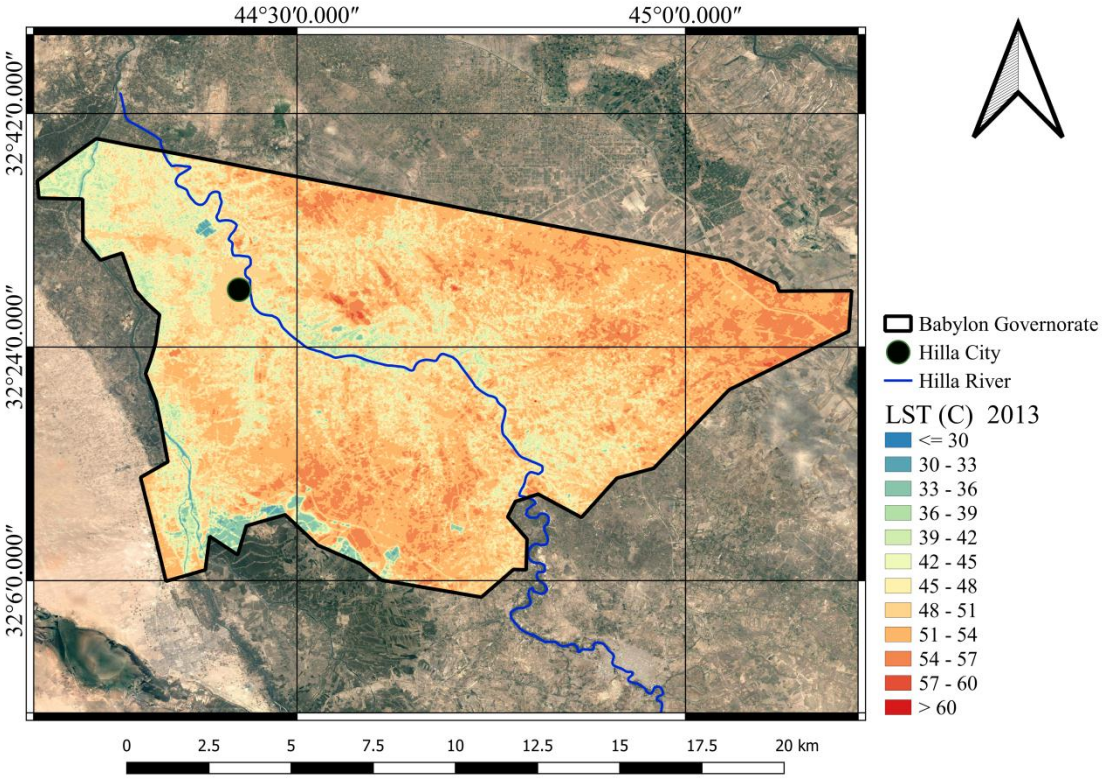

Land Surface Temperature 2013

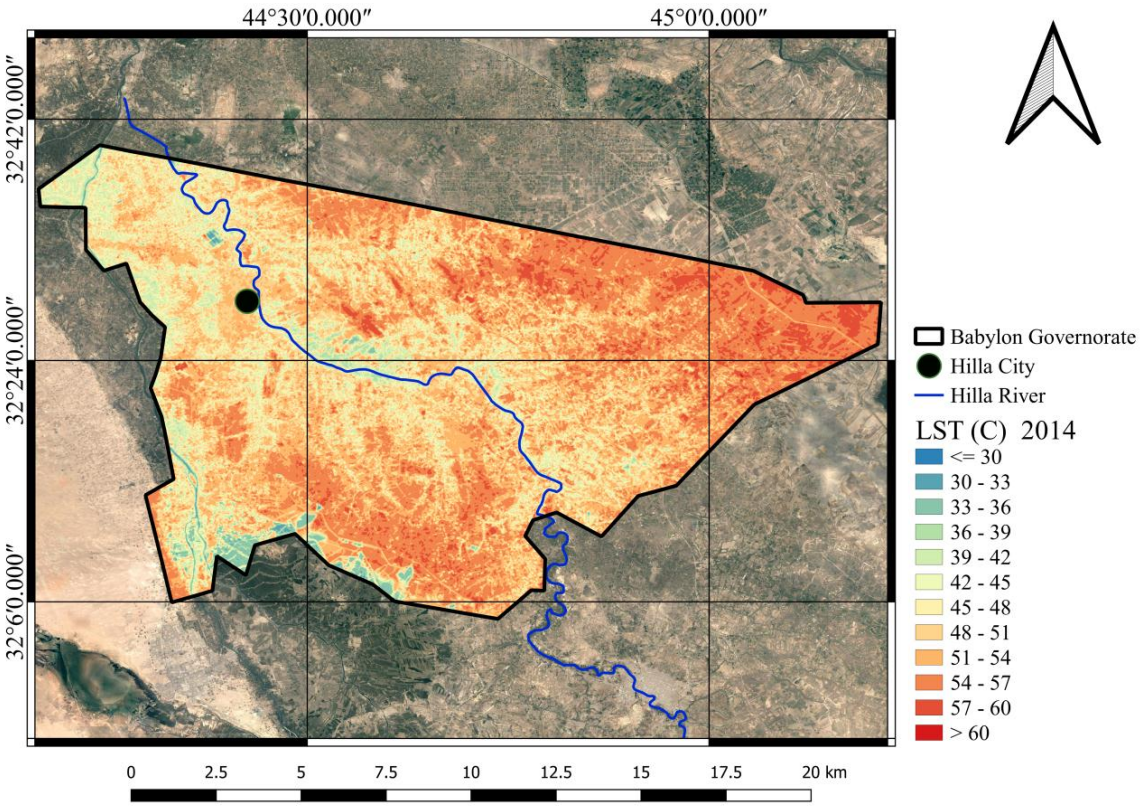

Land Surface Temperature 2014

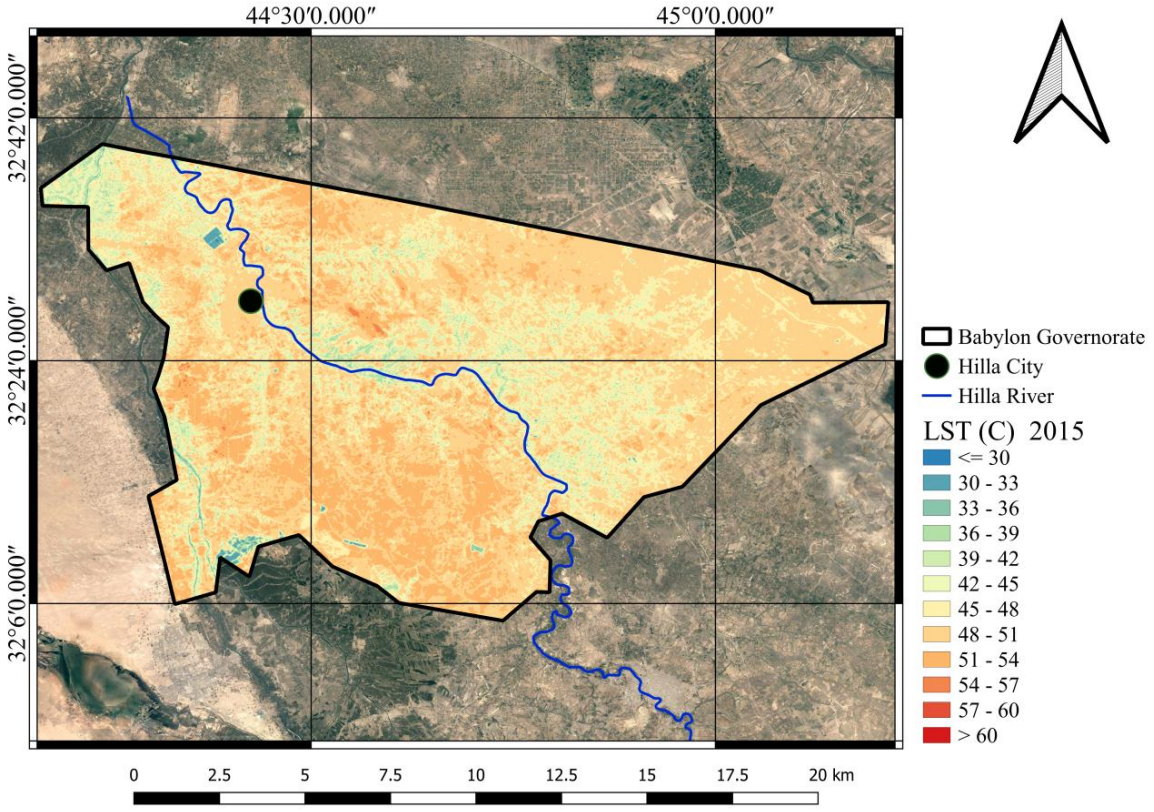

Land Surface Temperature 2015

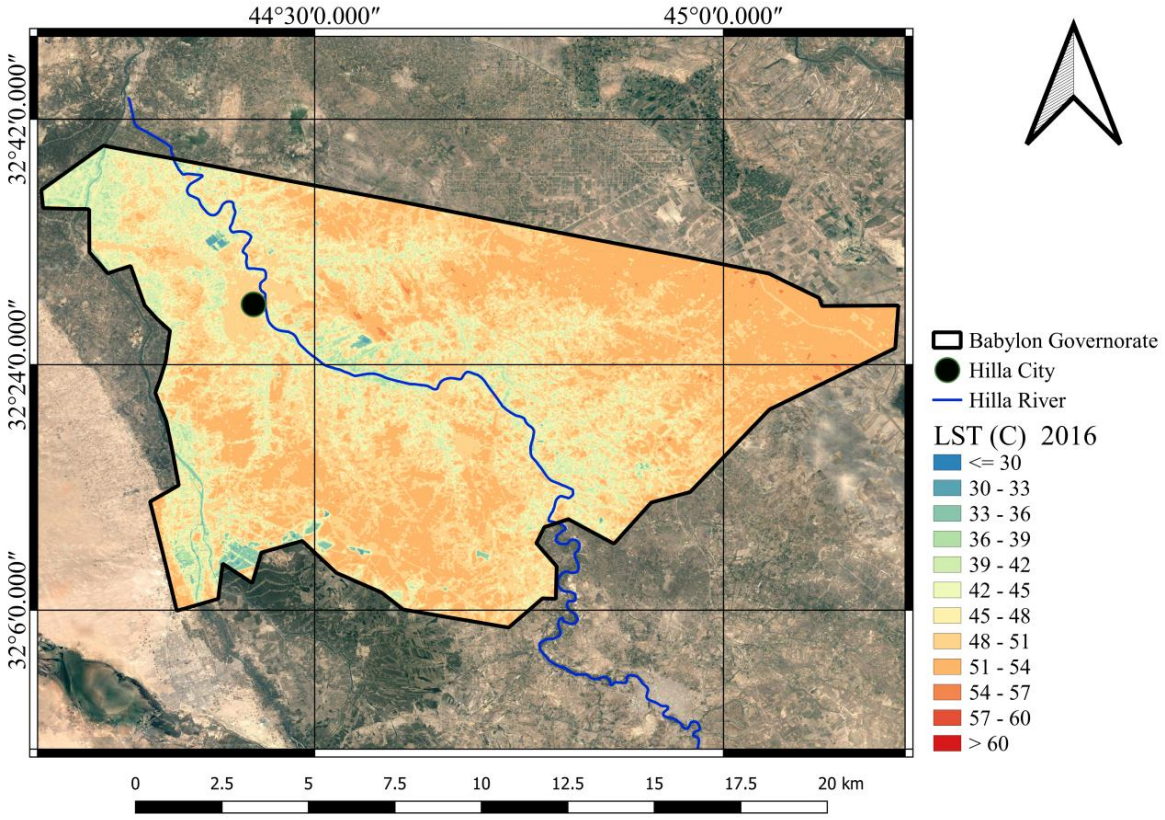

Land Surface Temperature 2016

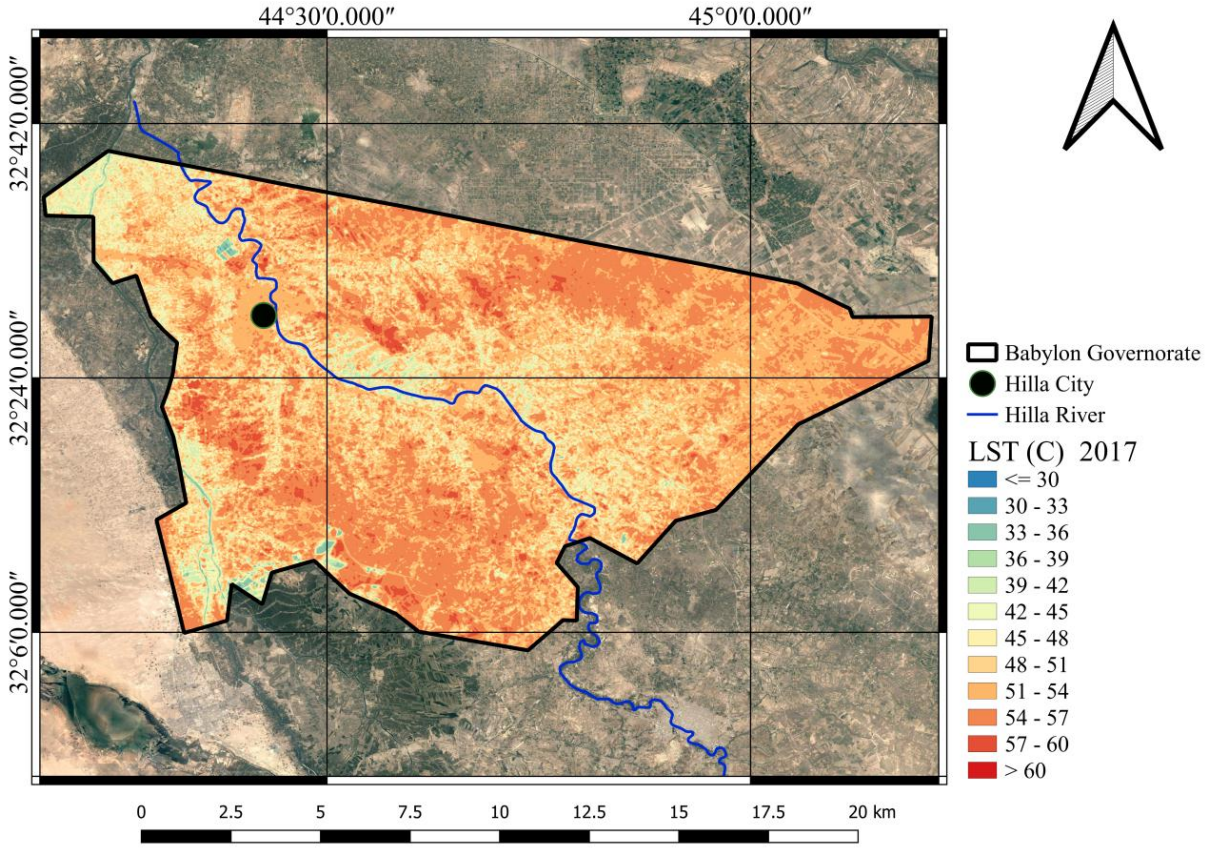

Land Surface Temperature 2017

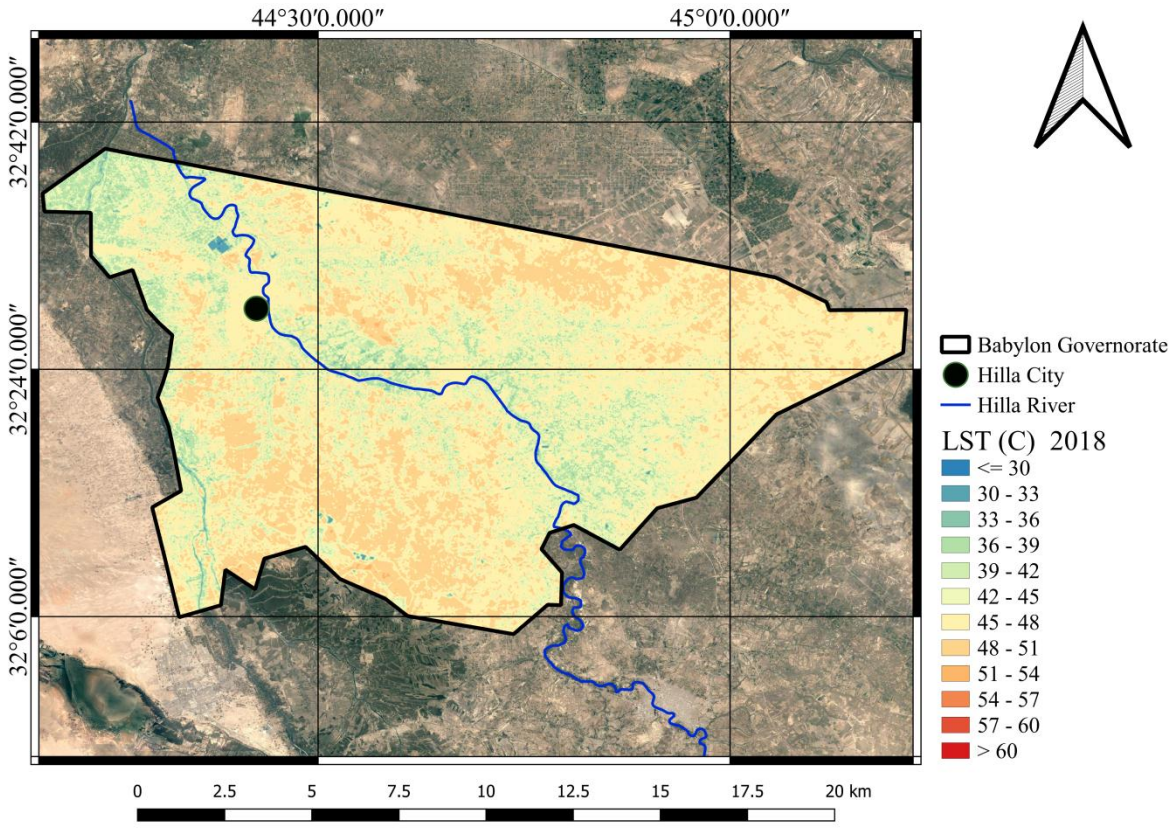

Land Surface Temperature 2018

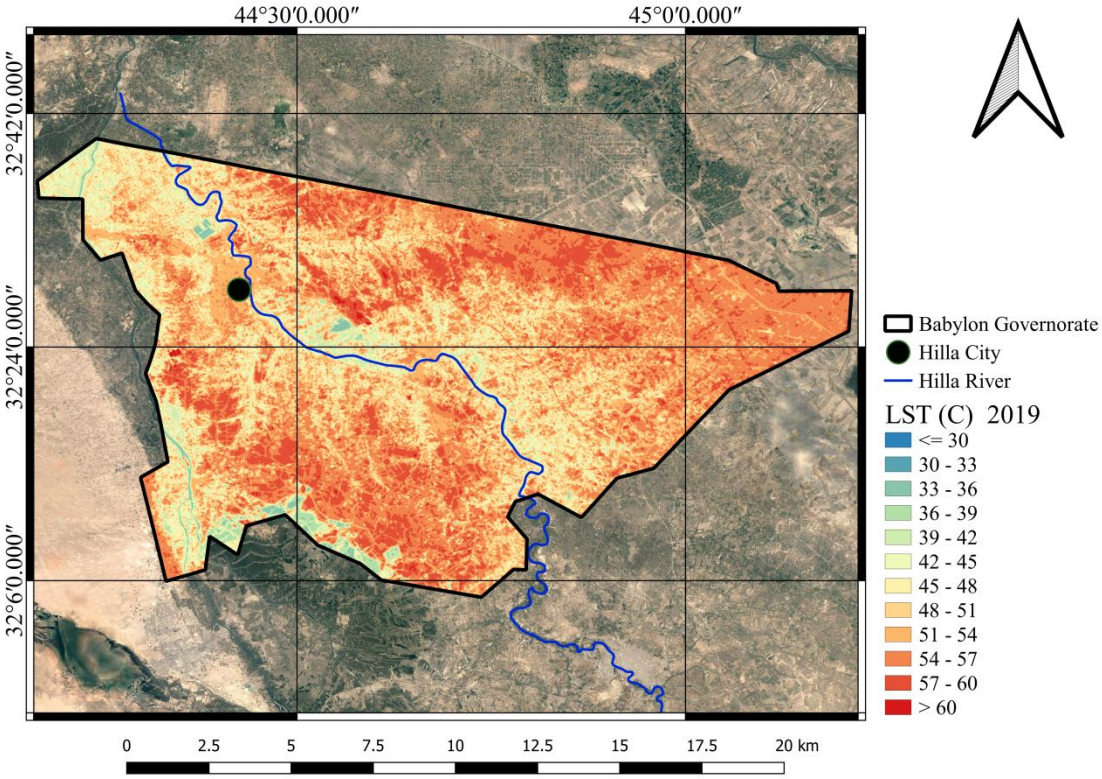

Land Surface Temperature 2019

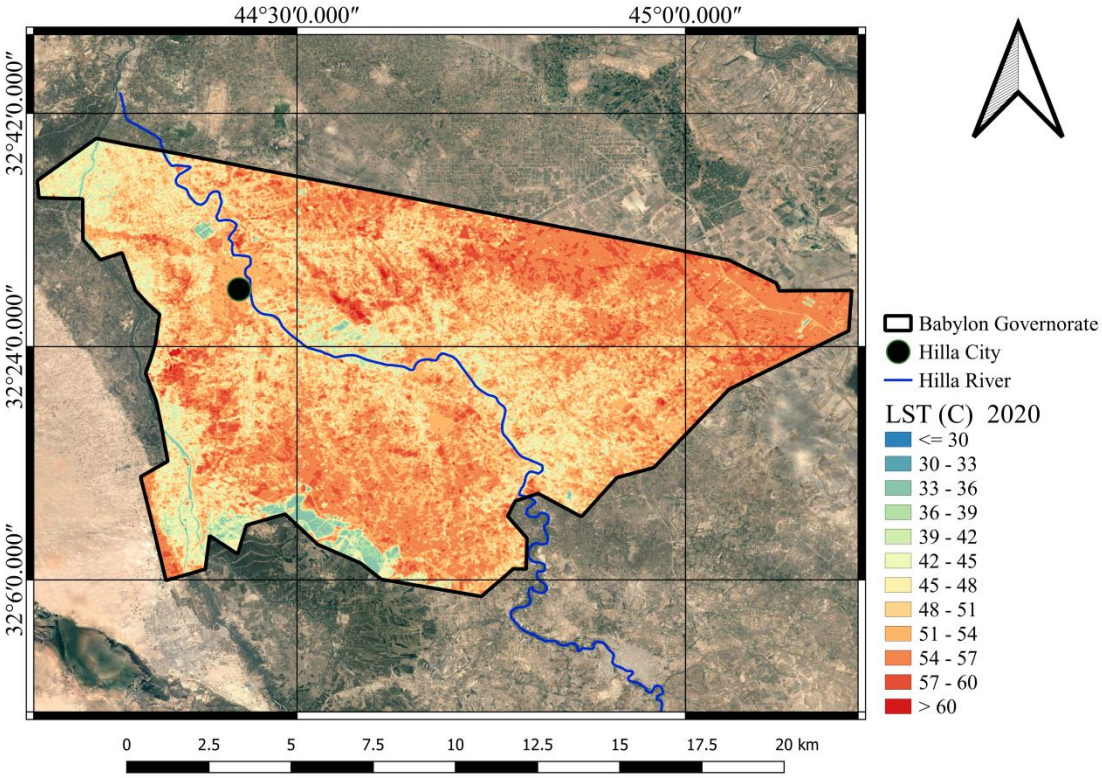

Land Surface Temperature 2020

Appendix C

Land Cover Classification

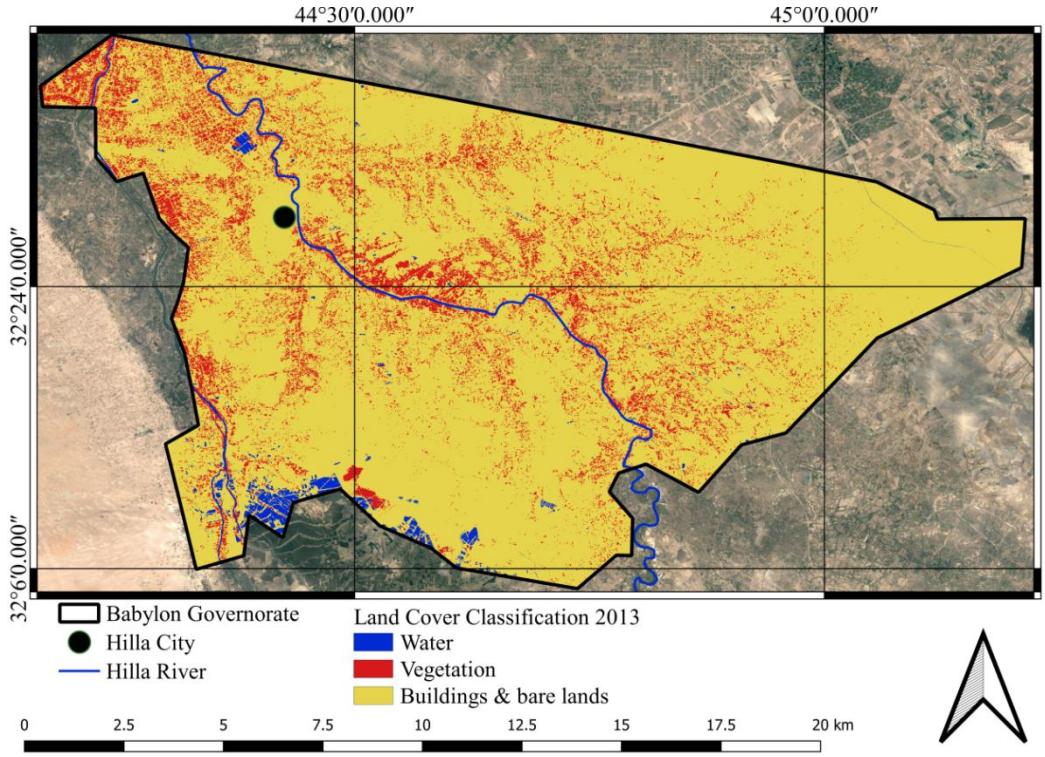

Land Cover Classification 2013

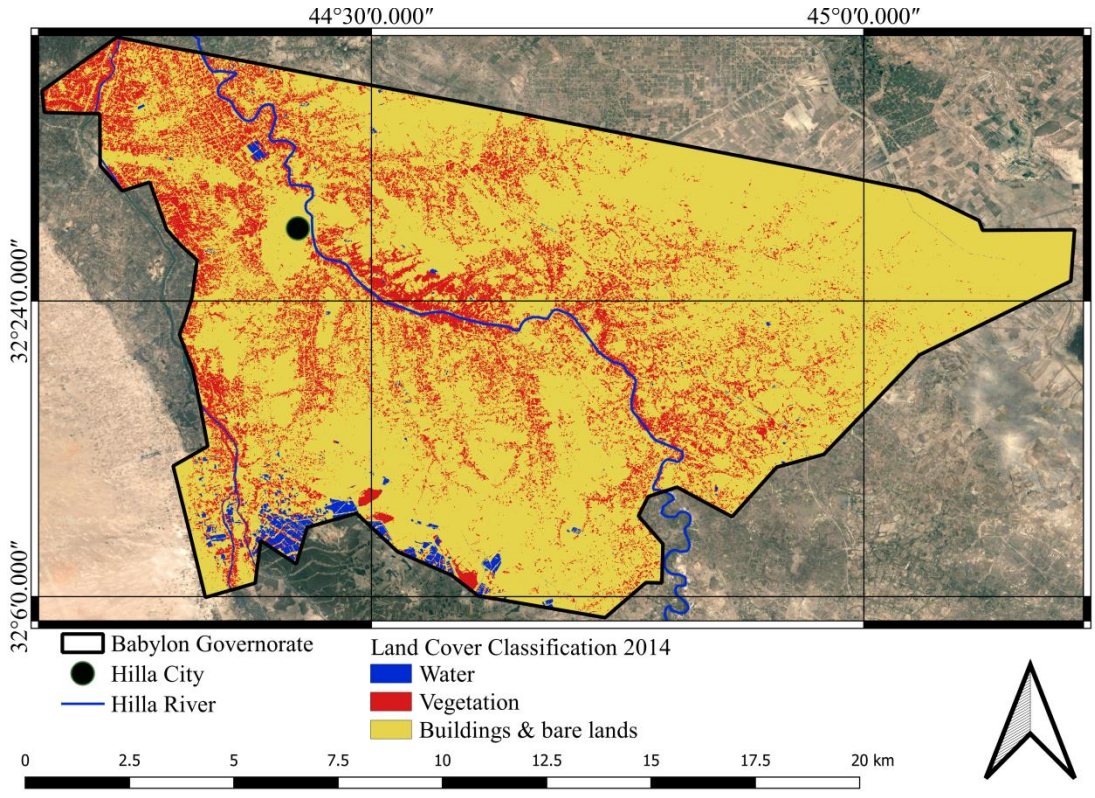

Land Cover Classification 2014

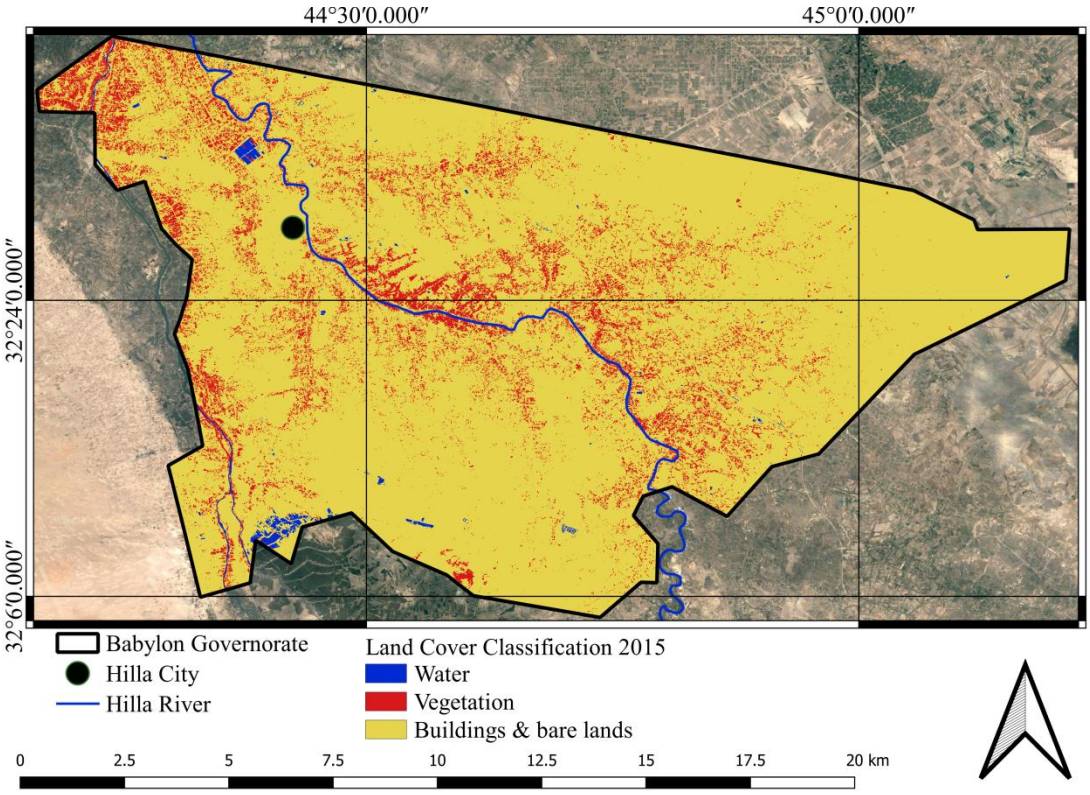

Land Cover Classification 2015

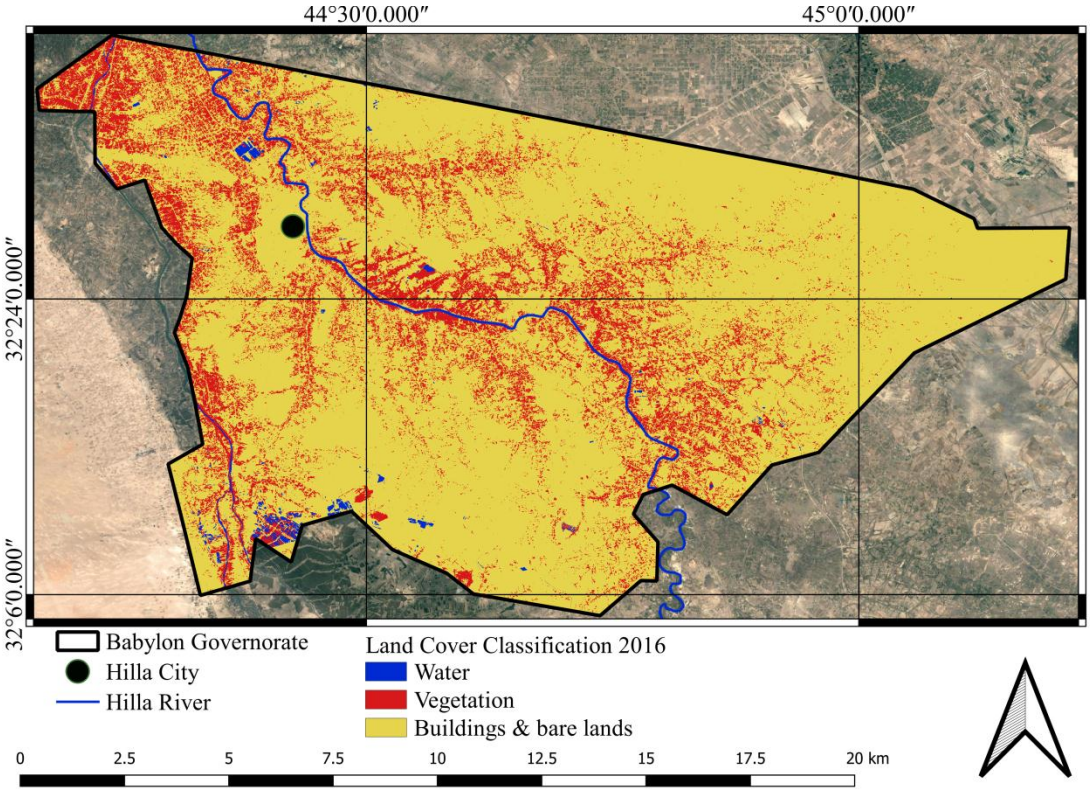

Land Cover Classification 2016

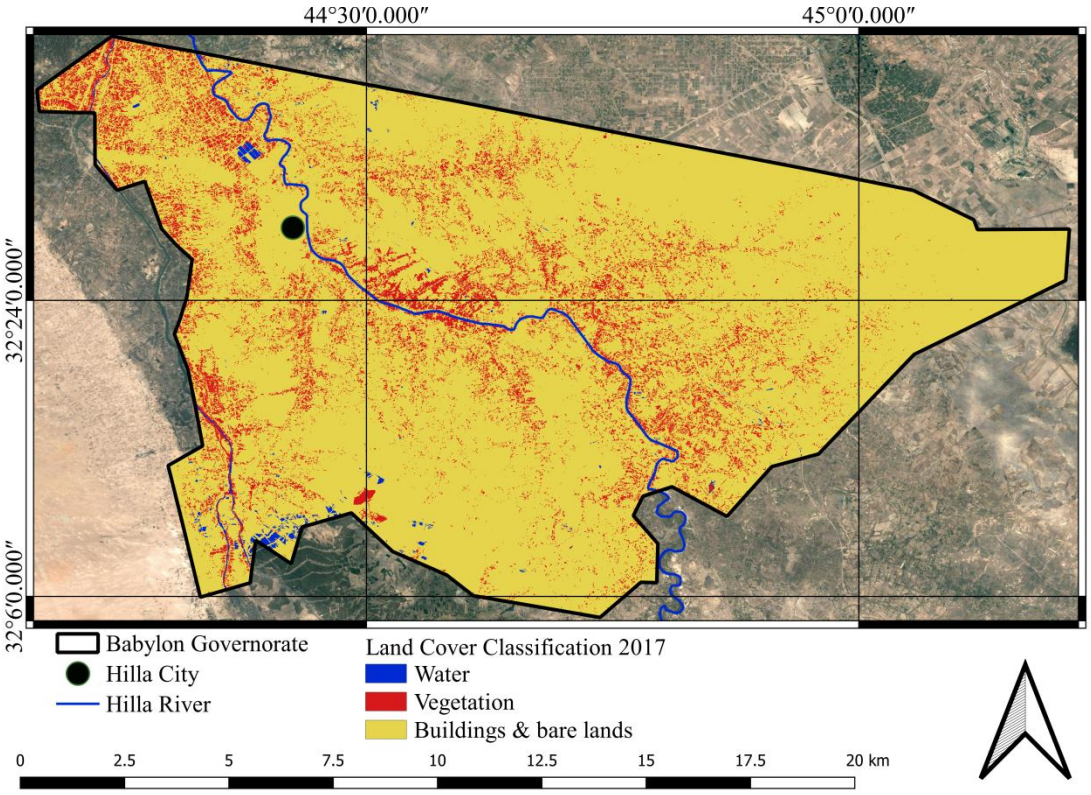

Land Cover Classification 2017

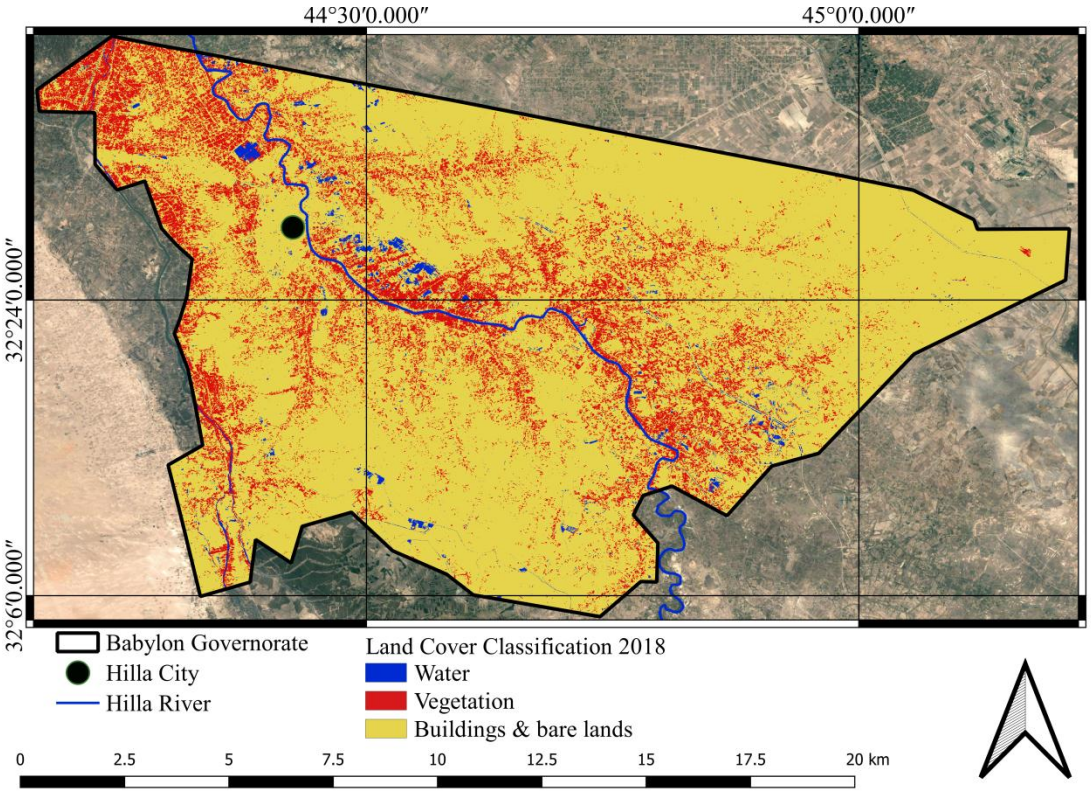

Land Cover Classification 2018

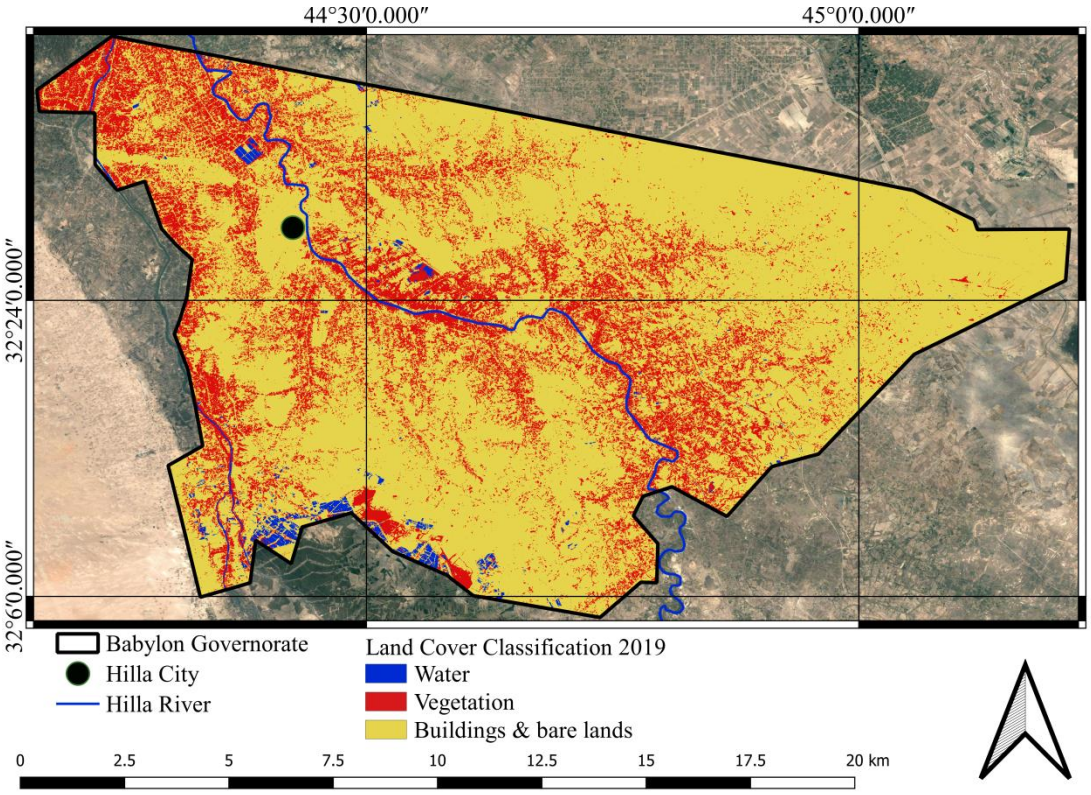

Land Cover Classification 2019

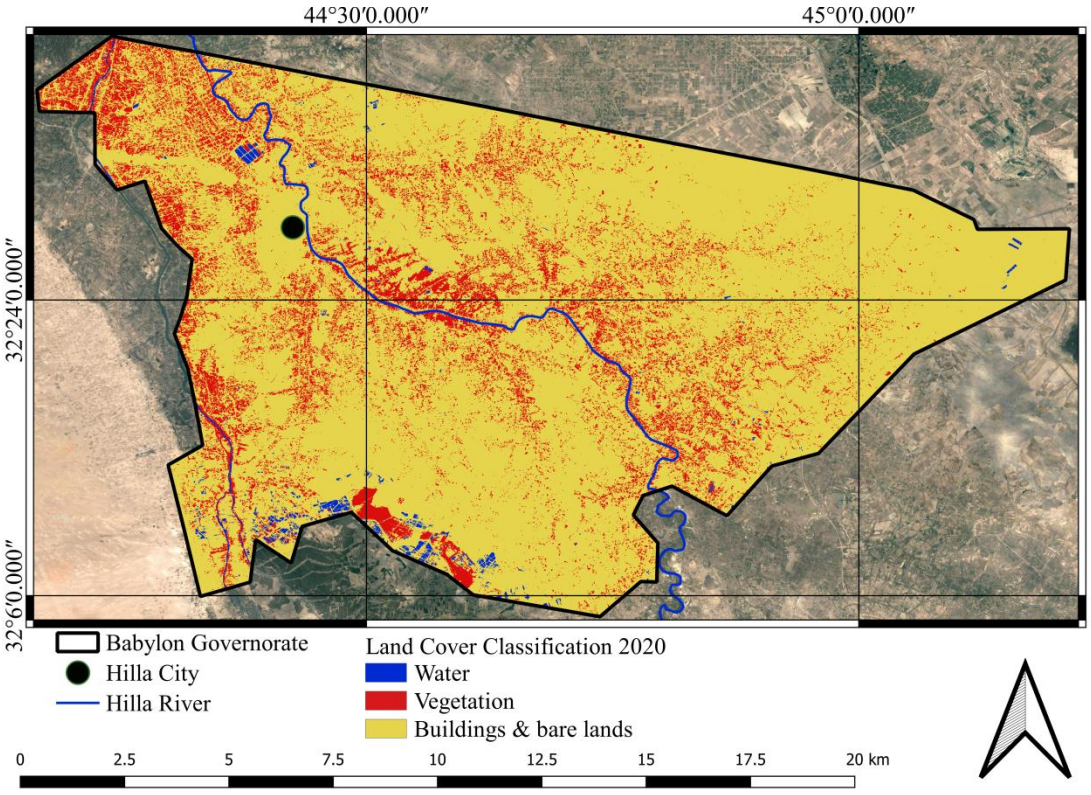

Land Cover Classification 2020

Appendix D

Normalized Difference Vegetation Index

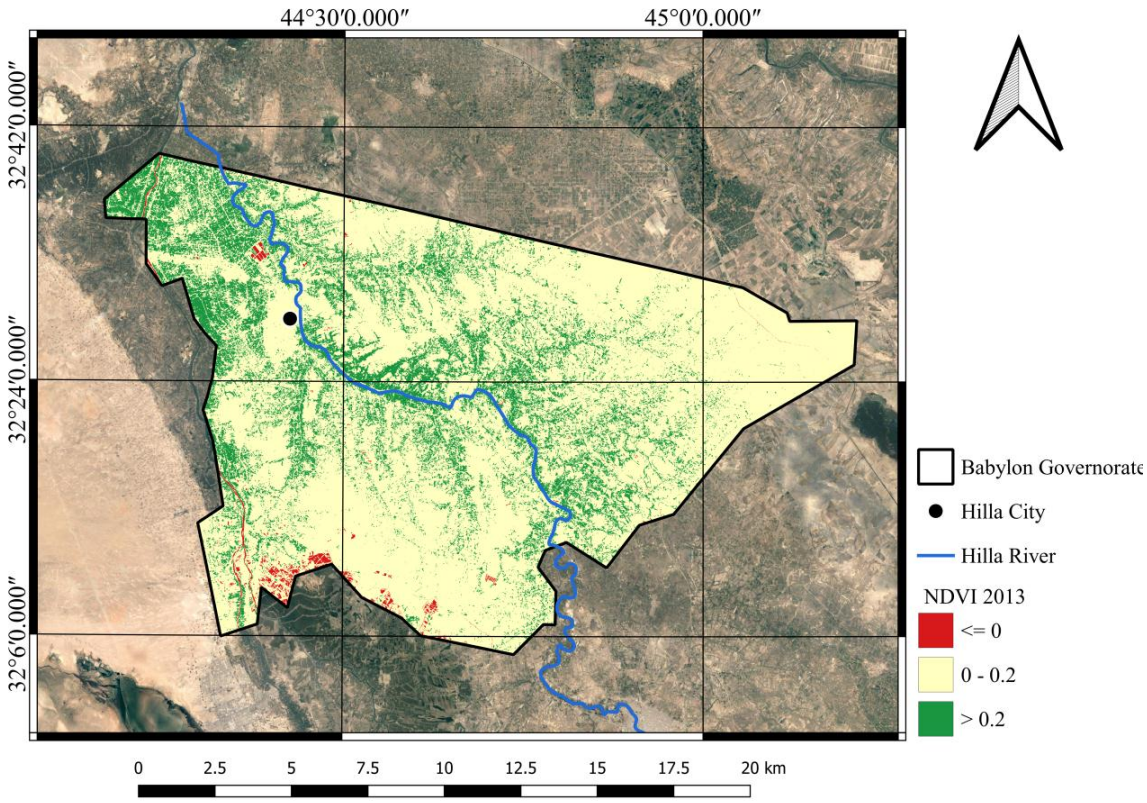

Normalized Difference Vegetation Index 2013

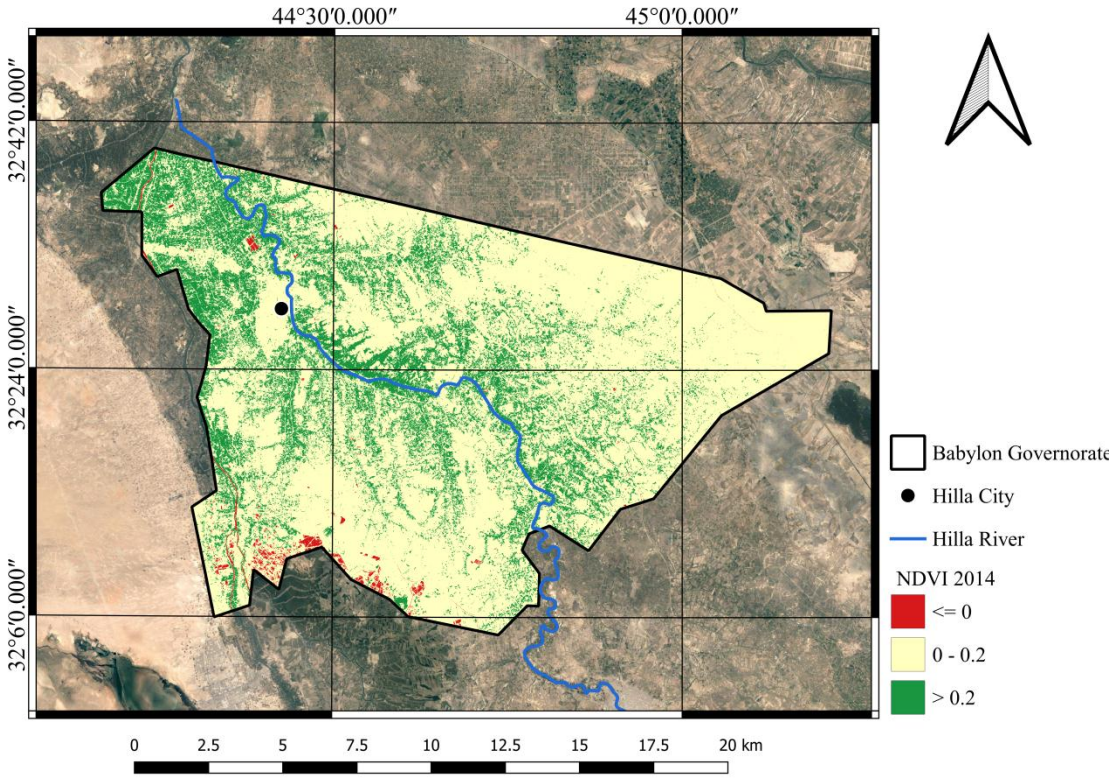

Normalized Difference Vegetation Index 2014

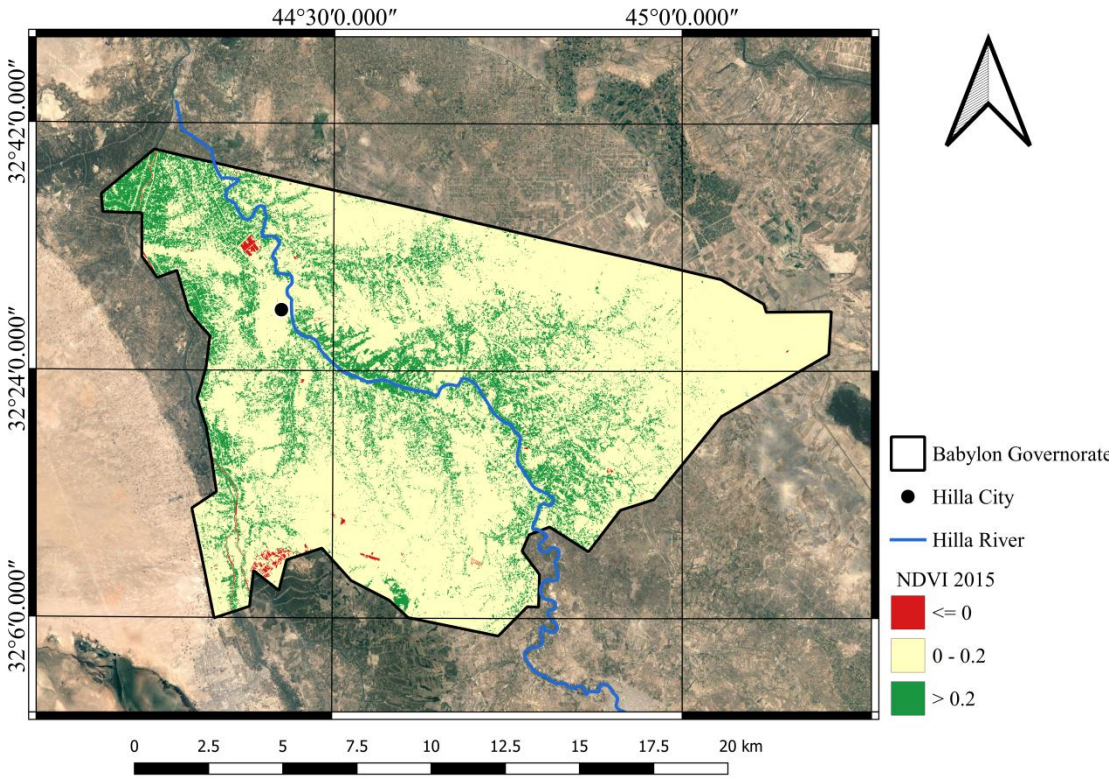

Normalized Difference Vegetation Index 2015

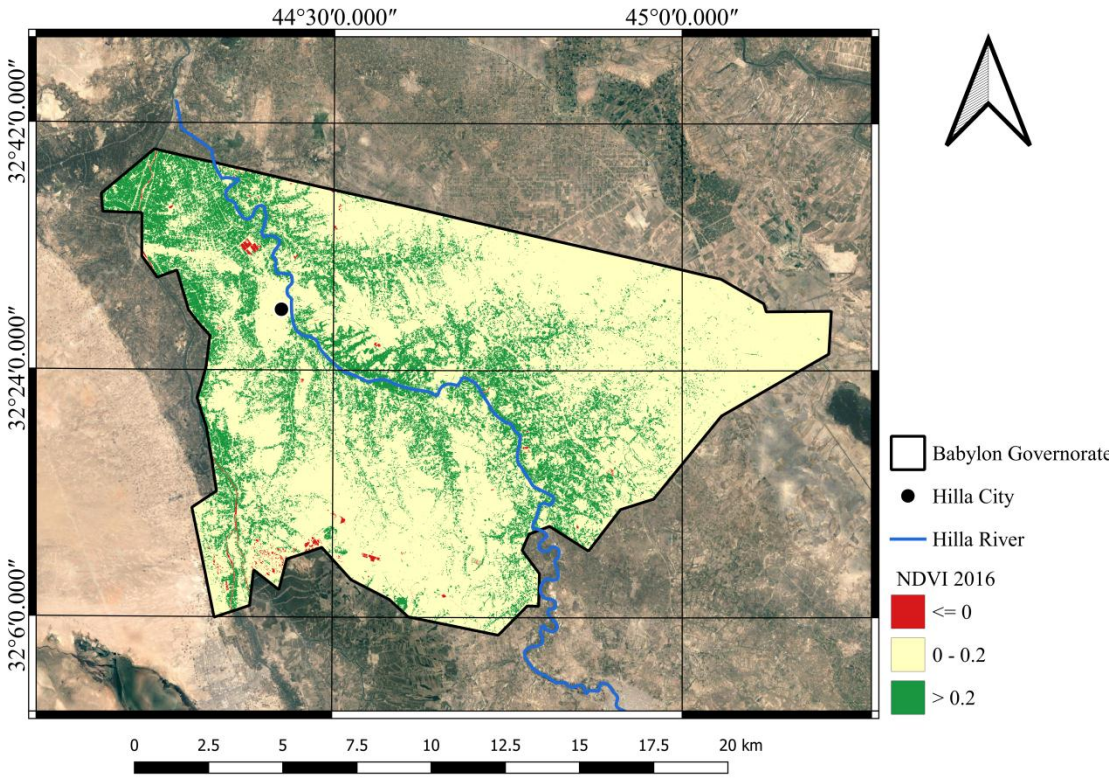

Normalized Difference Vegetation Index 2016

Appendix D

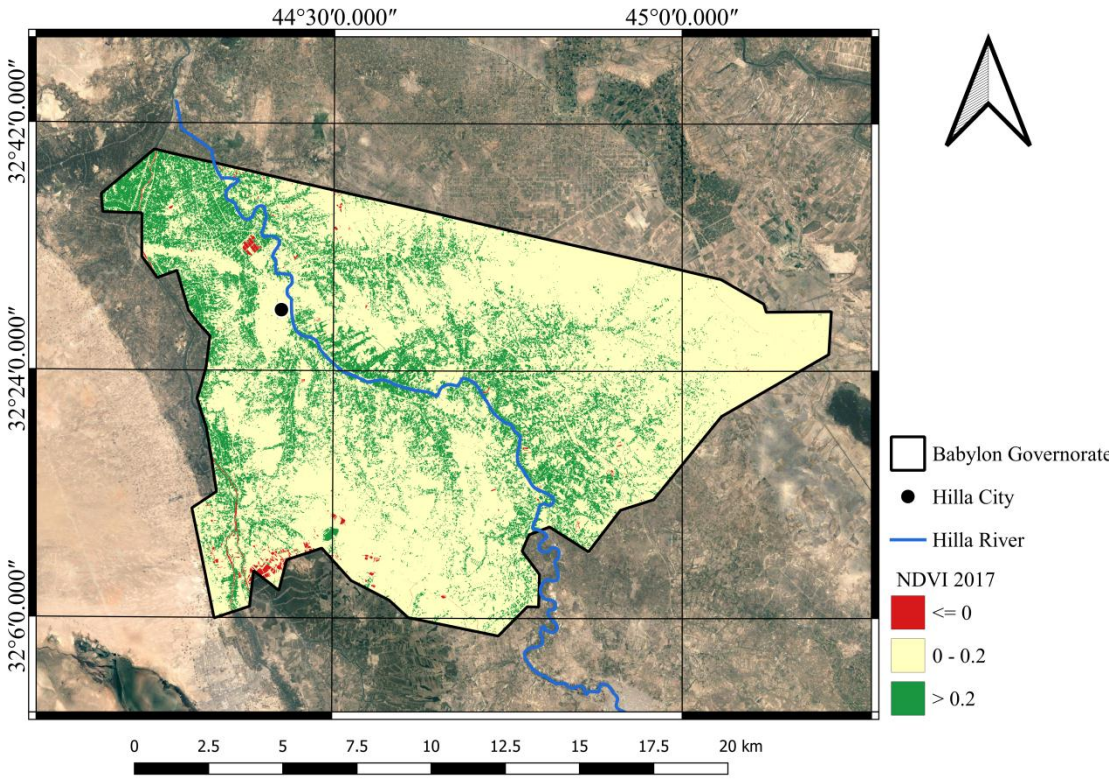

Normalized Difference Vegetation Index 2017

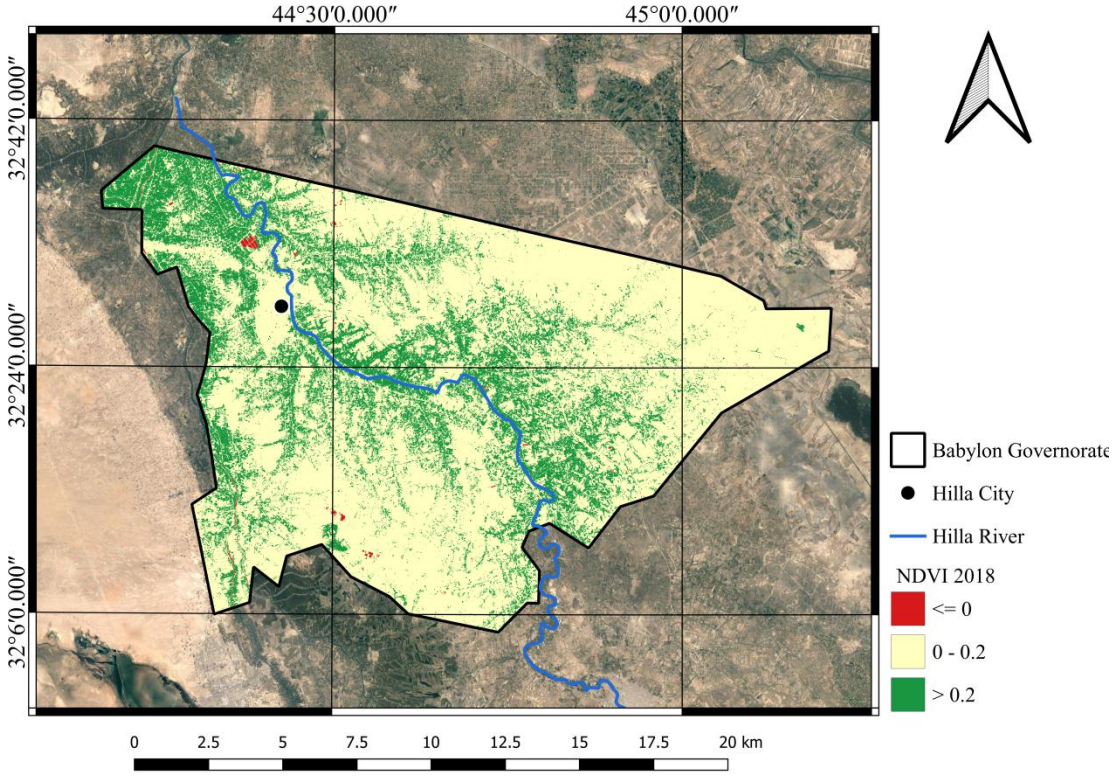

Normalized Difference Vegetation Index 2018

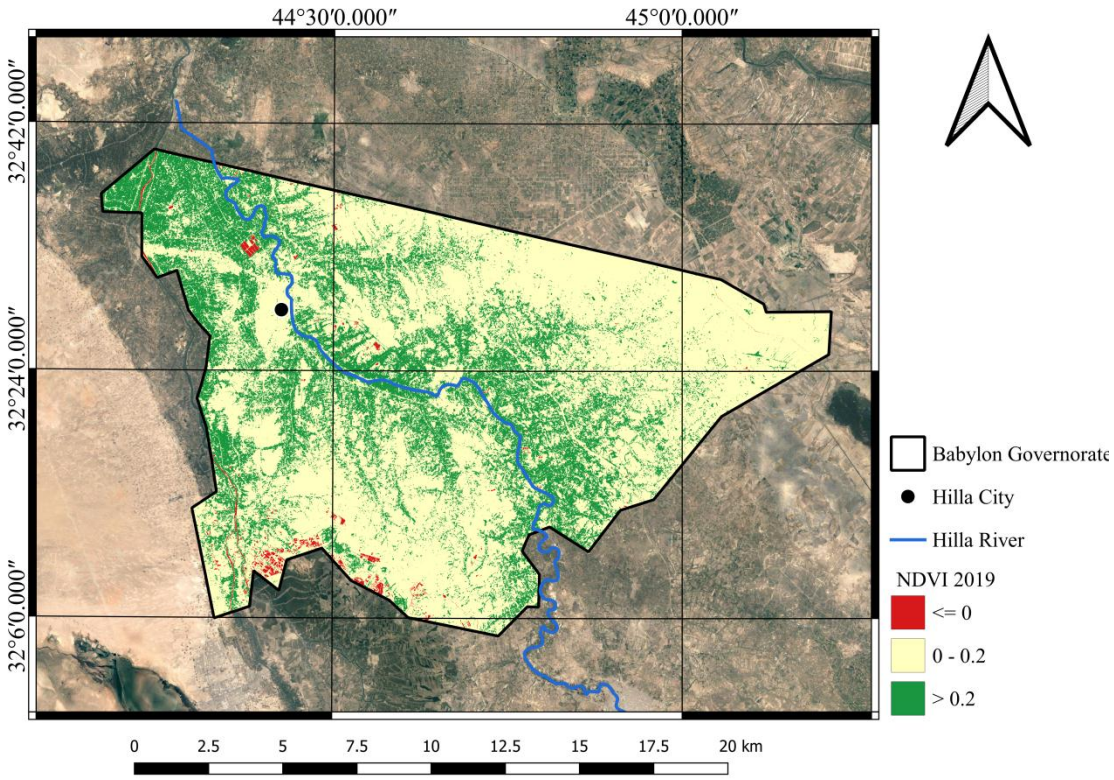

Normalized Difference Vegetation Index 2019

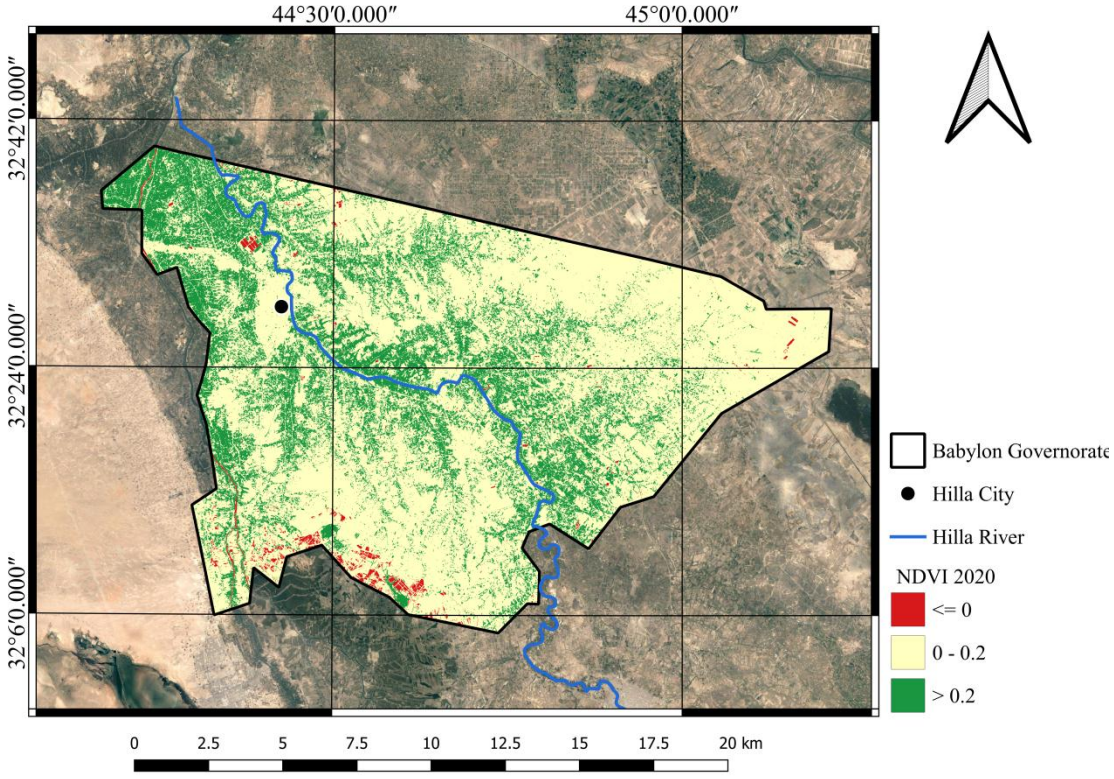

Normalized Difference Vegetation Index 2020

جمهورية العراق
وزارة التعليم العالي والبحث العلمي
جامعة بابل
كلية الهندسة
قسم الهندسة البيئية

نظم المعلومات الجغرافية و الأستشعارعن بعد
لاستجابات نهر الحلة لتغيرات درجات الحرارة الجوية في العراق

رسالة مقدمه الى
قسم الهندسة البيئية كلية الهندسة
في جامعة بابل كجزء من متطلبات نيل
درجة الماجستير في الهندسة / الهندسة البيئية

من قبل
هبه جاسم عوده جاسم المسعودي

اشراف
أ.م.د. حسين علي مهدي الزبيدي

1443 هـ 2022 م

الخلاصة

في البلدان النامية ، يؤدي التحضر إلى تباين في الغطاء الأرضي. وهذا يؤدي إلى تغيرات مكانية وزمانية في درجة حرارة سطح الأرض. يسلط هذا البحث الضوء على كيفية اختلاف درجة حرارة سطح الأرض (LST) مكانياً وزمانياً فوق مدينة بابل ، العراق. تم اخذ صورملتقطة من Landsat-8 خلال الفترة من 2013 إلى 2020 ومعالجتها في برنامج QGIS للإشارة إلى التغيرات في درجة حرارة سطح الأرض وربط هذا التباين بمؤشر الفرق الطبيعي للغطاء النباتي (NDVI).

أشارت النتائج إلى أن المناطق القاحلة أعطت أعلى درجة حرارة. بحدود 62 درجة مئوية ، وتراوح متوسط درجة الحرارة من 45 إلى 51 درجة مئوية ، وكان الحد الأدنى 30 درجة مئوية تقريبًا. بالإضافة إلى ذلك ، كانت القيم المتوسطة لمؤشر فرق الغطاء النباتي بين 0.15 و 0.17. تتراوح درجات الحرارة بين درجات الحرارة المرتفعة والمنخفضة والأراضي الجرداء (المبنية) والغطاء النباتي والمياه المغطاة بالتقريب (76.1 - 89)٪ و (10.2 - 22.6)٪ و (0.6 - 1.6)٪ من إجمالي مساحة الدراسة على التوالي. أشار إلى أن توزيع درجات الحرارة في المنطقة المختارة قد تأثر بالتطور الحضري.

علاوة على ذلك ، تم إعداد نماذج خطية صالحة للتنبؤ بـ LST من حيث NDVI مباشرة. أظهرت المقارنة بين درجة حرارة الهواء التي تم جمعها من محطات الأرصاد الجوية ودرجة حرارة سطح الأرض المحددة أن هناك علاقة ارتباط عالية بين القيم المقدرة والملاحظة مع اختلاف 3 درجات مئوية. كما أظهرت النتائج أن الأراضي الصخرية في مركز حوض نهر الحلة كانت أعلى من المناطق الأخرى داخل المحافظة. بدأت درجات الحرارة في الارتفاع عام 2013 ، ثم ارتفعت تدريجياً في 2014 و 2015 لتصبح مرتفعة بشكل ملحوظ في 2016 و 2017 و 2018 و 2019 ، لكن في عام 2020 انخفضت درجة الحرارة قليلاً عن السنوات السابقة.

أظهرت نتائج حي الصحة زيادة في الأراضي العارية والمبنية في السنوات الثماني الماضية ، حيث زادت المساحة من 2.6 كيلومتر مربع في عام 2013 إلى 2.8 كيلومتر مربع في عام 2020. وانخفضت المحاصيل والغطاء النباتي من 0.31 في عام 2013 إلى 0.18 كيلومتر مربع في عام 2020. علاوة على ذلك ، لوحظ انخفاض في المسطح المائي من 0.11 في عام 2013 إلى 0.06 كيلومتر مربع. أيضًا ، يتراوح LST من 36 إلى 50 درجة مئوية في عام 2013 ومن 40 إلى 54.6 درجة مئوية في عام 2020. في الدراسة ، وجد أيضًا أن الحد الأقصى من LST لكامل الأرض تم رفعه بمقدار 4 درجات مئوية من 2013 إلى 2020 ، وزادت درجة الحرارة الدنيا بنفس المعدل من 36 إلى 40 درجة مئوية. يمكن أن يعزى ذلك إلى التحضر واستبدال الغطاء النباتي بالمباني.

فضلا عن ذلك. أظهرت المقارنة بين بيانات درجة الحرارة من موقع ناسا ودرجة الحرارة المحسوبة اتفاقًا جيدًا للغاية من حيث RMSE و MAE فيما يتعلق بالمجسم المائي والنباتات والأراضي. كان RMSE

للمسطحات المائية 0.9 درجة مئوية والنباتات 1.20 درجة مئوية ، بينما كان للأراضي 1.5 درجة مئوية. كانت قيم MAE 0.6 و 0.9 0 درجة مئوية للمياه والنباتات ، على التوالي ، بينما كانت قيمتها 1.3 درجة مئوية للأراضي.